Infrastructure, Operations, and Circuits Design of an Undersea Power System

Shuai Lu

A dissertation submitted in partial fulfillment of
the requirements for the degree of

Doctor of Philosophy

University of Washington

2006

Program Authorized to Offer Degree: Electrical Engineering

University of Washington
Graduate School

This is to certify that I have examined this copy of a doctoral dissertation by

Shuai Lu

and have found that it is complete and satisfactory in all respects,
and that any and all revisions required by the final
examining committee have been made.

Chair of the Supervisory Committee:

____
Mohammed A. El-Sharkawi

Reading Committee:

____
Mohammed A. El-Sharkawi

____
Bruce M. Howe

____
Kai Strunz

Date: __________________________

University of Washington

Abstract

Infrastructure, Operations, and Circuits Design
of an Undersea Power System

Shuai Lu

Chair of the Supervisory Committee

Professor Mohammed A. El-Sharkawi
Department of Electrical Engineering

Natural processes in the oceans take place in an episodic or intermittent fashion: massive storms, submarine volcanoes, earthquakes, marine mammal feeding and hunting patterns, for example [1]. Traditionally, the oceans have been studied with ships, satellites, and instrumented moorings, all of which have been limited by time, space, power and communication capabilities. The NEPTUNE program will deploy a regional cabled ocean observatory on the seafloor of the northeast Pacific Ocean, enabling the continuous study of the ocean processes over this large region. This dissertation investigates the approaches to designing the NEPTUNE power system.

Located on the seafloor, the NEPTUNE power system poses a number of design challenges: it requires high reliability and compact sizes, cannot use commercial off-the-shelf components for power conversion and protection, lacks measurements to identify topology changes and to locate faults, and has no communications available to assist in the system startup. Solutions to these challenges are proposed in this dissertation.

First, a novel backbone circuit configuration aimed at increased reliability is described. Based on this configuration, the system operation modes are presented. An automated and coordinated protection scheme, which does not require dedicated communication capability between protection units, is presented. Then algorithms to detect an opened switch and to detect and locate a fault in an interconnected power network are proposed. Appropriate models and approaches for analyzing the various types of stability problems in a large scale dc power system are proposed or summarized. The operation design and implementation circuits for the branching unit system and the science node startup system are presented and their functionality is verified through lab tests.

With increasing research interest on the Earth's oceans, similar observatory systems will be needed and constructed. The solutions proposed in this dissertation address the typical constraints and difficulties in building power systems for this type of observatories. They may find more applications as scientists conceive methods to explore the ocean environment.

Table of Contents

Page

List of Figures

Figure Number Page

List of Tables

Acknowledgements

I would like to express my gratitude to my advisor, Professor Mohamed A. El-Sharkawi, for his support, patience, and guidance throughout my studies in pursuing my PhD. I was given the freedom of thinking independently, and encouraged to find innovative solutions to problems. I could not have fully understood what the essence of academic research is, otherwise.

I am also grateful to the engineers in the NEPTUNE power group, Dr. Harold Kirkham, Dr. Vatche Vorperian, Professor Bruce Howe, Professor Chen-Ching Liu, Tim McGinnis, Dr. Skip Kolve, and others. Working with them has been a good fortune to me. I saw how a large project was organized and operated effectively in a collaborative manner, and learned valuable engineering methodologies and knowledge from them. The work on the NEPTUNE power system was funded by the National Science Foundation grant OCE 116750, "Development of a Power System for Cabled Ocean Observatories".

I thank the members of my supervisory committee including Professor Kai Strunz, and Professor Mark Damborg for their help and advice on the research work and this dissertation.

My thanks also go to the graduate students in the Computational Intelligence Applications laboratory, David Krout, Patrick Ngatchou, Judy Klein, Anahita Zari, and others for their friendship and many interesting and good-spirited discussions that have affected my studies in some way. They have made working in the lab so much fun and enjoyable.

Thanks also to the many undergraduate students who have been working with me in the lab collecting information, designing and testing circuits, etc. The work has become a more joyful experience because of their participation.

Last, but not least, I would like to thank my wife Chunlian Jin, not only for her love, understanding, and support throughout the entire process of research and writing of dissertation, but also the information and comments she provided relating the technical details in my research. My parents receive my deepest gratitude and love for their dedication and faith in me, and allowing me to be however ambitious I am.

Dedication

To

My family

Chapter 1

Introduction

1.1 Background of NEPTUNE project

North-East Pacific Time-series Undersea Networked Experiments (NEPTUNE) observatory system is an underwater power and communications network for scientific experiments. It is proposed for the ocean floor of the Juan de Fuca tectonic plate in the northeast Pacific Ocean. NEPTUNE project represents a new generation of ocean research, which is based on the significant progress in electric power, underwater telecommunications and other related technologies. This section gives the background of the project.

1.1.1 Motivations

Scientific research on the world's ocean system is important in both providing us with a better understanding of the Earth and improving our life quality. Oceans occupy 70% of the Earth's surface and greatly affect global climate, biological diversity, geological activities, and many other global eco-system processes. Through the observation and study of the ocean system, natural hazards like hurricanes, earthquakes and tsunamis can be better comprehended, human's impact on the oceans can be evaluated, and natural resources in the ocean system can be managed and exploited for the long-term benefits of the human society.

The traditional way of doing ocean research has been an intermittent expeditionary mode. A ship is sent to a location of interest to collect data when environmental conditions allow. The time and space coverage of the information that can be collected is very limited. In contrast, ocean systems, complex and interactively dynamic, require us to understand their variation on many temporal and spatial scales. This need is compelling scientists to move beyond the expeditionary mode to building long-term ocean observatories, which enable the production of sustained time series data sets.

1.1.2 Types of ocean observatories

A. Mooring buoy

One type of ocean observatory is mooring buoys. It consists of buoys on the surface and junction boxes on the seafloor. The buoys are equipped with satellite communication ports and a power supply, either a generator or a large capacity battery. The buoys send continuous power to the seafloor junction boxes where the scientific sensors are operating, and transmit data back to shore via telecommunications satellites. It allows for real time data collection and transmission. However, finite battery life or limited fuel quantity for generators necessitates regular maintenance periods that constrain time and geographic scope of the observations. An example of this kind of ocean observatory (OceanNet) is shown in Figure 1.1 [2]. It was first deployed in August 2001 off the coast of Sardinia in the Mediterranean Sea at the depth of 2,300 m. It provides a 1Mb/s communication bandwidth between the observatory and shore. The fuel supply in the buoy lasts for seven months.

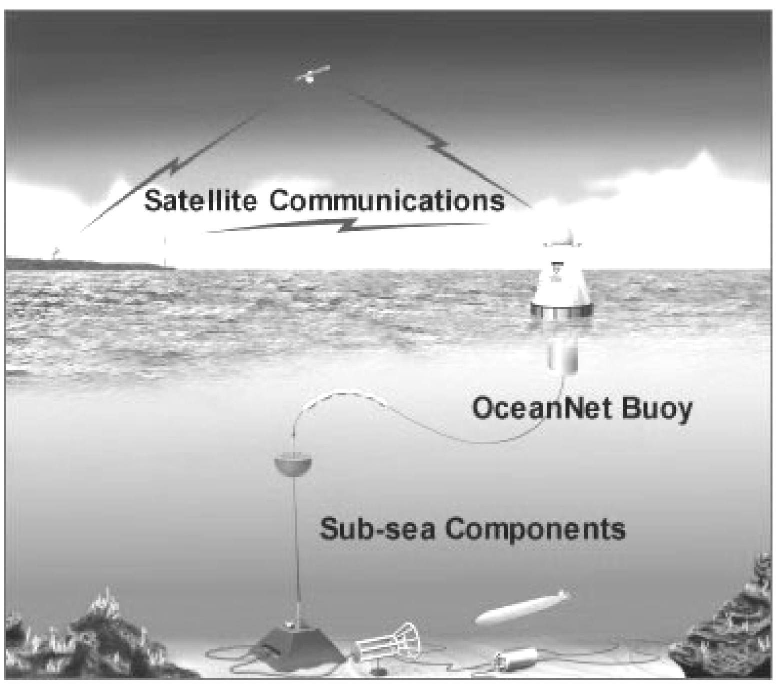

Figure 1.1 Schematic of OceanNet observatory

B. Cabled observatory

Ocean observatories can also be designed with a fiber optic/power cable connecting multiple science nodes on the seafloor to the terrestrial power system and communication network. This cabled observatory system can provide much more power in a "permanent" way and larger communication throughput to the science node research instruments than the buoy-type observatories. Using commercial-off-the-shelf (COTS) submarine telecommunication cables, hundreds of kW power can be sent to the observatories with up to 1Tb/s data bandwidth. Several experimental projects with a single node connected to shore through fiber optic/power cable have been built in the U.S., such as LEO-15 (Long-term Ecosystem Observatory), H2O (Hawaii-2 Observatory), and HUGO (Hawaii Undersea Geo-Observatory). A functional block diagram of the H2O system is shown in Figure 1.2 [3].

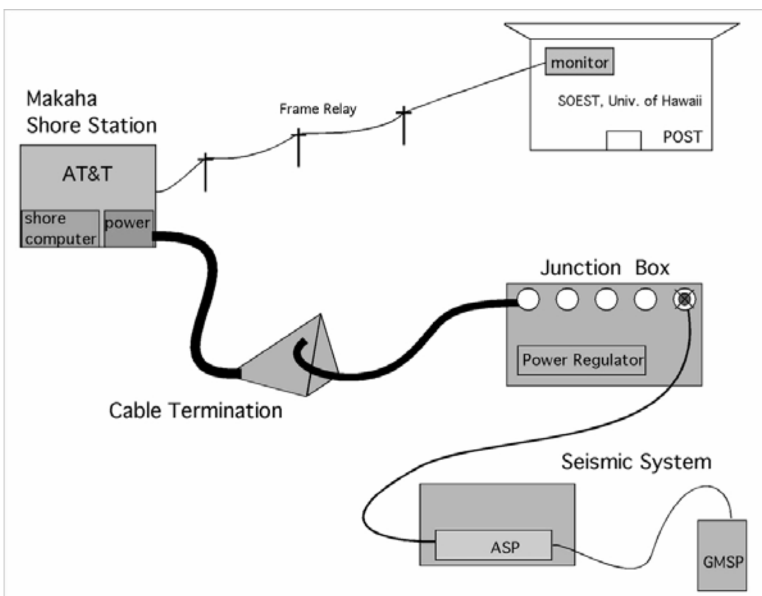

Figure 1.2 Functional diagram of H2O cabled observatory system

Presently, three cabled ocean observatory networks are being developed worldwide. They are NEPTUNE in North America, ARENA in Japan and ESONET in Europe. All are aiming to provide facilities for multidisciplinary ocean research with different priorities. Information regarding ARENA and ESONET can be found on their websites [4, 5], and will not be covered in this dissertation. One comparative observation, however, is warranted. Being designed independently and taking different tradeoffs, the configurations of the three systems have shown great differences in their most fundamental aspects. For example, NEPTUNE is using a parallel topology with constant voltage for power delivery, while ARENA is using a series method with constant current. While both topologies will work fine, they are determined by different design priorities. The detailed explanation of these differences can be found in [6].

1.1.3 Overview of NEPTUNE project [1, 7]

The NEPTUNE project will deploy 3,000 kilometers of fiber-optic/power cable on the seafloor encircling the Juan de Fuca tectonic plate beneath the Northeast Pacific Ocean. It will provide large amounts of power and an Internet communications link at distributed junction box nodes sited along the cable. Instrumented observatories connected to these nodes can remotely interact with physical, chemical, and biological phenomena in the ocean across multiple scales of space and time, while data flow in real time from instruments to shore-based scientists, educators, decision makers, and learners of all ages. Figure 1.3 shows the essential elements in the NEPTUNE system.

The NEPTUNE facility consists of two major subsystems: power and communication. The purpose of this thesis is to provide a solution to the NEPTUNE power system, including the infrastructure, operations, stability analysis and the design of some important subsystems, such as the branching unit and science node startup system.

1.2 Engineering challenges in the NEPTUNE power system design

The NEPTUNE project raises many engineering challenges being the world’s first large scale undersea cabled observatory system [8]. Those related to the design of the NEPTUNE power system are summarized in the following.

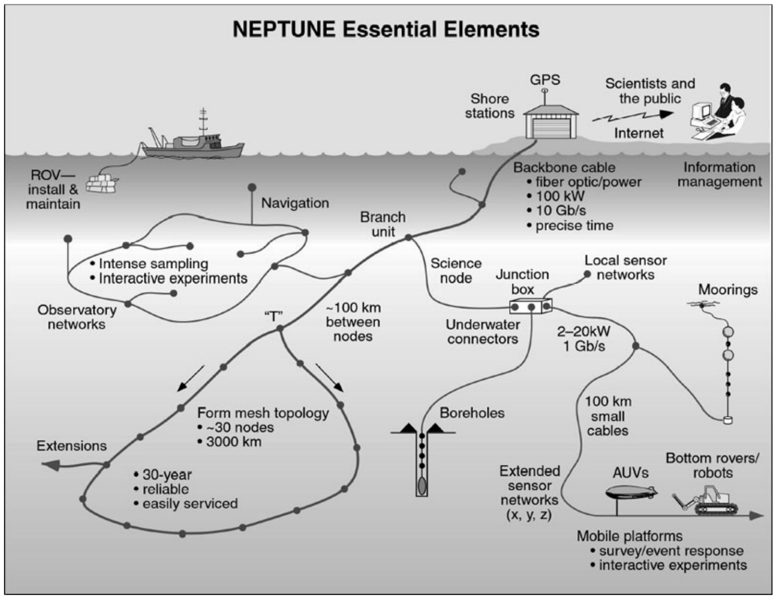

Figure 1.3 Essential elements in the NEPTUNE cabled observatory system

1.2.1 Location on the seafloor

A. Reliability

The location on the seafloor of the system makes it very difficult to access the hardware after installation. The system must be highly reliable to reduce the need for costly repairs. The system should also be maintenance free so that no replacement or service of components on a regular basis is needed. The impact of this constraint on system circuit design is, for example, that the use of a battery to supply auxiliary power on the seafloor is excluded, although it is a normal way to start a power system or to have a power supply backup in many other cases. An alternative to get a low voltage power supply to start the system on the seafloor must be found. The approach proposed by this dissertation is described in Chapter 5.

B. Size

NEPTUNE will take advantage of the submarine telecommunications technology for its backbone construction [9]. The standard branching units (BU) are slightly modified to provide housing for power switching and fault isolation devices [8]. Therefore, the size of the switching components in the BUs is limited. Oversized circuit breakers, high voltage capacitors, etc., which are commonly seen in a switchyard of a terrestrial power system, can not be used. Innovative approaches for power switching and fault isolation must be developed. The proposed solution can be found in Chapter 2 and Chapter 3.

C. Communications for operating the power system

The operation of the power system consists of multiple modes. Because the NEPTUNE power system should start functioning before the communication system, it must be autonomous so that the right operation mode can be identified at every science node. A novel power system design idea, which uses different voltage levels for various operation modes, is adopted in the operation design. In other words, the system voltage is used as a communication signal to recognize different operation modes. The design details are described in Chapter 3. The circuits for the BU system and science node startup system to carry out the designed operations are presented in Chapter 5.

1.2.2 Large scale dc power network

The NEPTUNE power system will be dc and parallel (the reasons for which are found in Chapter 2). Although dc power delivery systems have been used in various forms for a long time, they have never been operated before as interconnected networks [10]. Several issues must be solved in the design of the NEPTUNE power system:

A. Power conversion component

Dc power systems use dc-dc converters to step down the voltage from transmission level to distribution level, just as transformers function in ac power systems. Implementation of the NEPTUNE power system requires the development of a voltage-sourced dc-dc converter residing in the seafloor nodes and capable of operating at 5 to 10 kV range at several kW power level. COTS converters of this type do not exist [9]. The converter for NEPTUNE was developed by the Jet Propulsion Laboratory (JPL) at the California Institute of Technology and is briefly described in Chapter 5.

B. Protection device and scheme

Devices to interrupt dc fault current at 10 kV do not exist. Circuit breakers used in ac systems might be derated and used in the dc system. However, both the requirement for maintenance and the size of the circuit breakers are unacceptable for NEPTUNE (refer to Section 1.2.1). A dc circuit breaker that could interrupt load current has been developed in the Electrical Engineering Department at the University of Washington [7]. The current limiting capability at shore stations is utilized to work together with the dc circuit breaker to isolate a fault in the Version 1 design of the NEPTUNE power system. Based on this fault isolation approach, a current differential protection scheme was adopted in the Version 1 design [11]. However, because the Version 1 design requires low voltage power and communication capability in the BUs, which in turn depends on the availability of the connected science node, the backbone reliability is impacted by the performance of every science node. Further, because the current is limited by the shore stations during a fault, the backbone voltage close to the fault will drop to below the science node converter threshold voltage. Therefore, these science nodes may not be able to provide the power and communications required by the current differential protection scheme. To solve these problems with the Version 1 design, a Version 2 design was developed. In Version 2, an innovative fault isolation approach is adopted. This approach requires neither fault current interruption devices nor communication capability. The BUs can work independently of the science nodes. The details of the approach are found in Chapter 3.

C. Topology error identification and fault location

Topology errors in the NEPTUNE power system can be caused by unknown status change of the backbone switches. The changes should be identified for the system to have an accurate control over system loads. Similar problems exist in terrestrial power systems, for which various approaches have been proposed [12]. A common property among most of these approaches is to look at the state estimation residual. Schneider studies the characteristic of how the residual increases with the system voltage level when topology errors exist in the NEPTUNE power system [13], which provides an approach to detect falsely opened BU switches. The drawback is that the approach requires system voltage be varied in the normal operation mode to generate data, and the calculations are complex. Based on the assumption that only one switch status error exists any time in the NEPTUNE power system (considering the system only has 30 to 40 cable sections), a simpler approach is proposed, which can identify the topology error by analyzing the value of the residual vector.

Faults in the NEPTUNE cable system must be located automatically with good accuracy from shore for the convenience of repairing. Fault location is particularly important considering the NEPTUNE system's location on the seafloor and its network topology. This type of problem also exists in terrestrial power systems. However, because NEPTUNE is a dc system and there are not enough measurements available on the backbone, usually required by the ac system fault location techniques, an approach to locate a short circuit fault in the NEPTUNE system must be developed. In Chapter 3 this new approach, based on combined state and parameter estimation with the weighted least square (WLS) method, is presented.

D. Stability

The NEPTUNE power system consists of a large number of power electronic converters. These converters are connected to the shore stations through long distance undersea cables up to several thousand kilometers. The power electronic converters maintain constant power output regardless of the input voltage variations. This property introduces potential stability issues to the system. The effect of this property on a dc power system's small-signal stability has been intensively investigated. Small-signal models of the switching power converters were developed [14-17]. An impedance criterion was established [18]. Many impedance specifications for system stability have been proposed [19-21]. For large-signal stability study (which is necessary because of the nonlinearity in power sources, converter controllers, etc.), the model of converter switches given by [22, 23] and the model for current mode controller given by [17, 24, 25] and many other variations can be used in time domain simulations. All these approaches can be adopted in the stability study for NEPTUNE.

However, because the objective dc systems faced by the previous researchers were small scale systems from computer systems to space stations, no long distance cables were involved. An additional aspect of the stability issue induced by the long cables is steady-state stability, which is similar to the voltage stability concept in terrestrial power systems. The approaches to study this aspect are discussed in Chapter 4 for the NEPTUNE power system. Methods and circuit models for small-signal and large-signal stability analyses are summarized. The simulation results from large-signal power converter models match well with the results from lab tests. Therefore, the models can be used to study the stability of the entire NEPTUNE power system.

1.3 Organization of dissertation

In this dissertation, detailed solutions and algorithms for various design aspects are covered, including the NEPTUNE power system infrastructure, operations, stability analysis and circuit design for some important subsystems.

The chapters are organized as follows:

Chapter 2 addresses the most basic issues in the NEPTUNE power system infrastructure design, such as the voltage and current level, ac or dc, series or parallel topology, protection scheme, etc.

Chapter 3 discusses the operation modes designed for NEPTUNE, including system startup, fault isolation, fault location and related algorithms.

Chapter 4 investigates types of stability issues in NEPTUNE. Study approaches and appropriate circuit models for each type of stability analysis are either proposed or summarized.

Chapter 5 describes the circuit designs for some important NEPTUNE subsystems, including the branching unit and the science node startup system.

Chapter 6 presents the test results for the designs in Chapter 5.

Chapter 7 summarizes the contributions of this dissertation.

Chapter 2

Infrastructure

The power system infrastructure design for an ocean observatory system has particular constraints resulting from the system's location on the seafloor. These constraints require a unique power delivery approach compared with traditional terrestrial power system designs. The NEPTUNE power system design incorporates the fundamental aspects of voltage and current level, ac or dc source, system topology, and protection schemes. This chapter compares options in order to find an optimal solution which would enable the NEPTUNE power system to operate reliably over a 25-year lifetime in its particular environment and at a reasonable cost.

2.1 Design requirements

It is critical to consider a number of unique requirements of the NEPTUNE system infrastructure, which is driven by the needs of the scientific community. Top-level scientific requirements were developed through an iterative design process carried out by an interactive team of scientists and engineers [26]. In summary, the requirements include:

1) Lifetime: the cabled observatory shall meet all scientific requirements, with appropriate maintenance, for a design life of at least 25 years.

2) Cost: the cabled observatory shall be designed to minimize costs over the projected 25 year life span.

3) Controllability: the cabled observatory shall allow resources to be dynamically directed where scientific needs and priorities dictate.

4) Flexibility: the cabled observatory shall be expandable to facilitate the implementation of additional science nodes which meet the observatory reliability goals. These additional nodes can be placed at or near locations of interest that may develop in the future.

5) Upgradeability: the cabled observatory shall be upgradeable to accommodate future technological improvements.

6) Reliability: the primary measure of cabled observatory reliability shall be the probability of being able to send data to/from any science instrument from/to shore and/or from/to other science nodes, exclusive of instrument functionality.

7) Future casting: the cabled observatory shall have functionality and performance significantly beyond that required to support current use scenarios so that experiments and instruments that may reasonably be anticipated to develop over the expected life of the facility can be accommodated.

Guided by these requirements, the NEPTUNE power system design follows the principle of maintaining simplicity, reliability, and expandability at a limited cost. Commercially available high quality parts and equipment will be considered in order to achieve a high level of reliability and reduce development costs. These principles are applied throughout the design process, starting from the three very basic components of a power system: power source, delivery system and user interface. The components are described in Section 2.2.

2.2 NEPTUNE power system components

The NEPTUNE system is proposed to reside on the seafloor encircling the Juan de Fuca tectonic plate beneath the northeast Pacific Ocean. The proposed topology of the cable system is shown in Figure 2.1. There will be two shore stations: one on Vancouver Island in Canada, and the other on the Oregon coast of the USA. Three major components of the NEPTUNE power system will be the power source, delivery system and user interface. These components are described in the following.

1) Power source

The NEPTUNE system will be powered from shore stations which convert utility power into a form and level suitable for transmission by the delivery system. This method is more reliable and offers lower operating costs than using on site power supplies, such as fuel cell batteries and underwater nuclear power plants. The peak power output of each shore station is about 100 kW, including the total load plus the losses over the delivery cables.

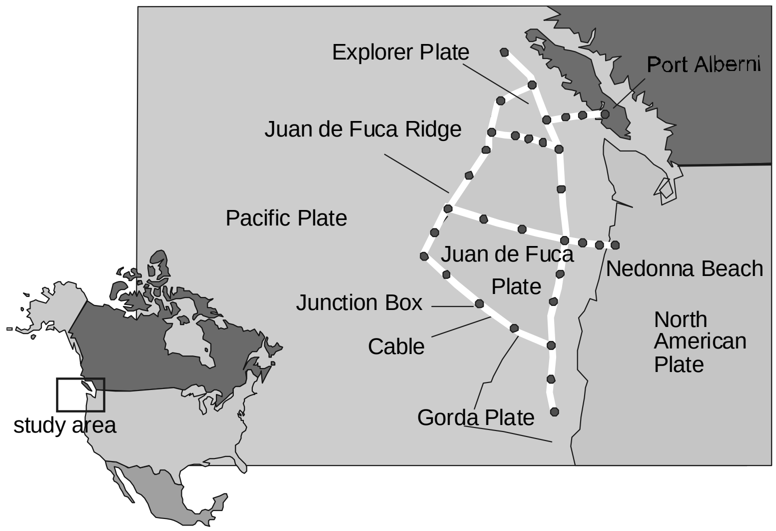

Figure 2.1 NEPTUNE cable system diagram

The shore stations will also have a control center to monitor and control loads via the communications system and user interface. Data on power usage by scientific instruments will be sent to the shore stations and analyzed for control purposes.

2) Delivery system

The delivery system will utilize submarine telecommunications cables to transmit both data and electric power. Submarine cables for the telecommunications industry have experienced over a hundred years of development, which has resulted in highly reliable COTS products. The design requirements for an ocean observatory cable, where data and power are to be delivered and distributed on a submerged network, are very compatible with the standard capabilities of telecommunications cable. An example is shown in Figure 2.2.

The NEPTUNE cable system will consist of a backbone network covering the entire service area, and spur cables reaching specific sites/science nodes. The backbone network will be comprised of 3000 km of cable connecting about 30 evenly distributed BUs. Each cable section will be less than 100 km. The dots in Figure 2.1 show the approximate locations of BUs. These BUs can be viewed as the switching yards in a terrestrial power system, while the power supplies in the shore stations can be seen as the generation units. When there is a cable fault, a protection scheme is carried out by the BU circuits with the coordination of shore stations to isolate the fault and minimizes the loss of science nodes. Science nodes are connected to the BUs through spur cables. The length of the spur cables can also be as long as 100 km, so that positions with some distance from the backbone can be accessed by the scientific instruments.

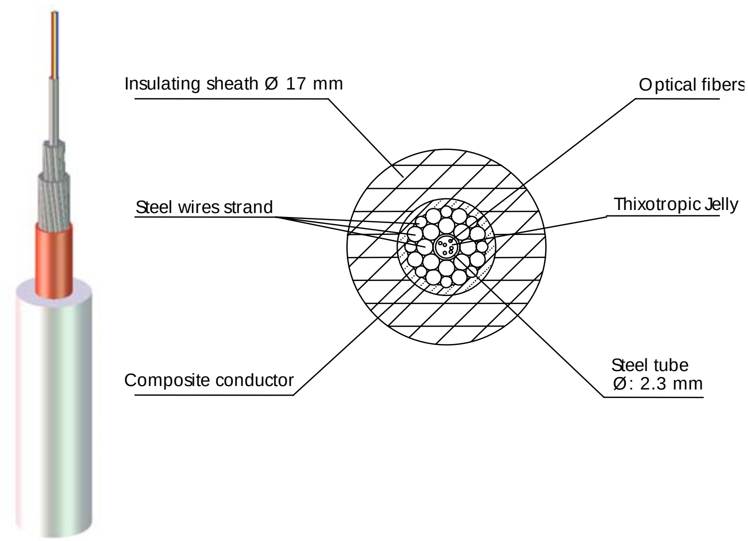

Figure 2.2 Proposed cable for the NEPTUNE system

3) User interface

User interfaces will be implemented in the undersea science nodes sited along the backbone power delivery network. Low voltage power output including 400 V and 48 V converted from the delivery voltage level is provided to the scientific instruments, as well as the data ports. Voltage at 48 V is a common standard, delivering moderate power at low current. 400 V is selected for users who require more power or who wish to transport over large distances.

Science loads will be controlled and monitored through the power controllers in the science nodes. The control center located at the onshore stations will communicate with the power controllers to perform load management tasks and thus form the power monitoring and control system (PMACS). In the event of a fault caused by a science load failure, the load will be isolated by PMACS and local protection circuit at the science node.

2.3 Fundamental aspects

Some fundamental aspects associated with a power system design include voltage and current rating of every part of the system, system topology, and ac or dc source. The optimal configuration will be determined based on a variety of considerations, such as technology availability, economics, reliability, and operation constraints. These fundamental design features of the NEPTUNE power system are addressed in [27] and are summarized in the following.

1) Voltage and current rating

Higher voltage can help reduce power delivery loss; however it is limited by the insulation levels of power supplies, cables and loads. The typical value for undersea telecommunication cables is 10 kV. These values will therefore be adopted in the NEPTUNE system, since cables are to be chosen before power supplies and loads. The current level is determined by considering the voltage level, power to be delivered and cable resistance. The resistance of the cable is around 1 Ω/km. With a large current, the cable voltage drop can approach its voltage rating in a few hundred kilometers. Hence, a current rating of 10 A is set for the backbone cables. However, the current rating is more of a reference value in NEPTUNE than being a constraint. The real current in the power delivery cables is determined by the load level in the system. As long as the system has enough stability margin (see Chapter 4, Stability Analysis), the operation is safe, because the thermal limit of the cables is much higher than the stability limit.

2) Power capacity

The total power capacity of the network will be 200 kW provided by two shore stations. Each of them is capable of providing 100 kW (10 kV at 10 A). A redundant power supply will be placed in each of the shore stations for backup.

3) Series or parallel

In a submarine telecommunication network, series connection of the sources and loads is used with a constant current flowing through. Since the spatial scales are similar, it should be viable for NEPTUNE. However, the loads in the two systems make a big difference. The loads in the NEPTUNE power system include scientific equipments, such as ROVs and under water drills. These equipments require a relatively large amount of power that is distributed irregularly over time, as compared with the loads of repeaters in a telecommunication network. Providing the scientific instruments with as much power as possible is a goal of the NEPTUNE power system. Thus, a more efficient method to deliver electric energy is preferred. Because the current decreases along the backbone cable of a parallel system, the I^2R loss in the delivery cables will certainly be less than in a series system with a constant current. Therefore, more power can be provided to loads along the same length of cable. This analysis leads to the choice of a parallel delivery scheme.

4) Ac or dc

In terrestrial power systems, electric power is mostly in the ac form. Ac power offers several advantages compared to dc. First, it is easier to raise voltage levels using transformers. Second, protection devices to interrupt fault current use natural zero crossing points with ac. Third, because the ac voltage across the insulation materials switches polarity in every cycle, charge trapping and charge migration problems accompanying dc voltage do not exist. However, because the cable capacitance is much larger than the overhead transmission lines in a large cable system, using ac will lead to unacceptable charging current. The shunt capacitance of a 100-km section of telecommunications cable used in NEPTUNE is about 0.2 μF/km, or 130 Ω at 60 Hz. The charging current at 5 kV ac will be 38 A. Although the problem can be solved by inserting compensation inductance, it is too expensive when considering both the materials and installation costs. Additional analysis shows that the electric field at 10 kV is very safe for the cable insulation, even under dc. Changing dc voltage level and interrupting dc fault current can be solved by applying modern power electronic techniques and proper system operation design. Therefore, dc is chosen for the NEPTUNE power system.

5) Current return path

The power delivery network will use a single conductor cable and the ocean will provide the return path for the current. There will be a sea electrode in every science node on the seafloor and a ground electrode at each shore station.

6) Voltage polarity

The undersea electrodes at the science nodes need to be at a positive potential compared to the cable input to avoid electrolytic corrosion, particularly from the chlorine in the seawater. Hence, the voltage of the shore station will be negative with respect to the seawater return.

7) Voltage output at science nodes

At each node, a dc-dc converter will be used to reduce the incoming voltage from 10 kV to 400 V. Another 10 kV converter will serve as a cold standby. Multiple low voltage dc-dc converters will produce additional 48 V outputs from the 400 V bus for the scientific instruments that require a lower voltage. Other low voltages will be generated for the internal loads to perform control and monitor functions.

2.4 Protection scheme and circuit architecture

The task of power system protection is to remove the faulted part, a load or a cable section from the system, in such a way that the remaining parts of the system will not be affected. Load faults in the NEPTUNE power system will be isolated locally at the science nodes. Therefore, the reliability of the entire system will not be compromised. The protection scheme handling faults on the power delivery cables has a much larger effect on the whole system availability, and it is also an influential factor in the power system circuit architecture design.

The protection design in the NEPTUNE power system began with a protective relaying scheme similar to the terrestrial power system protection. A different protection scheme was brought forward to mitigate reliability concerns. The two designs with related circuit architectures are referred to as Version 1 and Version 2 designs, respectively.

2.4.1 Version 1 design

In Version 1, the backbone cable is routed to the science node through passive BUs commonly used in submarine cables (Figure 2.3). The BU in this design has no switching elements and is used only as a junction box. The power is delivered to the node using two spur cables. Besides the dc-dc converters and communication circuits, the node also contains switching devices (circuit breakers) for connecting two cable sections and isolating cable faults. The switching devices locate in the science nodes because of their dimension and power requirement. The operation of the switching devices obtains power from the dc-dc converters in the science nodes. Therefore, the integrity of the backbone cable network is dependent on the dc-dc converters in each science node.

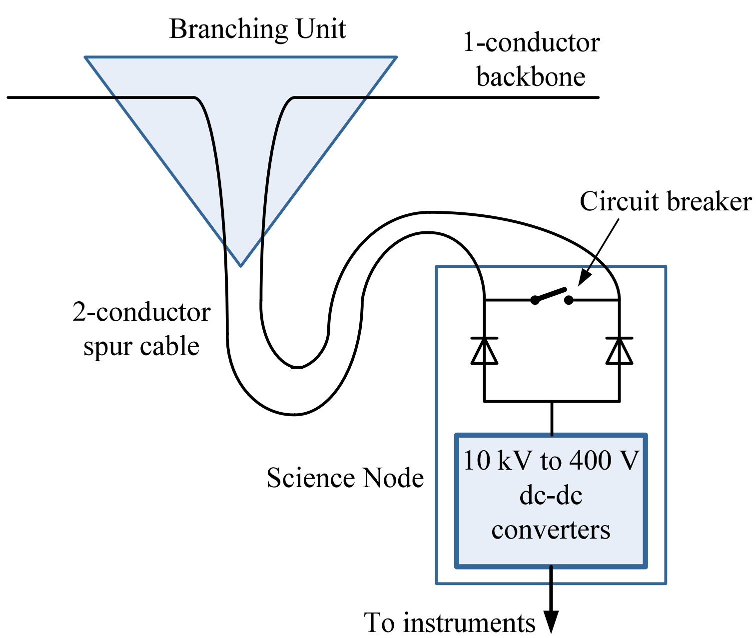

Figure 2.3 Connection between the backbone and science nodes in Version 1

When a cable fault occurs, the first line of defense is current differential protection. A comparison of the current input and output of a cable section is performed via the communication between two adjacent science node power controllers. Distance relaying is used as a backup to the current differential protection. Parameters such as cable length and resistance per kilometer are stored in science node controllers. The voltage and current at the end of a cable section is measured and the ratio of them is used to estimate the distance from the node to the fault. This distance is compared with the cable length to determine if the fault is in the node's protection zone.

Because there is no natural zero crossing in dc voltage, a specially designed dc circuit breaker is developed to be used in the science nodes. The breaker is composed of several elements that force a current zero in the isolation switch by diverting the electrical energy to a storage capacitor. With parameters designed properly, arcing and restrikes can be substantially reduced or eliminated when interrupting fault current [7]. Therefore, contact damage on the switches in the breaker can be largely alleviated. Maintenance, which is usually necessary for ac circuit breakers, should not be an issue for a long period.

2.4.2 Version 2 design

In Version 2, active BUs are housing the switching devices and their control circuits. The connection between a BU and a science node is shown in Figure 2.4. The dc-dc converters and the communication circuits are located in the science nodes. The node is powered through a single conductor spur cable from the BU.

In this active BU system, the power of the BU controller is tapped directly from the backbone cable instead of from the science node converters. The fault isolation approach is different from that in the Version 1 design. In Version 2, when a fault occurs, the fault current is limited by the shore stations and the entire NEPTUNE system goes into a mode at a much lower voltage and current level. The switches in the related BUs are then opened to isolate the fault. All the science loads are dropped during this process. However, the advantage is that the BU switches are not required to interrupt a large dc current. A fault is isolated by opening switches at a very low voltage. Thus, simple vacuum switches can be used instead of complicated dc circuit breakers.

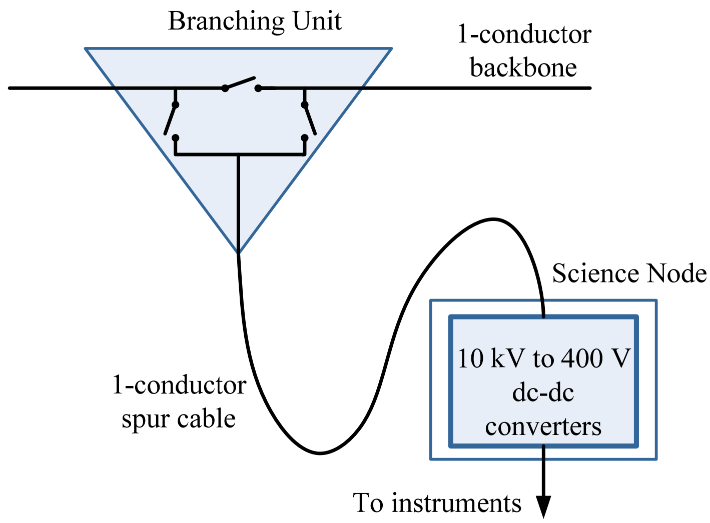

Figure 2.4 Connection between the backbone and science nodes in Version 2

The Version 2 design is based on the fact that faults in submarine cables are rare and will likely only happen a few times over the design lifetime of the project (25 years). Most of the cables are in deep water where faults due to fishing accidents or anchoring are virtually nonexistent. If a fault occurs, dropping the entire system loads is justifiable, provided that the isolation of the fault can be done in a short time.

2.4.3 Comparison of the two designs

There are several merits and demerits for each of the two designs. The key comparative features are shown in Table 2.1.

Through the comparison, the Version 2 design is shown to provide a more reliable backbone system that is immune to science node failures. Additionally, because fault current is not interrupted inside the BUs, the switching circuit for isolating cable faults is much simpler than in the Version 1 design. The tradeoff is that a single fault will bring down the entire NEPTUNE system and it takes longer for fault isolation. This is considered tolerable based on the assumption that faults will be very rare for the deep sea cables. Therefore, version 2 design looks more promising and is adopted by the NEPTUNE power group.

Table 2.1 Comparison of key features in Versions 1 and Version 2 design

Version 1	Version 2
All backbone circuit breakers depend on science nodes to operate. A single node failure (either dc-dc power converters or communications to the node power controller) can possibly cause failure to large sections of the network.	The backbone's integrity does not depend on science nodes. Any node failure (power or communication) has no impact on the operation of the remaining part of the system.
Fault current is interrupted by the node circuit breakers on the seafloor. Arcing and restrikes must be prevented to avoid maintenance.	Fault current is limited at the shore stations. Arcing and restrikes are avoided for the switches in the sub-sea system.
Two conductors in the spur cable are used, which implies a higher cost.	Single spur cable is used. It is a cheaper option.
There is communication between nodes, and between nodes and shore stations. Hence, the breakers connecting backbone cable sections can be fully controlled by the system operator.	The switches connecting backbone cable sections are contained in BUs, which do not have communication links. The operation of the switches in the BUs must be autonomous.
A cable fault will be isolated by circuit breakers. The remaining part of the system will not be affected or shortly affected, depending on the speed to interrupt the fault current.	A single cable fault leads to the lost of all science nodes before it is isolated. The isolation of the fault requires system wide change of operation mode, and it takes a much longer time, in the scale of minutes.

While Version 2 brings higher system reliability, it poses more challenges to the system operation and circuit design, which can be seen from the last two points of the comparison in Table 2.1. Circuits in BUs must carry out the tasks of connecting the system or isolating faults in the absence of communications. System operation modes must accommodate the particular fault isolation approach. The solution to these difficulties will be discussed in Chapter 3.

2.5 Summary

In this chapter, some fundamental aspects in the NEPTUNE power system design were discussed, including the main components, ac or dc form, voltage and current level, and parallel or series topology. Two versions of backbone circuit architecture and related protection schemes were compared. The comparison between them showed advantages of the design that is adopted and is the basis for the other aspects of the power system design.

Chapter 3

System Operations

System operation design focuses on how and through what procedures the NEPTUNE power system starts up, meets the power demand of loads, responds to disturbances, and shuts down when needed. Over the course of the last 100 years, these procedures have been thoroughly studied and developed for terrestrial power systems. They are valuable models from which the design of the NEPTUNE power system can borrow both ideas and practices. However, some fundamental aspects of the NEPTUNE power system, from the type of power source to circuit architecture, are quite different from those in a typical terrestrial power system. Therefore, the operation design for NEPTUNE requires new concepts to be developed to meet the particular constraints. The design is discussed in this chapter.

Chapter 3 is organized as follows: the operation mode design at the system level is first introduced; then the details regarding BU operations are explained; finally, as key aspects of the operation design, the fault isolation approach is discussed and fault location algorithms are proposed.

3.1 System operation modes

The NEPTUNE power system is similar to its terrestrial counterpart in the classification of operation modes. Operations in a terrestrial power system can be categorized into several groups such as normal operations, emergency operations, and system restorations, each corresponding to the various states of the system. The transition that takes place from one state to another is essentially incurred by faults (large disturbances) in the system. Similarly, based on the Version 2 design described in Chapter 2, the operations in the NEPTUNE power system are classified into four modes depending on the system fault condition: startup/restoration, fault location, fault isolation and normal mode. The transition between system modes is shown in Figure 3.1.

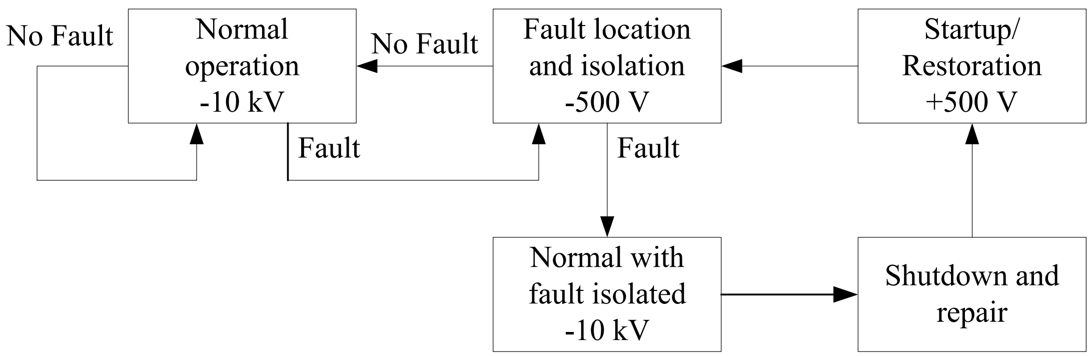

Figure 3.1 NEPTUNE power system modes transition diagram

3.1.1 Operation modes of the NEPTUNE power system

During startup, all the switches in the BUs are closed so that the NEPTUNE cable system is fully connected. This operation is the same as the system restore action after a faulted cable is repaired. Therefore, it is named the startup/restoration mode.

A fault may exist during system startup or after restoration (i.e., a new fault is developed). The shore stations make measurements of currents and voltages to locate the fault. Once the required measurements are collected, the system goes into a coordinated fault isolation mode, which involves all BUs and the shore stations, to isolate the faulted cable section. This is the fault location and isolation mode. After this, the system is brought back to normal mode.

In the normal mode, all system variables are within the normal range and no cables or science nodes are overloaded. The shore stations perform monitoring and control of system loads (power usage of various scientific instruments) by communicating with power controllers in the science nodes. The backbone node voltages and currents fluctuate when loads vary. If any node voltage becomes too low, the system could face voltage collapse and shut itself down. Therefore, the voltage profile of the delivery network must be maintained within allowable limits (This will be further discussed in Chapter 4 regarding stability issues.) Heavy load is the usual cause of voltage profile problems. The solutions include adjustment of the voltages at the shore stations and load shedding. These functions are performed in the normal mode as part of the PMACS operating in the science nodes and the control center in the shore stations. The functional block diagram of PMACS is shown in Figure 3.2 [28].

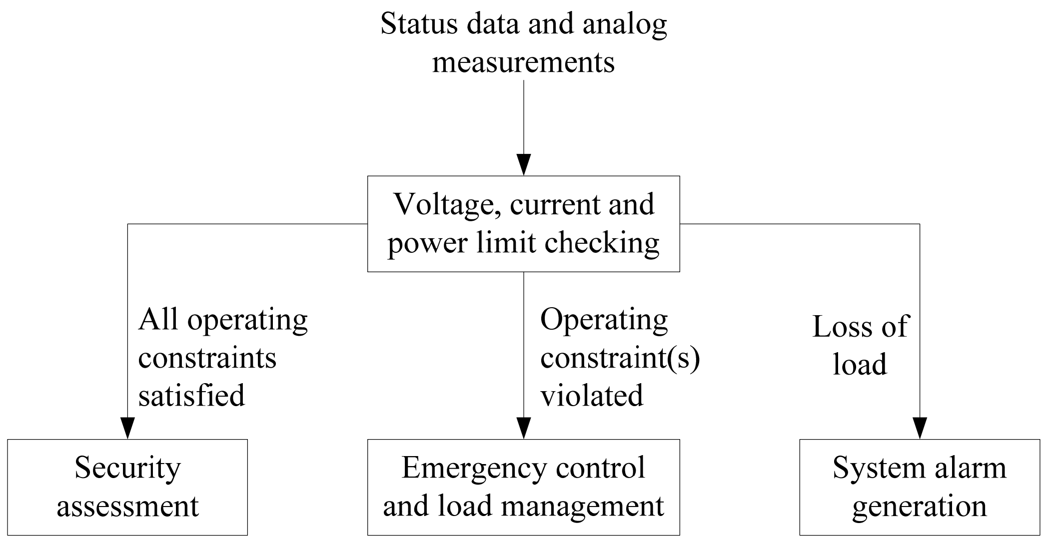

Figure 3.2 Functional block diagram of PMACS

If a severe fault occurs in the normal mode, which brings down part or all of the science nodes, the shore stations will decrease the system voltage and the backbone current will be limited to below 10 A. The system enters the fault location and fault isolation mode, similar to the one after the startup/restoration mode. After the fault is isolated, the system returns to normal mode with the faulty cable isolated. After the faulty cable section is repaired, the whole system starts in the startup/restoration mode and reconnects the repaired cable section.

3.1.2 Differences between NEPTUNE and terrestrial power systems

The operation sequence in Figure 3.1 is different from that in a terrestrial power system in two main aspects. The status transition diagram for a terrestrial power system is shown in Figure 3.3 for comparison.

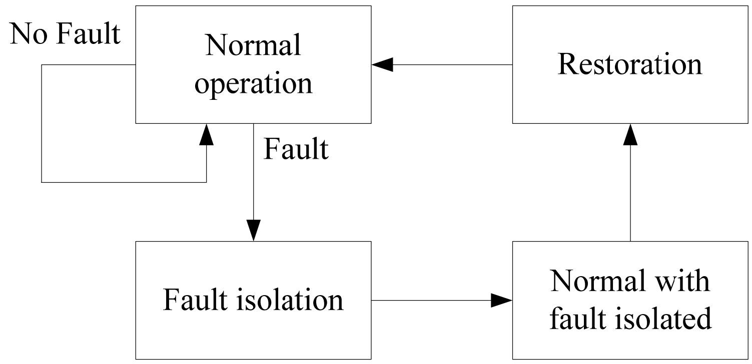

All operations are at regular voltage.

Figure 3.3 Status transition diagram of a terrestrial power system

The first key difference is the fault isolation approach in the power delivery network. In a terrestrial power system, the network is connected through circuit breakers. When a line fault occurs during normal operation mode, the relay protection circuit operates immediately to isolate the fault by opening related circuit breakers. The location of the fault is then determined and a repair crew is dispatched. In NEPTUNE, the relay protection system requiring immediate fault current interruption capability is not adopted, because such a protection scheme would be dependent on the science node converters. Hence, the overall system reliability would be compromised. Vacuum switches require less power to operate and occupy less space compared with circuit breakers. Therefore, they are used in BUs for the connection or isolation of cables. When a cable fault is detected, the fault isolation process is carried out after the shore station voltages are lowered to below 500 V and the backbone current is limited to within 10 A (a power level safe for operating vacuum switches). Details about the fault isolation approach are described in Section 3.3. The detection of fault and fault location algorithms are discussed in sections 3.4 through 3.6.

The second difference exists in the voltage levels at which the system operations are performed. The NEPTUNE power system has multiple voltage levels, while in a terrestrial power system all operations are carried out at about the system's nominal voltage. This difference results from the method in which BUs coordinate with the shore stations. The counterparts of BUs in a terrestrial power system are substations.

Commands from the system operator and data collected by the substations are exchanged via communication lines between the substations and the control center. In NEPTUNE, however, BUs have no communication capability. The operation mode in the BUs (see details in Section 3.2) has to be determined in the absence of communications. The solution adopted here is to use the backbone cable voltage as an information carrier: +500 V and -500 V are used as the commands to restore cable connections and isolate faults, respectively; at -10 kV, a voltage level for normal operations, all BU switching actions are inhibited. Therefore, different voltage levels in the shore stations means different system operations are intended.

3.2 BU operations

BU circuits coordinate with the shore stations to carry out the operations described in Section 3.1. The functions of BU circuits can be summarized as follows:

1) To connect the backbone and spur cables by closing switches;

2) To isolate faulted backbone or spur cables by opening switches.

The operation of the BUs focuses on how to implement these two functions. The process includes the following steps and is illustrated in Figure 3.4.

1) After the shore stations energize the cable with +500 V, all backbone and spur cable switches are closed during t_1, which should be long enough for all the BUs in the network to act.

2) After the startup/restoration mode or when a fault occurs, the shore stations are applied with low negative voltages of below 500 V. Upon seeing this voltage, a delay of t_2 is imposed on the BUs to allow time for fault location measurements taken in the shore stations. After t_2, any spur cable with a fault is immediately isolated. The delay time t_2 is identical in all BUs.

3) At the end of time t_2, the protection circuit that will isolate backbone cable faults is activated. Another delay of t_3 is initiated. After t_3, any faulted backbone cable is isolated.

4) Following a suitable further delay, the shore stations can raise the voltage to the level required for normal operations.

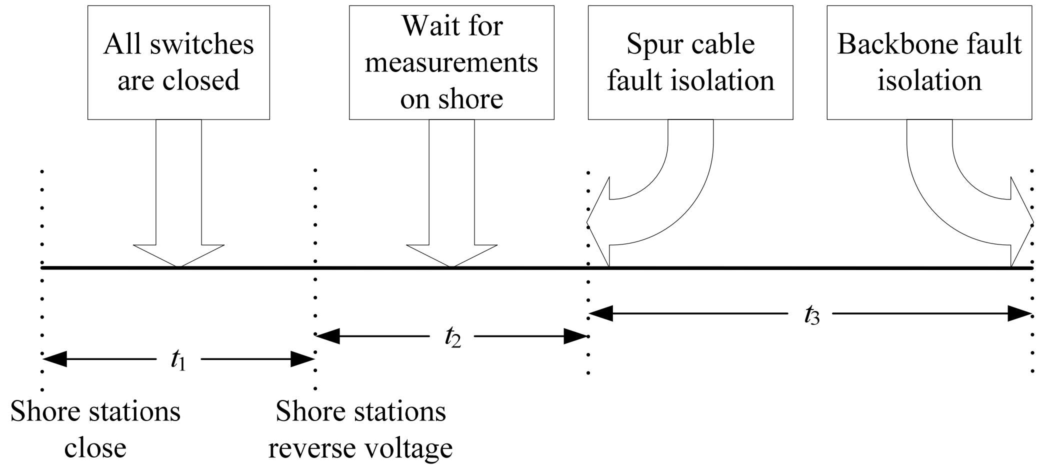

Figure 3.4 BU operations timing chart

3.3 Fault isolation

Fault isolation is carried out by switches inside the BUs at the times described in Section 3.2. Details of the approach are explained in this section.

3.3.1 Isolating a spur cable fault

As shown in Figure 3.4, spur cable fault is isolated at the end of time t_2. The fault is detected by looking at the current in the spur cable. With the system voltage being -500 V, the dc-dc converters in the science nodes remain unstarted. Any current flowing in the spur cable indicates the existence of a fault on that cable or the connected science node. The related BU opens the switches connecting the backbone and the spur cable upon detection of such a current.

3.3.2 Isolating a backbone cable fault

The controller in each BU uses an isolation algorithm that is triggered at the end of t_2 to determine if any switching action is needed to isolate a backbone fault. The algorithm, which may be implemented in hardware rather than software, is simply to trip the corresponding switches at a time determined by the voltage measured at the BU, as in (3.1), where v is the BU voltage and c is a positive constant.

$$t_3 = c \cdot v \tag{3.1}$$

For BUs A and B, for example, if $v_A > v_B$, then $t_{3A} > t_{3B}$. Thus, the BU closest to the fault, which has the lowest voltage in the system, will trip first. After the two BUs at both ends of the faulty cable section open their backbone switches, the faulty cable will be isolated from the network. The fault current is ceased and the backbone voltage goes up to the shore station level. Seeing the above changes as a signal suggesting that the fault has been cleared, the other BUs will stop their timers from counting and inhibit any further actions.

If a BU closest to the fault fails to open its switches, the neighboring BU will act as a backup, because it has the next shortest trip time. Also for this reason, the difference of the trip time between two neighboring BUs should be large enough so that the uncertainty in the timing process and switch operation time will be negligible. This can be achieved by carefully designing the constant "*c*" in (3.1).

The BU circuit needed to implement the above operations will be described in Chapter 5.

3.4 Detection of opened BU switches and high impedance faults

Abnormal events that may occur to the NEPTUNE power system include BU switch malfunction (mainly falsely opened), cable faults (which also result in opened BU switches after fault isolation) and load faults. Load faults can be identified by science node controllers monitoring the power usage of each connected scientific instrument, and then are isolated by opening the load switches. No coordination between BUs are needed. Switch malfunctions and cable faults, compared with load faults, are more difficult to deal with. Examples of switch malfunctions in the BUs and the cable faults are shown in Figure 3.5. They can only be detected from shore stations and corrected through BU switching operations [29].

If the switches connecting a science node and the backbone are falsely opened, as shown in Figure 3.5 (a), the science node will lose communication with the shore stations, thus it can be easily detected and the operation of the rest of the system is not affected.

When a cable fault is severe (the cable is grounded through low impedance) as in Figure 3.5 (c), multiple science nodes, or even the entire system may be put out of service. The voltages of the BUs close to the fault will drop to below the converter threshold, or the backbone current will exceed the limit. In either case, the measurements at the science nodes can no longer be sent to the shore stations. The NEPTUNE power system switches into the fault isolation mode. The faulted cable section is isolated by opening the related BU switches. The approach will be discussed in Section 3.5.

In the case of switch malfunction, which results in the disconnection of backbone cables, as in Figure 3.5 (b), or in the case of a high impedance cable fault as in Figure 3.5 (d), the BU voltages do not drop much and the science node converters are still operable. The problem may not be observed from the shore stations. The approach to find these situations is described in Section 3.4.1. For convenience, hereafter a fault will refer to both the opened BU switches and the high impedance fault.

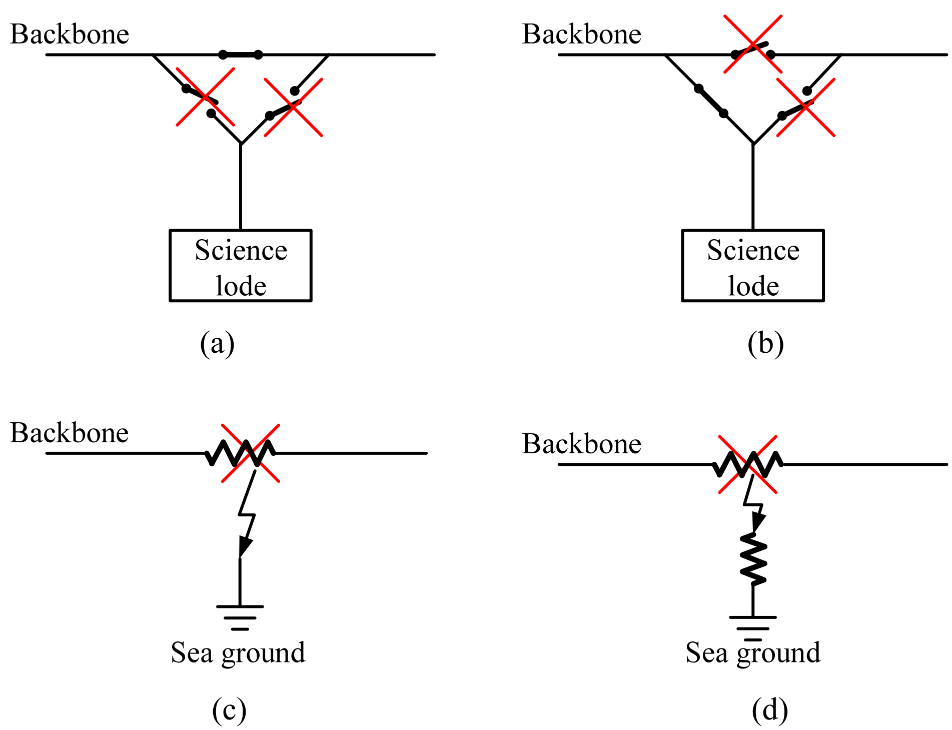

Figure 3.5 Types of abnormal events in NEPTUNE power system

3.4.1 Algorithm for fault detection and location

Detection of opened switches has been studied in the terrestrial power systems as a topology error identification problem. Various approaches have been proposed [12]. Schneider studies the characteristic of how the residual of system measurement equations increases with the system voltage level when topology errors exist in the NEPTUNE power system [13]. This approach provides a solution to detect opened BU switches in NEPTUNE. The drawback is that it requires system voltage be varied in the normal operation mode to generate data, and the calculations are complex.

High impedance fault detection and location in terrestrial power systems has also been difficult. Many proposed approaches require measurements not obtainable in NEPTUNE and do not apply to the networked environment.

An algorithm that solves the above two problems together for the NEPTUNE power system and does not require complicated calculations is proposed in this section.

A. Data requirement

A simplified circuit diagram of a backbone cable section is shown in Figure 3.6. A difficulty in detecting opened BU switches and high impedance faults in the NEPTUNE power system is related to the lack of measurements at the BUs. The current flow into and out of every BU is unknown. Therefore, the current differential algorithm normally used in a terrestrial power system to detect high impedance faults is not applicable.

The proposed algorithm for NEPTUNE assumes there is only one fault in the system and the availability of the following information:

1) Network information, including system topology and resistance of every cable section (which is proportional to the cable length)

2) Estimation of node voltages on the backbone (i.e., voltage at BUs) and node current injections (spur cable currents flowing from BUs into the sea ground)

Node voltages at the BUs can be derived from the input voltage and current at each science node, given the parameter of the spur cables between them.

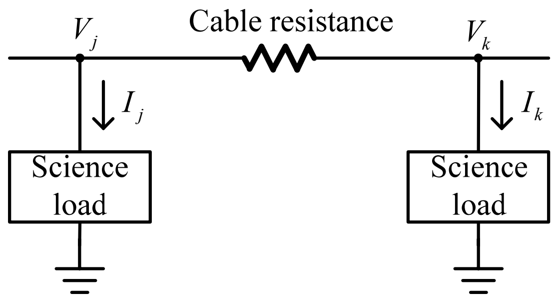

Figure 3.6 Measurements required for the proposed fault location algorithm

B. Algorithm description

In a power system, the node voltage and current injection at each node satisfy the nodal voltage equations (or KCL)

$$\begin{bmatrix} Y_{11} & Y_{12} & \cdots & Y_{1n} \\ Y_{21} & Y_{22} & \cdots & Y_{2n} \\ \cdots & \cdots & \cdots & \cdots \\ Y_{n1} & Y_{n2} & \cdots & Y_{nn} \end{bmatrix} \begin{bmatrix} V_1 \\ V_2 \\ \cdots \\ V_n \end{bmatrix} + \begin{bmatrix} I_1 \\ I_2 \\ \cdots \\ I_n \end{bmatrix} = \mathbf{0} \tag{3.2}$$

where

n is the total number of nodes in the network

Y_{kk} is the self admittance of node k

= sum of all the admittances terminating at node k

Y_{jk} is mutual admittance between nodes j and k

= negative of the sum of all admittance between nodes j and k

V_k is the voltage to ground at node k

I_k is the current flowing from the network into ground at node k

The elements in the $\boldsymbol{Y}$ matrix is given by

$$Y_{jk} = -G_{jk} \text{ when } k \neq j\text{, and}$$

$$Y_{jj} = \sum_{\substack{k=1 \\ k \neq j}}^{n} G_{jk}$$

where $G_{jk} = 1/R_{jk}$, with R_{jk} being the resistance between node j and node k. It is proportional to the length of the cable section between the two nodes.

When there is a fault, equation (3.2) will not hold. The right side of it becomes non-zero. (Noises in the voltage and current measurements have the same effect, but we will discuss the noise issue later.)

Define

$$\boldsymbol{\delta} = \boldsymbol{Y}\boldsymbol{V} + \boldsymbol{I} \tag{3.3}$$

where

$\boldsymbol{\delta}$ is the error vector, and $\boldsymbol{\delta} = (\delta_1, \delta_2, \cdots, \delta_n)^T$

$\boldsymbol{V}$ is the node voltage vector, and $\boldsymbol{V} = (V_1, V_2, \cdots, V_n)^T$

$\boldsymbol{I}$ is the current injection vector, and $\boldsymbol{I} = (I_1, I_2, \cdots, I_n)^T$

Inserting into (3.2) the voltage and current measurements shown in Figure 3.6, we can make the following observations:

1) If there is no fault in the network, then

$$\boldsymbol{\delta} = \boldsymbol{0}$$

2) If there is a fault on the connection between node j and k, then

$\delta_j \neq 0$ and $\delta_k \neq 0$, while all other elements of $\boldsymbol{\delta}$ are 0.

Based on the value of $\boldsymbol{\delta}$, we can identify both the existence of a fault and on which cable section the fault is located. Further information can be obtained by analyzing $\boldsymbol{\delta}$ as the following.

3) If the fault is an open circuit as shown in Figure 3.7, then

$$\delta_j = -\delta_k \neq 0$$

Because it is impossible for a cable to break without causing a fault current at the shore stations (the system uses sea water as the return path), an open circuit most likely means that switches at the ends of the faulted link are opened (abnormal event (b) shown in Figure 3.5).

4) If the fault is a short circuit fault with some impedance as shown in Figure 3.8, then

$$\delta_j \neq 0,\ \delta_k \neq 0 \text{ and } \delta_j \neq \delta_k .$$

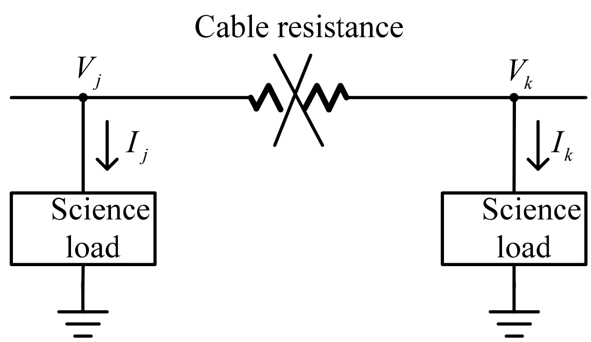

Figure 3.7 Cable section with open circuit fault

Furthermore, as is shown in Section 3.4.2, the resistance between the fault and node j can be obtained using

$$\frac{R_{jf}}{R_{jk}} = \frac{\delta_k}{\delta_j + \delta_k} \tag{3.4}$$

Because the cable resistance is proportional to its length (approximately 1 Ω/km), the distance between the fault and node j can therefore be determined.

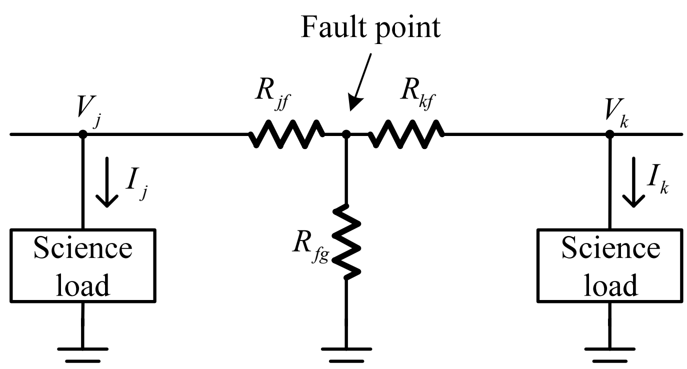

Figure 3.8 Cable section with short circuit fault

3.4.2 Proof of the fault detection and location algorithm

From equation (3.3), the jth element of error vector $\boldsymbol{\delta}$ is

$$\begin{aligned} \delta_j &= \sum_{i=1}^{n} Y_{ji} V_i + I_j \\ &= \sum_{\substack{i=1 \\ i \neq k}}^{n} Y_{ji} V_i + I_j + Y_{jk} V_k \end{aligned} \tag{3.5}$$

$$= \sum_{\substack{i=1 \\ j \neq k}}^{n} G_{ji}(V_j - V_i) + I_j + G_{jk}(V_j - V_k)$$

When a fault occurs between node *j* and node *k*, it changes the conductance G_{jk}, while the other parameters in the system remain the same. Therefore, we can see immediately that δ_j and δ_k deviate from 0 when any fault exists. The elements of **δ** corresponding to all other nodes are still zero. Hence, observation 2) is proved.

When the cable section *jk* is an open circuit, $G_{jk} = 0$. Inserting this "de facto" value of G_{jk} into (3.5), and using $\delta_j^{'}$ to represent the result, the nodal voltage equation for node *j* becomes

$$\begin{aligned} \delta_j^{'} &= \sum_{\substack{i=1 \\ i \neq k}}^{n} G_{ji}\left(V_j - V_i\right) + I_j + G_{jk}\left(V_j - V_k\right) \\ &= \sum_{\substack{i=1 \\ i \neq k}}^{n} G_{ji}\left(V_j - V_i\right) + I_j \\ &= 0 \end{aligned} \tag{3.6}$$

Applying the "original" value of G_{jk} into (3.5) to calculate δ_j, with consideration of (3.6), yields

$$\begin{aligned} \delta_j &= \sum_{\substack{i=1 \\ i \neq k}}^{n} G_{ji}\left(V_j - V_i\right) + I_j + G_{jk}\left(V_j - V_k\right) \\ &= G_{jk}\left(V_j - V_k\right) \end{aligned}$$

Similarly, for node k

$$\delta_k = G_{kj}\left(V_k - V_j\right)$$

Because $G_{jk} = G_{kj}$, then

$$\delta_j = -\delta_k$$

Thus, observation 3) is proved.

If the fault is a short circuit fault with some impedance as shown in Figure 3.8, the number of nodes is *n*+1 because the fault point becomes an additional one. KCL gives

$$\begin{aligned}\delta_j' &= \sum_{i=1}^{n+1} Y_{ji} V_i + I_j \\ &= \sum_{\substack{i=1 \\ i \neq f,k}}^{n+1} Y_{ji} V_i + I_j + Y_{jf} V_f + Y_{jk} V_k \\ &= 0\end{aligned} \tag{3.7}$$

Assuming $Y_{jf} = -G_{jf}$, and $Y_{jk} = -G_{jk}^{'}$, substitution for them in (3.7) yields

$$\begin{aligned}\delta_j' &= \sum_{\substack{i=1 \\ i \neq f,k}}^{n+1} G_{ji} \left(V_j - V_i\right) + I_j + G_{jf} \left(V_j - V_f\right) + G_{jk}^{'} \left(V_j - V_k\right) \\ &= 0\end{aligned}$$

In the faulted network, $G_{jk}^{'} = 0$, so

$$\sum_{\substack{i=1 \\ i \neq f,k}}^{n+1} G_{ji} \left(V_j - V_i\right) + I_j = -G_{jf} \left(V_j - V_f\right) \tag{3.8}$$

When using (3.5) to calculate δ_j, we obtain

$$\delta_j = \sum_{\substack{i=1 \\ i \neq k}}^{n} G_{ji} \left(V_j - V_i\right) + I_j + G_{jk} \left(V_j - V_k\right)$$

Notice that

$$\sum_{\substack{i=1 \\ i \neq k}}^{n} G_{ji} \left(V_j - V_i\right) = \sum_{\substack{i=1 \\ i \neq f,k}}^{n+1} G_{ji} \left(V_j - V_i\right)$$

Using the result from (3.8), yields

$$\delta_j = -G_{jf} \left(V_j - V_f\right) + G_{jk} \left(V_j - V_k\right) \tag{3.9}$$

Similarly, for node k

$$\delta_k = -G_{kf} \left(V_k - V_f\right) + G_{kj} \left(V_k - V_j\right) \tag{3.10}$$

Using the relations $G_{jk} = G_{kj}$ and $\frac{1}{G_{jf}} + \frac{1}{G_{fk}} = \frac{1}{G_{jk}}$ (from $R_{jf} + R_{kf} = R_{jk}$), we can solve (3.9) and (3.10) for

$$\frac{R_{jf}}{R_{jk}} = \frac{\delta_k}{\delta_j + \delta_k}$$

Observation 4) is thus proved.

3.4.3 Error propagation analysis

Ideally, when no fault exists, $\boldsymbol{\delta} = \mathbf{0}$. In reality, $\boldsymbol{\delta}$ should be nonzero because of the existence of computer round-off errors and measurement noise. The round-off error is usually much smaller than the required accuracy of the calculation. The objective of the error analysis here is to find out how the noise in the measurements propagates through the equations and affects the final result.

Let $\boldsymbol{\varepsilon}_V$ and $\boldsymbol{\varepsilon}_I$ be the random noise in system voltage and current measurements, respectively. They have normal distribution with zero mean. $\boldsymbol{\varepsilon}_\delta$ is the error in $\boldsymbol{\delta}$ caused by $\boldsymbol{\varepsilon}_V$ and $\boldsymbol{\varepsilon}_I$. $\boldsymbol{\varepsilon}_\delta$ is determined by

$$\boldsymbol{\delta} + \boldsymbol{\varepsilon}_\delta = \boldsymbol{Y}\left(\boldsymbol{V} + \boldsymbol{\varepsilon}_V\right) + \left(\boldsymbol{I} + \boldsymbol{\varepsilon}_I\right)$$

Using (3.2) to eliminate the deterministic terms, we obtain the relationship between the errors

$$\boldsymbol{\varepsilon}_\delta = \boldsymbol{Y}\boldsymbol{\varepsilon}_V + \boldsymbol{\varepsilon}_I$$

We can find the variance of $\boldsymbol{\varepsilon}_\delta$ by

$$\begin{aligned} E\left\{\boldsymbol{\varepsilon}_\delta \boldsymbol{\varepsilon}_\delta^T\right\} &= E\left\{\left(\boldsymbol{Y}\boldsymbol{\varepsilon}_V + \boldsymbol{\varepsilon}_I\right)\left(\boldsymbol{Y}\boldsymbol{\varepsilon}_V + \boldsymbol{\varepsilon}_I\right)^T\right\} \\ &= E\left\{\boldsymbol{Y}\boldsymbol{\varepsilon}_V\boldsymbol{\varepsilon}_V^T\boldsymbol{Y}^T + \boldsymbol{Y}\boldsymbol{\varepsilon}_V\boldsymbol{\varepsilon}_I^T + \boldsymbol{\varepsilon}_I\boldsymbol{\varepsilon}_V^T\boldsymbol{Y}^T + \boldsymbol{\varepsilon}_I\boldsymbol{\varepsilon}_I^T\right\} \end{aligned}$$

Let $\sigma_{V_k}^2 = E\left\{\varepsilon_{V_k}^2\right\}$, $\sigma_{I_k}^2 = E\left\{\varepsilon_{I_k}^2\right\}$ and $\sigma_{\delta_k}^2 = E\left\{\varepsilon_{\delta_k}^2\right\}$, representing the error variances at node k. Supposing all measurements are independent, we then have the variance of the δ_j given by

$$\begin{aligned} \sigma_{\delta_j}^2 &= E\left\{\varepsilon_{\delta_j}^2\right\} \\ &= \sum_{k=1}^{n} G_{jk}^2 \sigma_{V_k}^2 + \sigma_{I_j}^2 \end{aligned} \tag{3.11}$$

If all voltage and current measurements have the same variance σ_V^2 and σ_I^2, respectively, (3.11) can be simplified into:

$$\sigma_{\delta_j}^2 = \sigma_V^2 \sum_{k=1}^{n} G_{jk}^2 + \sigma_I^2 \tag{3.12}$$

Now we can estimate $\sigma_{\delta_j}^2$ as long as $\sum_{k=1}^{n} G_{jk}^2$ is known.

To make the calculations convenient, we normalize the voltage and current data, thus σ_V^2 and σ_I^2 will be a percentage. Take voltage base V_B = 10 kV and current base I_B = 10 A, which yields R_B = 1 kΩ. In the NEPTUNE system, the shortest cable length is greater than 50 km (i.e., cable resistance is larger than 50 Ω.) Therefore

$$\begin{aligned}\sum_{k=1}^{n} G_{jk}^2 &\le \sum_{k=1}^{n} \left(\frac{1}{50/R_B}\right)^2 \\ &= R_B^2 \sum_{k=1}^{n} \left(\frac{1}{50}\right)^2\end{aligned}$$

Also consider that every backbone node has, at most, three cable connections to other nodes, so

$$\begin{aligned}\sum_{k=1}^{n} G_{jk}^2 &\le 3R_B^2 \left(\frac{1}{50}\right)^2 \\ &\approx 1200\end{aligned}$$

Inserting the value of $\sum_{k=1}^{n} G_{jk}^2$ into (3.12) yields

$$\sigma_{\delta_j}^2 \le 1200\sigma_V^2 + \sigma_I^2 \tag{3.13}$$

This shows that the variance of voltage measurements σ_V^2 is dominant in determining σ_δ^2, while σ_I^2 does not carry as much influence. σ_V^2 must be reduced to get an acceptable σ_δ^2. This can be obtained by

1) Using more accurate voltage sensors and

2) Making a multitude of repeated measurements and using the average in the calculation of $\boldsymbol{\delta}$.

Let n_V and n_I be the number of repeated measurements for voltage and current, respectively. The variance of $\boldsymbol{\delta}$ is given by

$$\sigma_{\delta_j}^2 \le 1200\frac{\sigma_V^2}{n_V} + \frac{\sigma_I^2}{n_I} \tag{3.14}$$

For example, if $\sigma_V = 0.1\%$, $\sigma_I = 1\%$, n_V = 12, and n_I = 1, then

$$\begin{aligned}\sigma_{\delta_j}^2 &\le 1200\frac{(0.1\%)^2}{12} + \frac{(1\%)^2}{1}\\ &= 2(1\%)^2\end{aligned}$$

Using Taylor expansions, from (3.4) we get

$$\Delta\left(\frac{R_{jf}}{R_{jk}}\right) \approx \frac{-1}{\left(\delta_j + \delta_k\right)^2}\Delta\delta_j + \frac{\delta_j}{\left(\delta_j + \delta_k\right)^2}\Delta\delta_k \tag{3.15}$$

Let $\theta = \dfrac{R_{jf}}{R_{jk}}$, and ε_θ be the error in θ caused by the error in δ_j and δ_k. Then from (3.15) we get

$$\varepsilon_\theta \approx \frac{-1}{\left(\delta_j + \delta_k\right)^2}\varepsilon_{\delta_j} + \frac{\delta_j}{\left(\delta_j + \delta_k\right)^2}\varepsilon_{\delta_k} \tag{3.16}$$

ε_θ can be approximated by a linear combination of ε_{δ_j} and ε_{δ_k}, and therefore can still be seen as random noise satisfying normal distribution with zero mean. But the variance of ε_θ is dependant on δ_j and δ_k, which in turn depends on the particular system voltage and current profile, making it impossible to have a general estimate of the variance of θ.

For the purpose of getting an accurate fault location result, making a large number of repeated measurements for the same set of system voltages is preferable. However, it is usually not realistic to have many simultaneous measurements for every node voltage in the system. Measurements made at different times are affected by system load changes. They can not be averaged, as in (3.14). Instead, the following procedures are proposed:

1) Make a snapshot of the system voltage and current measurements from both the shore stations and science nodes

2) Process the data with a state estimation program to obtain good voltage and current estimations for every node

3) Use the estimated voltage and current data to calculate the error vector $\boldsymbol{\delta}$ with (3.3)

4) Find the two nodes corresponding to the two largest elements in $\boldsymbol{\delta}$; the fault is most likely located on the cable between these two nodes

5) Make judgments on whether the fault is open circuit or short circuit fault based on the observations stated in Section 3.4.1

6) Calculate the fault location parameter θ with (3.4) if it is recognized as a short circuit fault

7) Repeat 1) to 6) consecutively for a number of times and throw away obviously erroneous fault location results, such as values of θ outside (0, 1)

For an open circuit fault, most of the results from 5) should be pointing to the same cable section; for a short circuit fault, use the average of all reasonable fault location results from 7) as an estimate.

Because the location of the fault (represented by θ) is constant regardless of the system load level, the series of random variable θ obtained in 7) should have the same mean value. But as already discussed, they do have different variances. Therefore, an unbiased estimation of $E\{\theta\}$ should be calculated with a weighted average approach. However, when the system load variation is slow or normally distributed, a simple average of θ series can be taken for the estimation of $E\{\theta\}$, eliminating the need for calculating the variance of every θ. This simple approach was used in the test case and was found to give satisfying results.

3.4.4 Test case

A simplified version of the NEPTUNE network is shown in Figure 3.9. There are ten backbone nodes and two voltage sources. The blocks between the backbone nodes and the ground represent science loads. Between the two backbone nodes are the cable resistances. The cable resistivity is 1 Ω/km.

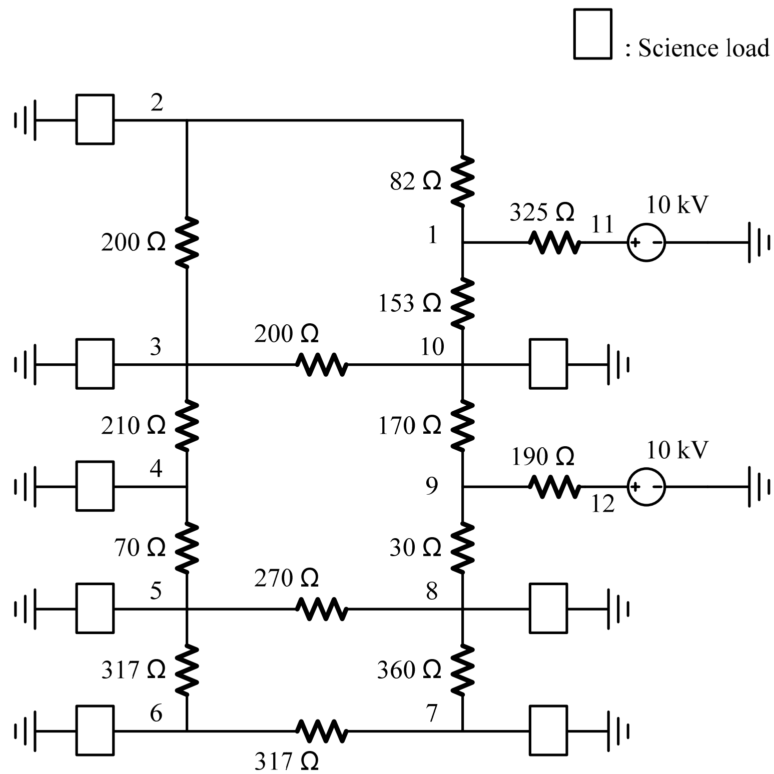

Figure 3.9 A simple dc power network to verify the fault location algorithms

In the simulation, $\sigma_V = 0.1\%$, $\sigma_I = 1\%$, and system voltage and current measurements are repeated 100 times. Science load variation has a normal distribution with zero mean and 20% standard deviation.

Because of the existence of noise, there are times when the right fault type and location can not be recognized. In the test simulations, fault identification accuracy (FIA) is defined as the number of right or acceptable results versus the total number of calculations (100). The test was carried out for 1000 times for both open circuit and short circuit cases. The mean and the standard deviation of FIA from the 1000 tests are given. But because the fault location result from each calculation is not a stationary random process, the statistical data of FIA may vary.

A. Detection and location of opened switches

An open circuit is simulated between node 2 and node 3. The value of error vector $\boldsymbol{\delta}$ in one calculation is shown in Figure 3.10. The elements corresponding to node 2 and node 3 are the largest and are approximately equal in amplitude, which verifies the theoretical analysis in Section 3.4.1.

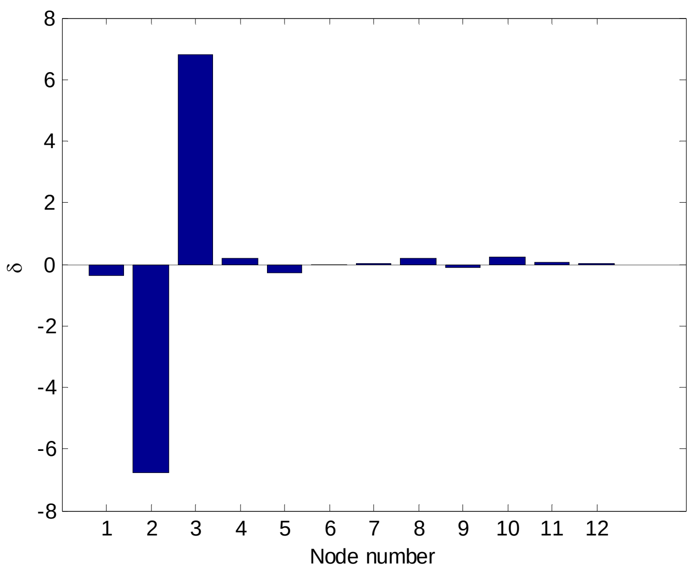

Figure 3.10 Value of $\boldsymbol{\delta}$ for open circuit

B. Detection and location of a high impedance fault

A fault with a grounding resistance of 2 kΩ is put between node 2 and node 3. The distance between the fault and node 2 is 60 km. The total length of the cable between node 2 and node 3 is 200 km. Thus, the fault location parameter θ is 60/200=0.3.

The mean value of FIA from 1000 tests is 87%, and its standard deviation is 25%.

The value of $\boldsymbol{\delta}$ in one calculation is shown in Figure 3.11. Node 2 and node 3 have the two largest elements in $\boldsymbol{\delta}$. Using (3.4), the value of θ is calculated for 100 times based on 100 consecutive measurements in a simulation test. The series of θ calculated from this test is shown in Figure 3.12. The average of θ is 0.3000 with a standard deviation of 0.0319.

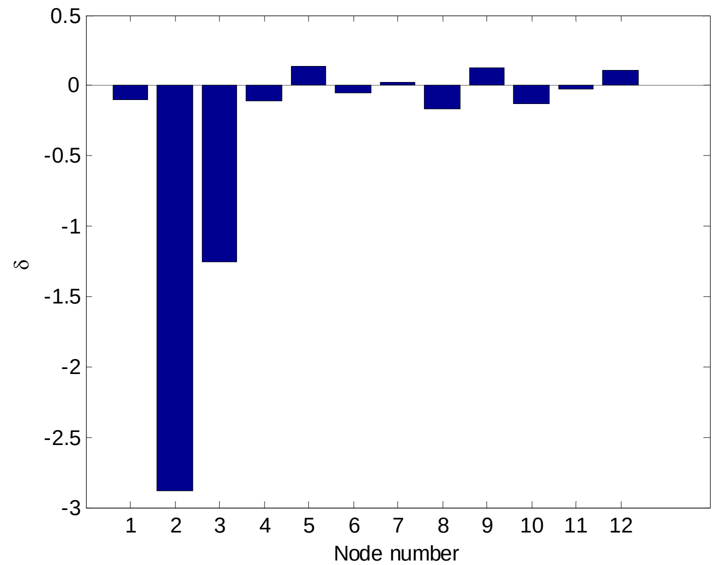

Figure 3.11 Value of $\boldsymbol{\delta}$ for high impedance fault

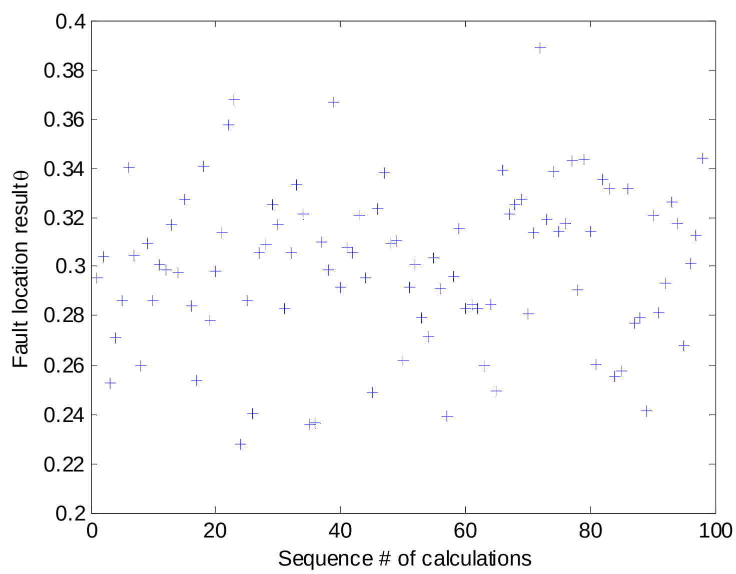

Figure 3.12 Fault location calculation results for high impedance fault

The mean value of FIA from 1000 tests is 93%, and its standard deviation is 7%.

The simulation on the simplified NEPTUNE network shows that the algorithm proposed to detect opened BU switches and a high impedance fault is effective and practical even with some measurement noise. The algorithm requires obtaining data from every operating science node in the system. In the case of some nodes being down, the network admittance matrix discussed in Section 3.4.1 A needs to be changed accordingly to use this algorithm. For example, if a science node under the BU_m is down and BU_m is between BU_j and BU_k, then in the system topology information, node *m* should be eliminated and cable sections *jm* and *mk* become one single section *jk*. Then the algorithm can be applied to the "new" system.

3.5 Location of a severe fault

When the system encounters a severe fault, system voltage is lowered to below 500 V. BU switches adjacent to the fault are opened to isolate the faulted cable section. Then the system is brought back to normal mode. Through the approach discussed in Section 3.4, opened BU switches can be detected, and thus the faulted cable section is identified. The exact location of the fault point requires the system to be shut down and restarted through the procedure described in Section 3.1. The isolated cable section is reconnected during the startup/restoration mode. Then in the fault location mode, a low negative voltage is applied to the system and measurements (voltage and current) are made in the shore stations. Based on the measurement data and the knowledge of the faulty cable section, the exact location of the fault can be calculated. The fault is then isolated again and the system voltage is brought up to normal values.

3.5.1 Calculations to locate a severe fault

The data obtained in the fault location mode include voltage and current measurements in the two shore stations. The network equations become nonlinear because the location of the fault (which affects the conductance between nodes) adds an extra unknown variable in the admittance matrix.

The system nodal voltage equations (3.2) can be written as

$$\begin{bmatrix} \boldsymbol{Y}_{NN} & \boldsymbol{Y}_{NS} \\ \boldsymbol{Y}_{SN} & \boldsymbol{Y}_{SS} \end{bmatrix} \begin{bmatrix} \boldsymbol{V}_N \\ \boldsymbol{V}_S \end{bmatrix} + \begin{bmatrix} \boldsymbol{I}_N \\ \boldsymbol{I}_S \end{bmatrix} = \boldsymbol{0} \tag{3.17}$$

where

$\boldsymbol{Y_{NN}}$ is the matrix containing admittances between non-voltage source nodes

$\boldsymbol{Y_{NS}}$ is the matrix containing admittances between non-voltage source nodes and voltage sources

$\boldsymbol{Y_{SN}} = \boldsymbol{Y_{NS}}^T$

$\boldsymbol{Y_{SS}}$ is the matrix containing admittances between voltage sources

$\boldsymbol{V_N}$ is the voltage vector of non-voltage source nodes

$\boldsymbol{V_S}$ is the voltage vector of voltage source nodes

$\boldsymbol{I_N}$ is the current injections vector into ground from non-voltage source nodes

$\boldsymbol{I_S}$ is the current injections vector into ground from voltage source nodes

From (3.17) we get

$$\boldsymbol{Y}_{NN}\boldsymbol{V}_N + \boldsymbol{Y}_{NS}\boldsymbol{V}_S + \boldsymbol{I}_N = \boldsymbol{0} \tag{3.18}$$

and

$$\boldsymbol{Y}_{SN}\boldsymbol{V}_N + \boldsymbol{Y}_{SS}\boldsymbol{V}_S + \boldsymbol{I}_S = \boldsymbol{0} \tag{3.19}$$

In the fault location mode, system voltage is around -500 V, therefore, no science loads are connected. Thus

$$\boldsymbol{I}_N = (\underbrace{0,\cdots,0}_{N-1}, I_f)^T \tag{3.20}$$

where N-1 is the number of non-voltage source nodes in the system, excluding the fault point, and I_f is the current injection into the ground from the fault point. I_f can be obtained through

$$I_f = -\sum_{i=1}^{M} I_{Si} \tag{3.21}$$

where M is the number of voltage sources in the system, and I_{Si} is the current injection into the ground from the ith voltage source.

We use the same variable θ as in Section 3.4 to represent the fault location. Some of the elements in the system admittance matrix are changed by the presence of the fault. For example, if the fault is located on a cable section connecting a voltage source to the network, the related elements in $\boldsymbol{Y_{NS}}$ and $\boldsymbol{Y_{SN}}$ become functions of θ. If the fault is located inside the network, the elements related to the faulted cable section in $\boldsymbol{Y_{NN}}$ are functions of θ. In both cases, from (3.18) we have

$$\boldsymbol{V_N} = -\boldsymbol{Y_{NN}}^{-1}(\boldsymbol{Y_{NS}}\boldsymbol{V_S} + \boldsymbol{I_N}) = \boldsymbol{V_N}(\theta) \tag{3.22}$$

From (3.19) we have

$$\boldsymbol{Y_{SN}}(\theta)\boldsymbol{V_N}(\theta) + \boldsymbol{Y_{SS}}\boldsymbol{V_S} + \boldsymbol{I_S} = \boldsymbol{0} \tag{3.23}$$

Let

$$\boldsymbol{h}(\theta) = \boldsymbol{Y_{SN}}(\theta)\boldsymbol{V_N}(\theta)$$

and

$$\boldsymbol{b} = -\boldsymbol{Y_{SS}}\boldsymbol{V_S} - \boldsymbol{I_S}$$

Then we get a set of non-linear equations of θ:

$$\boldsymbol{h}(\theta) - \boldsymbol{b} = 0 \tag{3.24}$$

3.5.2 Weighted least square method solving non-linear equations

Non-linear equations like (3.24) can be solved using the WLS method as follows.

Let θ^* be the solution to (3.24), using Taylor expansions we get

$$\begin{aligned} \boldsymbol{h}(\theta) &= \boldsymbol{h}(\theta^* + \Delta\theta) \\ &= \boldsymbol{h}(\theta^*) + \left.\frac{\partial \boldsymbol{h}(\theta)}{\partial \theta}\right|_{\theta=\theta^*} \Delta\theta + h.o.t. \end{aligned} \tag{3.25}$$

where $h.o.t$ represents the high order terms.

Let

$$\boldsymbol{H} = \left.\frac{\partial \boldsymbol{h}(\theta)}{\partial \theta}\right|_{\theta=\theta^*}$$

and

$$\boldsymbol{z} = \boldsymbol{h}(\theta) - \boldsymbol{b}$$

From (3.25), ignoring the *h.o.t.*

$$\boldsymbol{z} \approx \boldsymbol{h}(\theta^*) + \boldsymbol{H}\Delta\theta - \boldsymbol{b} = \boldsymbol{H}\Delta\theta$$

Write the above equation in the following form

$$\boldsymbol{H}\Delta\theta - \boldsymbol{z} = 0 \tag{3.26}$$

$\Delta\theta$ can be found by minimizing an objective function

$$J = \boldsymbol{r}^T \boldsymbol{W} \boldsymbol{r}$$

where

$\boldsymbol{r} = \boldsymbol{H}\Delta\theta - \boldsymbol{z}$

$\boldsymbol{W} = \boldsymbol{R}^{-1}$, with $\boldsymbol{R}$ being the covariance matrix of the measurements.

The objective function is minimized when

$$\frac{dJ}{d\boldsymbol{z}} = 2\boldsymbol{H}^T \boldsymbol{W}(\boldsymbol{H}\Delta\theta - \boldsymbol{z}) = 0$$

Therefore

$$\Delta\theta = (\boldsymbol{H}^T \boldsymbol{W} \boldsymbol{H})^{-1} \boldsymbol{H}^T \boldsymbol{W} \boldsymbol{z} \tag{3.27}$$

Then the solution to (3.24) is

$$\theta^* = \theta - \Delta\theta \tag{3.28}$$

3.5.3 Procedures to solve equations to locate a severe fault

For the particular fault location equations in (3.24), we have

$$\boldsymbol{H} = \frac{d\boldsymbol{Y}_{SN}(\theta)}{d\theta} \boldsymbol{V}_N(\theta) + \boldsymbol{Y}_{SN}(\theta) \frac{d\boldsymbol{V}_N(\theta)}{d\theta} \tag{3.29}$$

Consider the case when a fault is inside the network. Only the elements related to the faulted cable section in $\boldsymbol{Y}_{NN}$ are functions of θ. Therefore

$$\frac{d\boldsymbol{Y}_{SN}(\theta)}{d\theta} = 0$$

Then from (3.29), we get

$$\boldsymbol{H} = \boldsymbol{Y}_{SN} \frac{d\boldsymbol{V}_N(\theta)}{d\theta} \tag{3.30}$$

From (3.18), we have

$$\frac{d\boldsymbol{Y}_{NN}(\theta)}{d\theta}\boldsymbol{V}_N(\theta) + \boldsymbol{Y}_{NN}(\theta)\frac{d\boldsymbol{V}_N(\theta)}{d\theta} = \mathbf{0}$$

Therefore

$$\frac{d\boldsymbol{V}_N(\theta)}{d\theta} = -\boldsymbol{Y}_{NN}(\theta)^{-1}\frac{d\boldsymbol{Y}_{NN}(\theta)}{d\theta}\boldsymbol{V}_N(\theta) \tag{3.31}$$

Inserting (3.31) into (3.30), we get

$$\boldsymbol{H} = -\boldsymbol{Y}_{SN}\boldsymbol{Y}_{NN}(\theta)^{-1}\frac{d\boldsymbol{Y}_{NN}(\theta)}{d\theta}\boldsymbol{V}_N(\theta) \tag{3.32}$$

Assume the fault is located on the cable section between node j and node k. Then the node admittance matrix $\boldsymbol{Y}_{NN}$ can be written as

$$\boldsymbol{Y}_{NN} = \begin{bmatrix} \boldsymbol{Y}_{NN}^{\ *} + \boldsymbol{Y}_{NN}^{\ f} & \boldsymbol{Y}_{Nf} \\ \boldsymbol{Y}_{fN} & \boldsymbol{Y}_{ff} \end{bmatrix} \tag{3.33}$$

where

$\boldsymbol{Y}_{NN}^{*}$ is the node admittance matrix of the network without faults

$\boldsymbol{Y}_{NN}^{f}$ is the change to node admittance matrix caused by the fault

$\boldsymbol{Y}_{Nf}$ is admittance vector between network nodes and the fault point

$\boldsymbol{Y}_{fN} = \boldsymbol{Y}_{Nf}^{T}$

$\boldsymbol{Y}_{ff}$ is the self admittance of the fault point

We also have

$$\boldsymbol{Y}_{NN}^{\ f}(j,j) = -Y_{jk} + \theta^{-1}Y_{jk}$$

$$\boldsymbol{Y}_{NN}^{\ f}(k,k) = -Y_{jk} + (1-\theta)^{-1}Y_{jk}$$

$$\boldsymbol{Y}_{NN}^{\ f}(j,k) = -Y_{jk}$$

$$\boldsymbol{Y_{NN}}^f(k,j) = -Y_{jk}$$

$$\boldsymbol{Y_{Nf}}(j) = -\theta^{-1}Y_{jk} = \boldsymbol{Y_{Nf}}(j)$$

$$\boldsymbol{Y_{Nf}}(k) = -(1-\theta)^{-1}Y_{jk} = \boldsymbol{Y_{fN}}(k)$$

$$\boldsymbol{Y_{ff}} = \theta^{-1}Y_{jk} + (1-\theta)^{-1}Y_{jk}$$

All the other elements in $\boldsymbol{Y_{NN}}^f$, $\boldsymbol{Y_{fN}}$ and $\boldsymbol{Y_{Nf}}$ are zero.

$\dfrac{d\boldsymbol{Y}_{NN}(\theta)}{d\theta}$ for (3.31) can be obtained from $\boldsymbol{Y_{NN}}$ immediately.

Similar to locating a high impedance fault in the normal mode, the accuracy of the above calculations can be compromised with the existence of measurement noise. Through repeated measurements and averaging the result from each calculation, accurate location of the fault can still be obtained.

Assuming the fault is inside the network, the procedure to locate a severe fault in the fault location mode is summarized below. (The approach is similar when the fault is on the cable between a shore station and the network.)

1) Obtain voltage $\boldsymbol{V_S}$ and current injections from the system $\boldsymbol{I_S}$ from the two shore stations.

2) Calculate $I_f = -\sum_{i=1}^{M} I_{Si}$, where M is the number of voltage sources in the system, and I_{Si} is the current injection into the system from the ith voltage source. $\boldsymbol{I}_N = (\underbrace{0,\cdots,0}_{N-1}, I_f)^T$,where N-1 is the number of non-voltage source nodes in the system, excluding the fault point.

3) Choose an initial value for θ, such as 0.2.

4) Based on the knowledge that the fault is located on the cable between node j and k (refer to Section 3.4), calculate the following:

$$\boldsymbol{Y}_{NN}(\theta) = \begin{bmatrix} \boldsymbol{Y_{NN}}^* + \boldsymbol{Y_{NN}}^f & \boldsymbol{Y_{Nf}} \\ \boldsymbol{Y_{fN}} & \boldsymbol{Y_{ff}} \end{bmatrix}$$

$$\boldsymbol{V}_N(\theta) = -\boldsymbol{Y}_{NN}^{-1}(\boldsymbol{Y}_{NS}\boldsymbol{V}_S + \boldsymbol{I}_N)$$

$$\boldsymbol{h}(\theta) = \boldsymbol{Y}_{SN}\boldsymbol{V}_N(\theta)$$

$$\boldsymbol{b} = -\boldsymbol{Y}_{SS}\boldsymbol{V}_S - \boldsymbol{I}_S$$

$$\boldsymbol{z} = \boldsymbol{h}(\theta) - \boldsymbol{b}$$

$$\boldsymbol{H} = -\boldsymbol{Y}_{SN}\boldsymbol{Y}_{NN}(\theta)^{-1}\frac{d\boldsymbol{Y}_{NN}(\theta)}{d\theta}\boldsymbol{V}_N(\theta)$$

$$\Delta\theta = (\boldsymbol{H}^T\boldsymbol{W}\boldsymbol{H})^{-1}\boldsymbol{H}^T\boldsymbol{W}\boldsymbol{z}$$

$$\theta = \theta - \Delta\theta$$

5) Repeat 4) until $\Delta\theta$ is small enough.

6) Adjust the shore station voltages, and repeat 1) to 5) for a number of times to obtain a series of estimates on the value of θ. Take the average of the estimates and use it as the location of the fault.

3.5.4 Test case

The same simplified network as in Section 3.4.4 is used to test the algorithm. In the simulation, standard deviations for voltage and current measurements are $\sigma_V = 0.1\%$, and $\sigma_I = 1\%$, respectively. System voltage and current are measured at two shore stations and repeated 100 times. The shore station voltages are randomly adjusted around -500 V each time the measurements are taken.

A short circuit fault with a grounding resistance of 2 kΩ is put between node 2 and node 3. The distance between the fault and node 2 is 60 km. The total cable length between nodes 2 and 3 is 200 km. Thus, the fault location parameter θ is 60/200 = 0.3.

Calculation results of θ from one simulation test are shown in Figure 3.13. The mean value as an estimate of θ from the data is 0.3003, and the standard deviation is 0.0742.

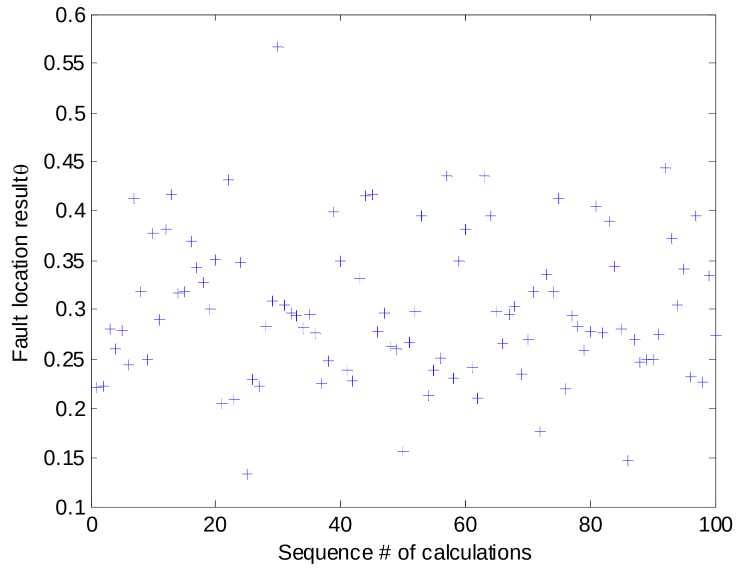

Figure 3.13 Fault location results for a severe fault

3.6 Combined fault location and state estimation

The high impedance fault location problem discussed in Section 3.4 can also be solved along with the task of estimating system voltages, when some measurement data are believed erroneous or not available. It thus becomes a combined parameter and state estimation algorithm.

3.6.1 Algorithm description

With the presence of a fault, the system nodal voltage equations become

$$\boldsymbol{Y}(\theta)\boldsymbol{V} + \boldsymbol{I} = \mathbf{0}$$

The formation of admittance matrix $\mathbf{Y}(\theta)$ requires the knowledge of the faulty cable section, i.e., between which two nodes the fault is located. This can be obtained by the calculation of the error vector $\boldsymbol{\delta}$ in (3.3). If there are abnormally large elements in $\boldsymbol{\delta}$, then the fault is located between the two nodes corresponding to the two largest elements. If it is a short circuit fault (refer to Section 3.4.1 for the determination of fault type from $\boldsymbol{\delta}$), $\boldsymbol{Y}(\theta)$ is formed in a way similar to $\boldsymbol{Y}_{NN}$ in (3.3) except that both voltage source and non-voltage source nodes are included in $\boldsymbol{Y}(\theta)$.

Using the node voltage and current injection measurements from the shore stations and science nodes yields the following

$$\begin{aligned} \boldsymbol{V} - \boldsymbol{V}_{meas} &= 0 \\ \boldsymbol{Y}(\theta)\boldsymbol{V} + \boldsymbol{I}_{meas} &= 0 \end{aligned} \tag{3.34}$$

where $\boldsymbol{V}_{meas}$ and $\boldsymbol{I}_{meas}$ are the node voltage and current injection measurements, respectively.

Let

$$\boldsymbol{x} = (\boldsymbol{V}, \theta)^T$$

and

$$\boldsymbol{b} = (\boldsymbol{V}_{meas}, -\boldsymbol{I}_{meas})^T$$

then (3.34) can be written as

$$\boldsymbol{h}(\boldsymbol{x}) - \boldsymbol{b} = \boldsymbol{0} \tag{3.35}$$

Equation (3.35) can be solved using the WLS method described in Section 3.5.2.

Similar to the other fault location algorithms, the accuracy of the above calculations can be compromised with the existence of measurement noise. Through repeated measurements and averaging the result of each calculation, accurate location of the fault can still be achieved.

The procedure of doing a combined fault location and state estimation in the normal mode is summarized below.

1) Obtain node voltage $\boldsymbol{V}_{meas}$ and current injections from the system to ground $\boldsymbol{I}_{meas}$ from the shore stations and science nodes.

2) Insert $\boldsymbol{V}_{meas}$ and $\boldsymbol{I}_{meas}$ into $\boldsymbol{\delta} = \boldsymbol{Y}\boldsymbol{V} + \boldsymbol{I}$ to evaluate the error vector $\boldsymbol{\delta}$. $\boldsymbol{Y}$ is the original admittance matrix for the system without a fault. If there are abnormally large elements in $\boldsymbol{\delta}$, then a fault is located between the two nodes corresponding to the two largest elements. If it is determined that a short circuit fault exists, then continue with the combined fault location and state estimation procedure.

3) Choose initial values for $\boldsymbol{V}$ and θ.

4) Let $\boldsymbol{x} = (\boldsymbol{V}, \theta)^T$, $\boldsymbol{h}(\boldsymbol{x}) = \boldsymbol{h}(\boldsymbol{V}, \theta) = \begin{bmatrix} \boldsymbol{V} \\ \boldsymbol{Y}(\theta)\boldsymbol{V} \end{bmatrix}$ and $\boldsymbol{b} = (\boldsymbol{V}_{meas}, -\boldsymbol{I}_{meas})^T$.

Calculate the following:

$$\boldsymbol{z} = \boldsymbol{h}(\boldsymbol{x}) - \boldsymbol{b}$$

$$\boldsymbol{H} = \frac{\partial \boldsymbol{h}(\boldsymbol{x})}{\partial \boldsymbol{x}}$$

$$\boldsymbol{\Delta x} = (\boldsymbol{H}^T \boldsymbol{W} \boldsymbol{H})^{-1} \boldsymbol{H}^T \boldsymbol{W} \boldsymbol{z}$$

$$\boldsymbol{x} = \boldsymbol{x} - \boldsymbol{\Delta x}$$

5) Repeat 4) until $\boldsymbol{\Delta x}$ is small enough.

6) Repeat 1) to 5) to obtain a series of estimates of the value of θ as well as the system node voltages. Take the average of the estimates of θ and use it as the location of the fault.

3.6.2 Test case

The same simplified network as in Section 3.4.4 is used to test the algorithm. In the simulation, standard deviations for voltage and current measurements are $\sigma_V = 0.1\%$, and $\sigma_I = 1\%$, respectively. System node voltage and current injections are measured 100 times. The science load variations at every time the measurement data is collected satisfy normal distribution with zero mean and 20% standard deviation.

Case 1: A short circuit fault with a grounding resistance of 2 kΩ is put between node 2 and node 3. The distance between the fault and node 2 is 60 km. The total length of cable between node 2 and 3 is 200 km. Thus, the fault location parameter θ is 60/200 = 0.3.

To test the state estimation result as well as the effect of bad or missing sensors on the fault location result, voltage and current data of node 8 are assumed erroneous, and given zero weight in the calculations. This is also equal to the situation when communications to node 8 are lost, thus, the data from it become unavailable.

Calculation results of θ from one simulation test are shown in Figure 3.14. The mean value as an estimate of θ from the data is 0.3037, and the standard deviation is 0.0349.

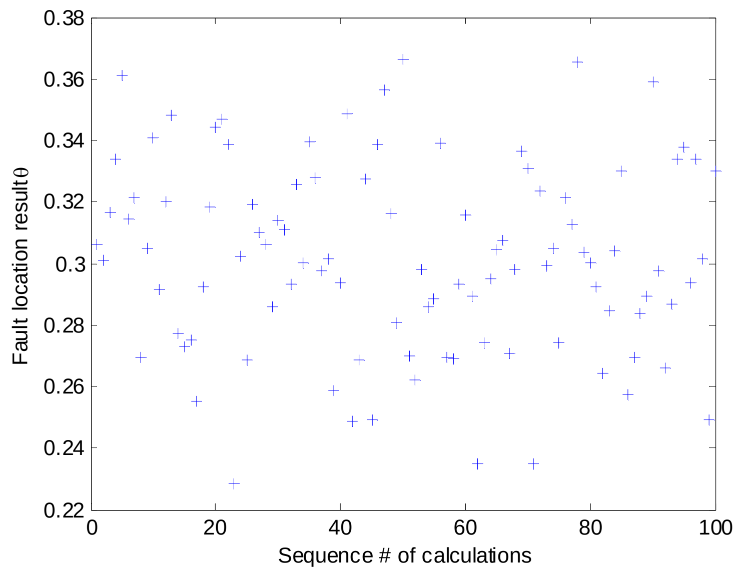

Figure 3.14 Fault location results in Case 1 using the combined fault location and state estimation method

The state estimation result from one calculation is shown in Figure 3.15. The voltage measurement data of node 8 is higher than the voltage source nodes, which indicates that it is bad data. In the estimation result, the estimated voltage is very close to the true value.

Case 2: A short circuit fault is put into the system at the same place as in Case 1, i.e., θ = 0.3 between node 2 and 3, but with a much smaller grounding resistance of 180 **Ω**. Voltage on node 2 is pulled down by the fault to below 5 kV, which will result in the loss of communications from node 2. All other measurements are assumed within the correct tolerance.

In the simulation, data of node 2 are set as: V_2 = 10 kV and I_2 = 1 A, because they will not be obtained from real measurements. The weight of the two variables is set to 0.01 (a value much smaller than the weights of other valid measurements).

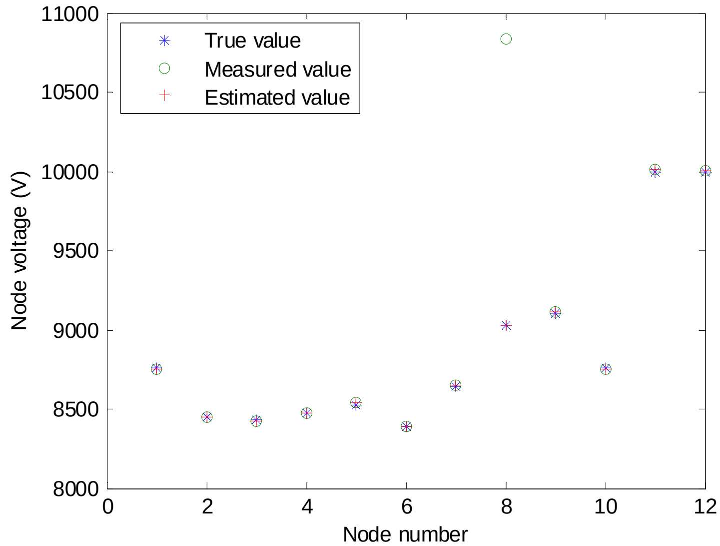

Figure 3.15 State estimation result in Case 1 using the combined fault location and state estimation method

Calculation results of θ from one simulation test are shown in Figure 3.16. The mean value of θ is 0.3151, and the standard deviation is 0.0059.

The state estimation result of one calculation is shown in Figure 3.17. The voltage of node 2 is set to 10 kV manually. In the estimation result, the estimated voltage is very close to the true value.

Case 1 and Case 2 demonstrate that when there is bad or missing data in the system measurements, it is still possible to locate the fault as well as getting a good estimate of the system voltages. This can not be achieved by using the method discussed in Section 3.4. However, the combined fault and state estimation method needs the analysis in Section 3.4 to provide knowledge of the faulty cable, and sometimes it does not converge. Therefore, both methods should be considered.

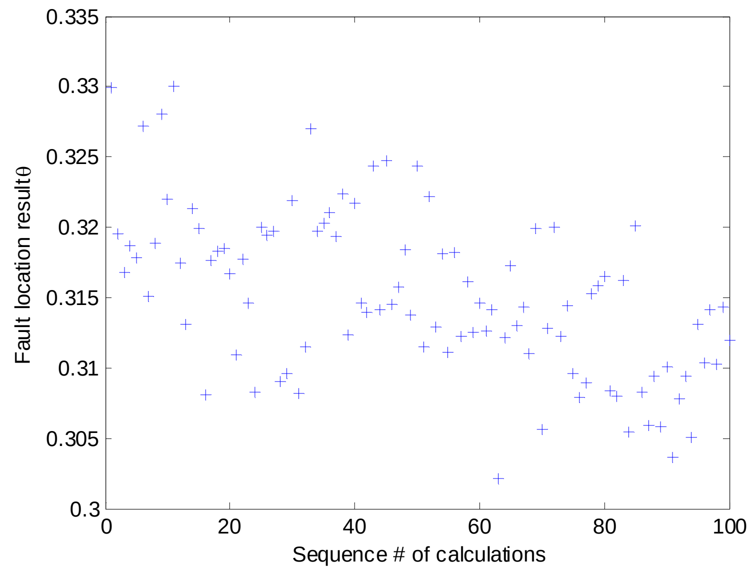

Figure 3.16 Fault location results in Case 2 using the combined fault location and state estimation method

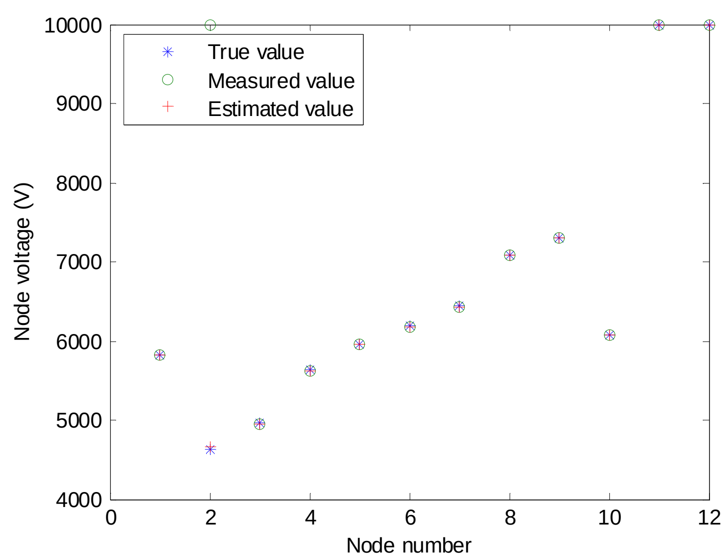

Figure 3.17 State estimation result in Case 2 using the combined fault location and state estimation method

3.7 Summary

In this chapter, the operation design for the NEPTUNE power system is described. This design involves new concepts such as fault isolation in an interconnected network. The problem of locating various types of faults is also addressed. Practical fault location algorithms showing satisfying results are proposed and verified through extensive simulation tests. The accuracy of the fault location results is affected by the location of the fault but limited by only the number of measurements.

Another important aspect to consider in building and operating a power system is the issue of stability. This is discussed in Chapter 4.

Chapter 4

Stability Analysis of the NEPTUNE Power System

The NEPTUNE power system consists of a large number of power electronic converters. Tens of 10 kV to 400 V dc-dc converters are connected to the shore stations through undersea cables up to several thousand kilometers long. In each science node, multiple low voltage converters are connected to the 10 kV converters to power the various science loads. The power electronic maintains a constant power output regardless of the variations with the input voltage. This characteristic introduces potential stability concerns to the system. This chapter will first examine the stability issues in a simplified dc power delivery system, and then describe the models and approaches used to study these issues in a large power network like the NEPTUNE power system. Finally, the stability problems in ac and dc power systems are compared to help gain a greater understanding of the issue.

4.1 Stability issues in a dc power system

Stability has been studied in small scale dc power systems such as space stations and computer systems. These systems usually are a compact size, which is characterized by cascaded converters connected with short cables or wires. Stability problems in a large dc power delivery system with thousands of kilometers of cables connecting power sources and converters have not been studied systematically. This section will investigate the type of stability issues in a large dc power delivery system by analyzing a simplified system model.

4.1.1 Steady-state stability

A power converter usually delivers a tight regulated voltage to its load, therefore, when the load remains the same, the converter outputs constant power regardless of the variation at its input. A simplified dc power delivery system in which a converter is powered by a voltage source through a cable is shown in Figure 4.1.

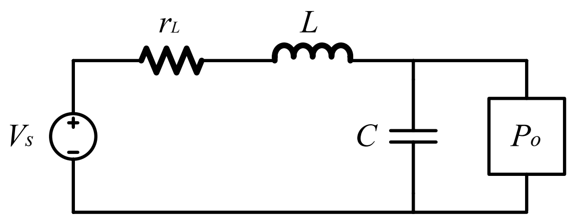

Figure 4.1 A simplified dc power delivery system

In Figure 4.1, V_s is the dc voltage source, r_L, L and C are the equivalent lumped parameters for the cable section, and P_o is modeling the load converter. The system dynamics can be studied using the following state equations

$$L\frac{di_L}{dt} = V_s - r_L \cdot i_L - v_C$$
$$C\frac{dv_C}{dt} = i_L - \frac{P_o}{v_C} \tag{4.1}$$

The system is nonlinear because of the term $\frac{P_o}{v_C}$ introduced by the constant power load property of the converter.

At equilibrium points, the system must satisfy

$$\frac{di_L}{dt} = 0$$
$$\frac{dv_C}{dt} = 0 \tag{4.2}$$

Therefore, equations of the system's equilibrium points are

$$V_s - r_L \cdot i_L - v_C = 0$$
$$i_L - \frac{P_o}{v_C} = 0 \tag{4.3}$$

Solving (4.3), yields

$$v_C = \frac{V_s \pm \sqrt{V_s^{\,2} - 4P_o r_L}}{2} \tag{4.4}$$

$$i_L = \frac{P_o}{v_C}$$

Because the value of the state variables must be real, for the equilibrium points to exist, the following condition must hold

$$V_s^2 - 4P_o r_L \geq 0 \tag{4.5}$$

When the voltage source V_s and cable parameter r_L are fixed, (4.5) specifies a constraint on the maximum output power to the load, which is

$$P_o \leq \frac{V_s^2}{4r_L} \tag{4.6}$$

The load voltage corresponding to the maximum power output is

$$v_C = \frac{V_s}{2} \tag{4.7}$$

Example 1:

Assuming the parameters for the system of Figure 4.1 are V_s = 10 kV, r_L = 1000 Ω (the resistance of 1000 km cable, approximately), the relation curve between load voltage v_C and P_o at equilibrium points is determined by (4.3) and is shown in Figure 4.2.

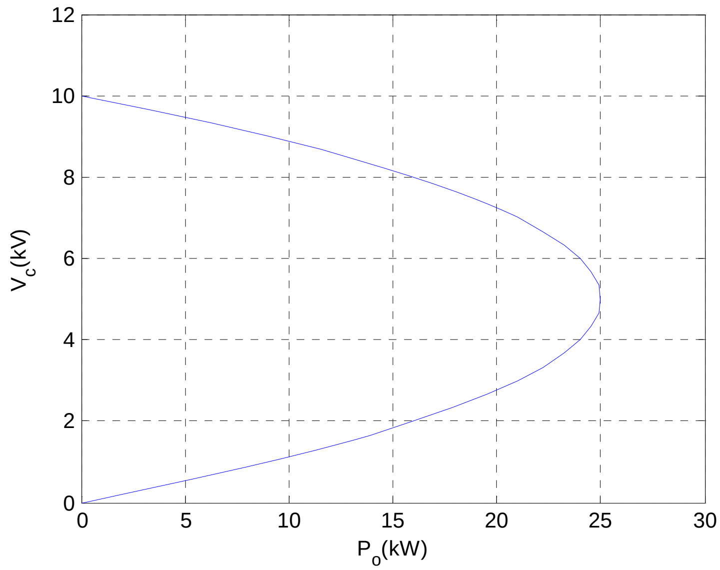

Figure 4.2 $v_C \sim P_o$ curve in the example system

From Figure 4.2 we can see that the maximum amount of power that can be delivered to the load is 25 kW, and the corresponding load voltage is 5 kV.

Other than the situation with maximum power, the system has two equilibrium points according to (4.4) and Figure 4.2. The point with higher voltage and lower current is the preferred equilibrium state. A satisfactory operating condition should be ensured by allowing for a sufficient "power margin."

Note:

Figure 4.2 suggests that the system remains at the preferred equilibrium point as long as the load voltage (V_C) is above one half of the source voltage (V_s). Therefore, reducing or totally shedding the load when V_C falls close to half of V_s will ensure the system's steady-state stability.

The constraint on output power, resulting from the steady-state analysis, essentially results from the law of energy conservation. Satisfaction of this constraint will guarantee the system has an equilibrium point. However, when disturbance occurs, the system will deviate from the equilibrium point. Whether the system can come back to equilibrium is determined by its dynamic stability characteristic. This is discussed in Section 4.1.2.

4.1.2 Dynamic stability

A. Small-signal stability

Small-signal stability is also called local stability or stability in the small. The system is said to be locally stable about an equilibrium point if, when subject to small perturbation, it returns to the original state as time increases (asymptotically stable), or it remains within a small region surrounding the equilibrium point but does not return to the same point (limit cycles). In practice, we are usually interested in asymptotic stability [30].

According to dynamical system theories (Hartman-Grobman Theorem), the stability characteristic of a nonlinear system around its equilibrium is the same as its linearization. Therefore, small-signal stability of a nonlinear system is analyzed by linearizing the system's state equations at the equilibrium point. The stability is given by the linearized system's eigenvalues (i.e., eigenvalues of the nonlinear system's Jacobian matrix).

For the system represented by (4.1), linearizing it at point (I_L, V_C) yields

$$\begin{aligned} L\frac{d\hat{i}_L}{dt} &= V_s - r_L \cdot \hat{i}_L - \hat{v}_C \\ C\frac{d\hat{v}_C}{dt} &= \hat{i}_L + \frac{P_o}{V_C^{\,2}}\hat{v}_C \end{aligned} \tag{4.8}$$

where $\hat{i}_L$ and $\hat{v}_C$ are the small deviations from the equilibrium point (I_L, V_C) the state variables experience after a small disturbance.

The system's Jacobian matrix can be obtained from (4.8)

$$A = \begin{bmatrix} -\frac{r_L}{L} & -\frac{1}{L} \\ \frac{1}{C} & \frac{P_o}{CV_C^{\,2}} \end{bmatrix} \tag{4.9}$$

The characteristic equation of A is

$$\lambda^2 + \left(\frac{r_L}{L} - \frac{P_o}{C{V_C}^2} \right) \lambda + \frac{1}{LC} = 0 \tag{4.10}$$

The condition of small-signal stability is that all roots of the system's characteristic equation have negative real parts. For (4.10), this condition is equivalent to

$$\frac{r_L}{L} - \frac{P_o}{C{V_C}^2} > 0 \tag{4.11}$$

Hence, the constraint for an equilibrium point to be small-signal stable is

$$V_C > \sqrt{\frac{P_o L}{r_L C}} \tag{4.12}$$

Note that V_C must be positive.

The stability depends on the cable parameters and power output to the load. This is shown in the following example.

Example 2:

For the same system of Figure 4.1, assume the cable has the parameters (same as the cable chosen for NEPTUNE):

$r = 1$ Ω/km, $l = 0.3947$ mH/km, and $c = 0.179$ μF/km.

Also assume the cable length is 1000 km:

$r_L = 1000$ Ω, $L = 0.3947$ H, and $C = 179$ μF.

The boundary between stable and unstable equilibrium points is shown in Figure 4.3.

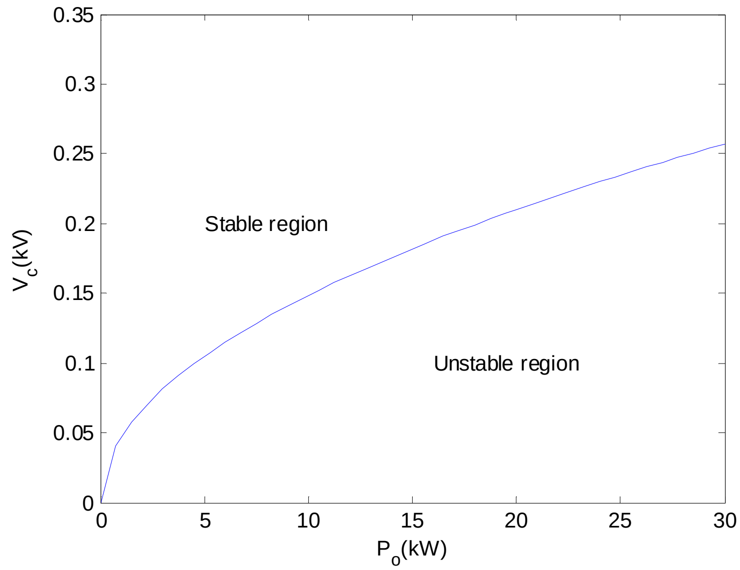

Figure 4.3 Boundary between stable and unstable region in small-signal sense for Example 2

Only the equilibrium points located within the stable region in Figure 4.3 can be reached in the steady state. In Figure 4.4, the stable region boundary curve and the equilibrium point curve of the same system are drawn together, so that those stable equilibrium points can be determined.

It can be seen from Figure 4.4 that most of the equilibrium curve is stable. Therefore, the example system will have two stable equilibrium points with any power output below 25 kW.

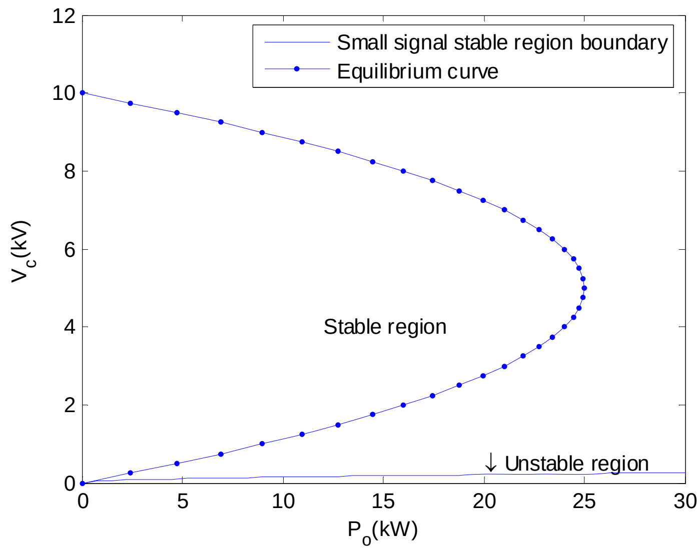

Figure 4.4 Small-signal stable region and equilibrium curve for Example 2

Because the small-signal stable region depends on the cable parameters, it can have a much smaller intersection with the equilibrium curve than is shown in Figure 4.4. This is shown in Example 3.

Example 3:

For the same system configuration as that of Example 2, with cable inductance increased to 39.47 mH/km, cable capacitance reduced to 0.0179 μF/km, and all other parameters remaining the same, the equilibrium curve and stable region can be drawn in Figure 4.5 for comparison.

In the case shown in Figure 4.5, the lower part of the equilibrium curve is located in the small-signal unstable region. It adds another constraint on the maximum power that can be delivered to the load, which is limited to the power at point A instead of 25 kW from the steady-state analysis.

Conclusion:

The maximum power that can be delivered to the load is reduced after considering the small-signal stability requirement under certain circuit parameters.

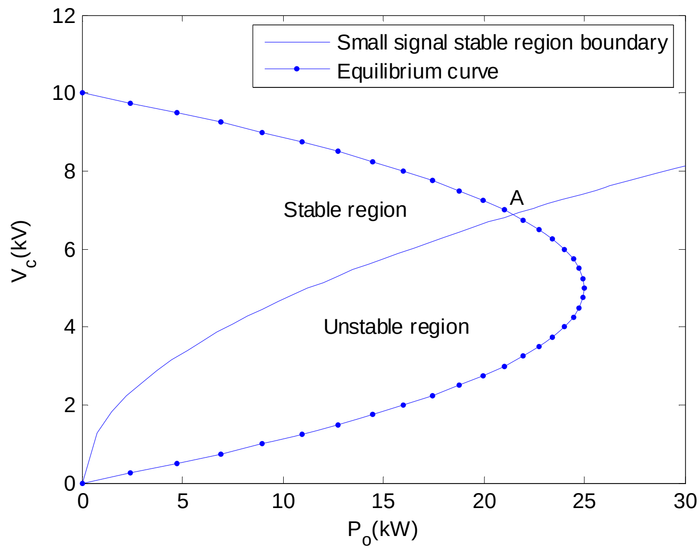

Figure 4.5 Small-signal stable region and equilibrium curve for Example 3.

The relative damping of each root of the characteristic equation of a system can be investigated to determine the system's relative stability. It is measured by the damping ratio ζ of each complex root pair. The classical form of a second order characteristic equation is

$$\lambda^2 + 2\zeta\omega_n\lambda + \omega_n^{\ 2} = 0$$

Hence, we can obtain ζ for the simplified dc power delivery system at equilibrium point through (4.10)

$$\zeta = \frac{\sqrt{LC}}{2}\left(\frac{r_L}{L} - \frac{P_o}{CV_C^{\ 2}}\right) \tag{4.13}$$

With the system parameters of Example 3, the relation between ζ and P_o is shown in Figure 4.6.

We see in Figure 4.6 that a larger output power P_o results in a smaller damping ratio ζ. Hence the system tends to oscillate at very heavy loads. Besides P_o, the damping ratio also depends on cable parameters as (4.13) shows.

Conclusion:

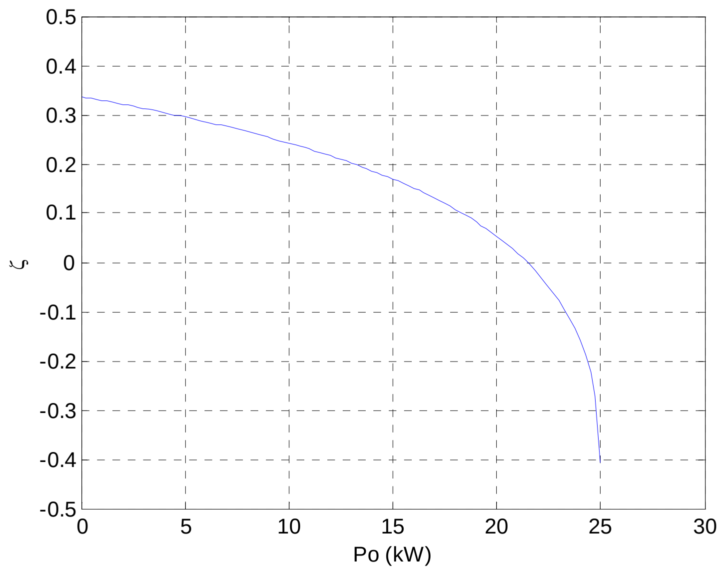

Figure 4.6 Relation between system damping ratio ζ and output power P_o

By examining (4.13), we find the system's damping ratio increases with the increase of resistance r_L and capacitance C, and decreases with larger inductance L and output power P_o. These are helpful guidelines for small-signal stability considerations in system design.

B. Large-signal stability

In a nonlinear system, the system state variables can not reach an equilibrium point from every starting point. The region on a phase plane around the equilibrium point, from where the system can reach equilibrium, is called the system's stable region. Usually caused by large external disturbances, the system can run away from the stable region, thus becoming unstable.

For the example systems, the stable region is determined by circuit parameters including V_s, cable parameters and P_o. The effect of P_o on the system's stable region is revealed by comparison of Figure 4.7 and Figure 4.8. Both figures plot the system's stable region on a phase plane with the inductor current and capacitor voltage being x and y axis, respectively. The system parameters are the same as those of Example 3, except in Figure 4.7 $P_o = 10$ kW, and in Figure 4.8 $P_o = 18$ kW.

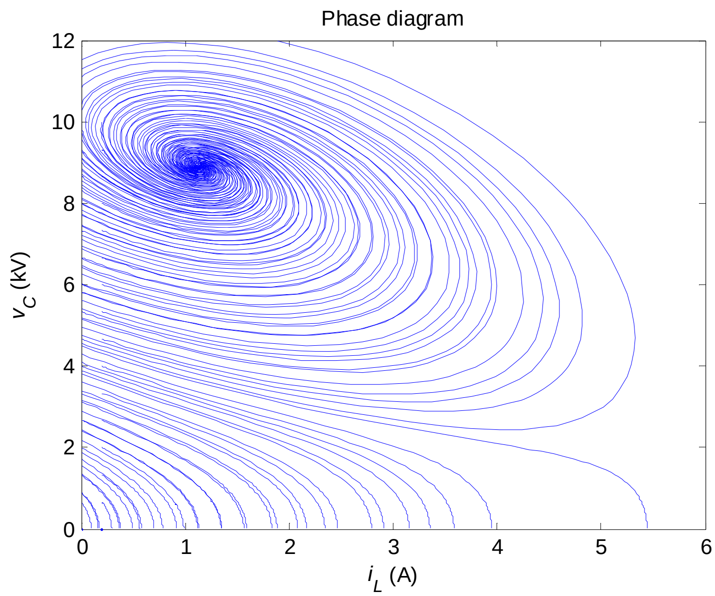

Figure 4.7 Phase diagram showing stable region for the example system with $P_o = 10$ kW

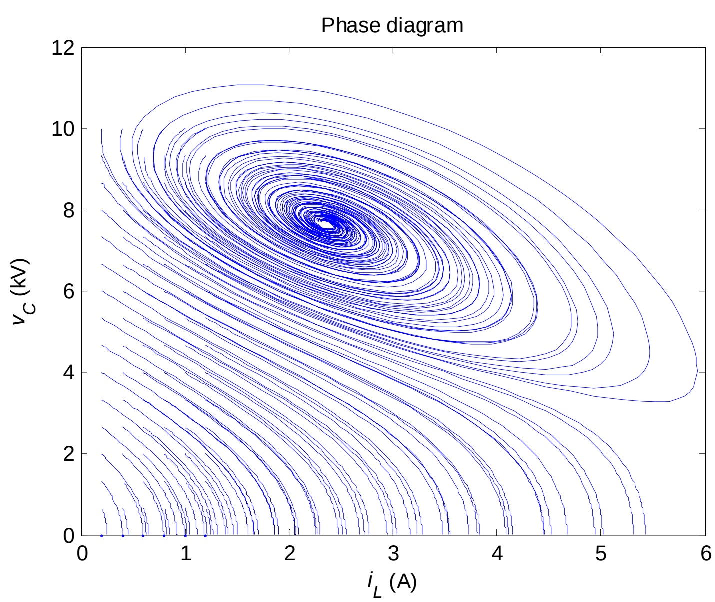

Figure 4.8 Phase diagram showing stable region for the example system with $P_o = 18$ kW

Figure 4.7 shows that if the initial value of i_L is 0 amp, the system will reach the equilibrium point with v_C higher than 5 kV, while in Figure 4.8, v_C tends to crash even starting from 8 kV.

Suppose the system is operating at its equilibrium point when a short circuit fault at the load suddenly occurs. The fault draws a large current from the capacitor (refer to the system circuit diagram in Figure 4.1) and v_C falls to 5 kV when the fault is cleared by protection circuits. We assume the fault clearance is fast so that i_L stays almost the same. Figures 4.7 and 4.8 show that if the normal power output P_o is 18 kW, the system will not be able to return to the equilibrium point, while with $P_o = 10$ kW it will. In conclusion, the system represented in Figure 4.7 can withstand larger disturbances than that of Figure 4.8.

One meaningful system operation design principle derived from the above discussion is that during system startup (right after Vs is turned on) P_o should be zero and then ramp up slowly to avoid going into the unstable region on the phase plane.

This section discussed several aspects that need to be addressed in the stability analysis for a dc power system with constant power load. Based on the discussion of the example systems, the stability of a networked power system similar to NEPTUNE is investigated in Section 4.2.

4.2 Stability analysis of large dc power systems

In a large dc power system, power sources and converters are interconnected and cascaded through cables. The system dynamics are influenced by this wide array of components. The analysis of the several stability aspects observed in Section 4.1 requires more complicated techniques to be used. In this section, the models and approaches for each type of analysis are proposed or summarized to study the stability of a large dc power system such as NEPTUNE. For each analysis, appropriate cable and converter models are first identified, then the approaches are described, and some examples are given to demonstrate the proposed approaches.

4.2.1 Steady-state stability

Section 4.1 discussed how the power delivered through a cable section is limited by its length. To maintain steady-state stability, the power at the load end must be lower than the maximum power that can be delivered. This is an important aspect in making system operating decisions. In the steady-state stability analysis, we are concerned about how far away the system's load level is to the power limit, in other words, the proximity to voltage instability. In a networked power delivery system like NEPTUNE, this type of stability can be analyzed based on the power flow analysis approach, similar to the methods used in ac power systems. Also, the stability under both normal circuit topology and topologies with certain types of defects (e.g., isolated cable sections) need to be studied.

A. Cable and converter models

Equation (4.6) shows that the steady-state power limit at a load is the function of power supply voltage and cable resistance, independent of cable inductance and capacitance. Therefore, in the circuit model for steady-state analysis, only cable resistance needs to be considered.

Converters can be modeled as constant power loads because in the steady state they always maintain constant power output regardless of input voltage changes.

B. V ~ P sensitivity analysis

From Figure 4.4 we observe that along the upper half of the equilibrium curve, load voltage V_c decreases monotonically with the increase of power P_o, and the derivative of V_c with regard to P_o increases monotonically. This suggests we may be able to get the relative position of an equilibrium point on the curve by looking at the derivative of V_c with regard to P_o, in other words, the sensitivity between load voltage and power.

From (4.4) we can get the relationship between load voltage and power at the upper half of the equilibrium curve

$$V_C = \frac{V_s + \sqrt{V_s^{\,2} - 4P_o r_L}}{2} \tag{4.14}$$

Choose the power limit given by (4.6) as the base value and normalize P_o

$$P_o = P_{\max} P^* = \frac{V_s^2}{4r_L} P^* \tag{4.15}$$

Substitution of P_o given by (4.15) in (4.14) yields

$$\frac{V_C}{V_s} = \frac{1+\sqrt{1-P^*}}{2} = V^* \tag{4.16}$$

The sensitivity between V^* and P^* is

$$\frac{dV^*}{dP^*} = -\frac{1}{4\sqrt{1-P^*}} \tag{4.17}$$

Therefore, the mapping from relative power level P^* to $V \sim P$ sensitivity is one to one. We can use $V \sim P$ sensitivity as an indicator for the proximity of P_o to P_{max}. This is an alternative method for steady-state stability analysis. It is explained below how the approach is applied in a network environment.

The relationships between load voltages and currents can be represented using the node admittance matrix

$$\begin{bmatrix} I_1 \\ I_2 \\ \cdots \\ I_n \end{bmatrix} = \begin{bmatrix} Y_{11} & Y_{12} & \cdots & Y_{1n} \\ Y_{21} & Y_{22} & \cdots & Y_{2n} \\ \cdots & \cdots & \cdots & \cdots \\ Y_{n1} & Y_{n2} & \cdots & Y_{nn} \end{bmatrix} \begin{bmatrix} V_1 \\ V_2 \\ \cdots \\ V_n \end{bmatrix} \tag{4.18}$$

where

n is the total number of nodes in the network

Y_{kk} is the self admittance of node k

= sum of all the admittances terminating at node k

Y_{jk} is mutual admittance between nodes j and k

= negative of the sum of all admittance between nodes j and k

V_k is the voltage to ground at node k

I_k is the current flowing into the network at node k

The power drawn from the network at node k is

$$P_k = -V_k I_k \tag{4.19}$$

Note that I_k is the current flowing *into* the network.

From (4.18), we get

$$I_k = \sum_{j=1}^{n} Y_{jk} V_k \tag{4.20}$$

Substitution of I_k given by (4.20) in (4.19) yields

$$P_k = -V_k \sum_{j=1}^{n} Y_{jk} V_j \tag{4.21}$$

At an equilibrium point with a specified load level, the power P and voltage V at every node in the network satisfy (4.21). The effect of power variation at load k on the network node voltages can be shown by linearizing (4.21) at the equilibrium point

$$\Delta P_k = -V_k \sum_{\substack{j=1 \\ j \neq k}}^{n} Y_{jk} \Delta V_j - 2 V_k Y_{kk} \Delta V_k \tag{4.22}$$

where ΔP and ΔV are the small changes of power and voltages, respectively.

Writing the relationship in (4.22) for every node in matrix form, we have

$$\begin{bmatrix} \Delta P_1 \\ \Delta P_2 \\ \cdots \\ \Delta P_n \end{bmatrix} = \begin{bmatrix} \frac{\partial P_1}{\partial V_1} & \frac{\partial P_1}{\partial V_2} & \cdots & \frac{\partial P_1}{\partial V_n} \\ \frac{\partial P_1}{\partial V_1} & \frac{\partial P_1}{\partial V_1} & \cdots & \frac{\partial P_1}{\partial V_1} \\ \cdots & \cdots & \cdots & \cdots \\ \frac{\partial P_n}{\partial V_1} & \frac{\partial P_n}{\partial V_2} & \cdots & \frac{\partial P_n}{\partial V_n} \end{bmatrix} \begin{bmatrix} \Delta V_1 \\ \Delta V_2 \\ \cdots \\ \Delta V_n \end{bmatrix} \tag{4.23}$$

Equation (4.23) is usually written in a simpler form in ac power system analysis as

$$\boldsymbol{\Delta P} = \boldsymbol{J \Delta V} \tag{4.24}$$

where $\boldsymbol{J}$ is called the Jacobian matrix.

With (4.24) we can, therefore, easily compute the expected small changes in V for small changes in P as long as $\boldsymbol{J}^{-1}$ exists. This sensitivity information is useful for estimating the steady-state stability of the system. Equation (4.17) shows that an increase on load power should decrease load voltage when the system is stable. Also, as the load power is close to its limit, $V \sim P$ sensitivity goes up rapidly. Therefore, it indicates instability if a large load voltage drop is accompanied by a small increase of load.

C. $V \sim P$ curves at a particular load

The distance to instability may be measured in terms of absolute load level. The margin is determined by subtracting the power limit by the present load level.

For a network with multiple distributed voltage sources and loads, the power limit at a specific load (referred to as load k) depends on every voltage source and every other load in the system. Using the following algorithm, a $V \sim P$ curve similar to Figure 4.4 can be computed for load k by fixing the source voltages and the power at all other loads:

1) Specify the source voltages and the power level at all other loads P

2) Choose the initial values for node voltages V

3) Choose the load level P_k at load k

4) Obtain the Jacobian matrix using (4.22)

5) Obtain ΔV using (4.24)

6) $V = V + \Delta V$

7) Repeat 4) to 6) until ΔV is small enough

8) Repeat 3) to 7) to calculate different points on the $V \sim P$ curve

We can slowly increase P_k at step 3) when doing the above calculations. If P_k exceeds the power limit at load k, ΔV_k (or $\Delta V_k / \Delta P_k$) will become abnormally large. Thus the limit can be found.

For a network of scale such as the NEPTUNE power system, the number of nodes is 30 to 40. The $V \sim P$ curves can be calculated with real time data, and then the power margin at every node can be determined.

For a larger network with more nodes, a real time stability margin may not be possible to obtain. In this case, a large number of power flow calculations can be executed in advance for different combinations of load levels to make the curves useful for real time operating decisions.

The suggested algorithm is used on the simplified system shown in Figure 4.9, which is the same system as in Figure 3.9.

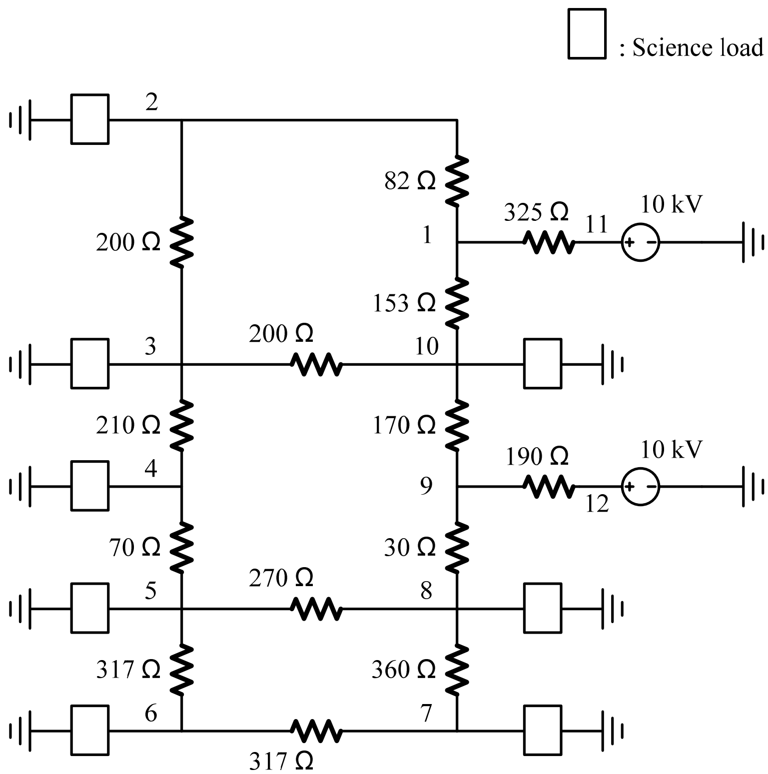

Figure 4.9 A simple dc power network to demonstrate $V \sim P$ relationship

Power flow calculations show that when every load in the system is the same, node 6 has the lowest voltage and voltage collapse will occur at about 15 kW. We set the other loads at 15 kW and draw a $V \sim P$ curve for node 6, which is shown in Figure 4.10.

In Figure 4.10, the abnormal shape at the end of the curve indicates that voltage collapse has occurred.

A group of $V \sim P$ curves of node 6 is shown in Figure 4.11, when the load level of other nodes varies from 0 to 15 kW.

With $V \sim P$ curves as shown in Figure 4.11, the stability margin of node 6 can be easily determined based on the present load level.

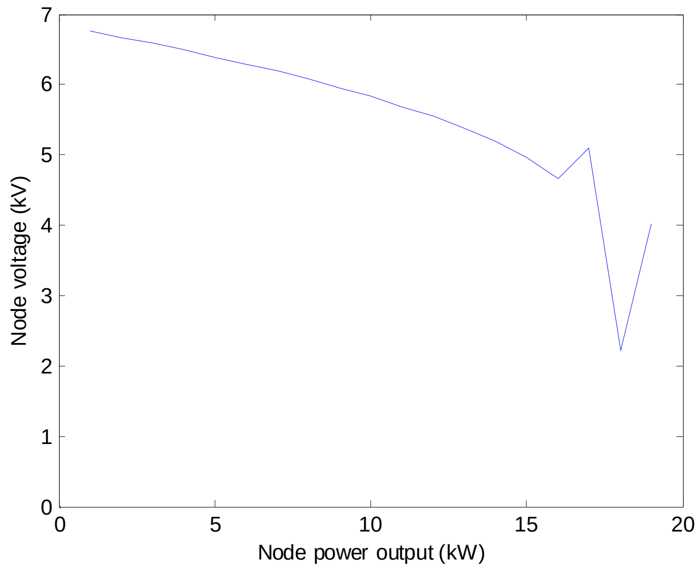

Figure 4.10 $V \sim P$ curve of node 6 in the simplified system when all other loads are at 15 kW

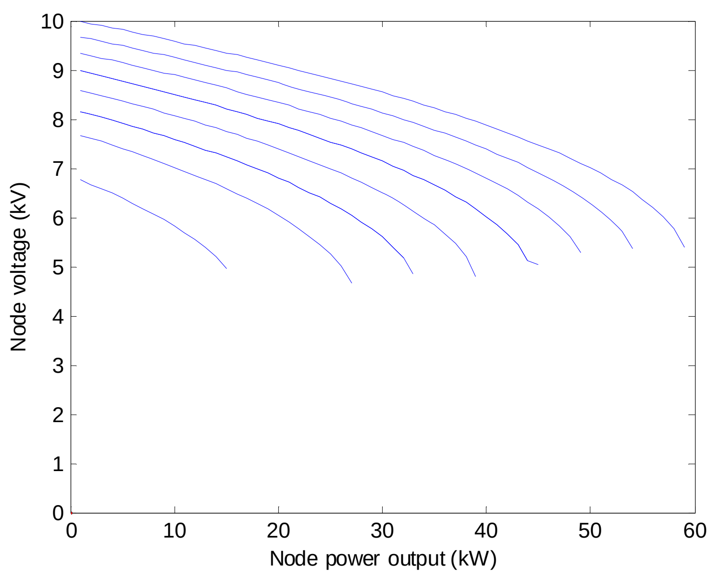

Figure 4.11 $V \sim P$ curves of node 6 in the simplified system when all other loads are at 0, 2, 4, 6, 8, 10, 12, 15 kW, from top to bottom, respectively.

D. Measures to improve steady-state stability

Equation (4.6) shows that the steady-state power limit is determined by power supply voltage and cable resistance. In the design phase of the system, choosing cables with lower resistance will achieve higher power delivery limits, thus steady-state instability is less likely to occur. Increasing the power supply voltages can also increase the power limits, hence, the steady-state stability is improved.

Figure 4.11 shows that voltage collapse occurs at about 5 kV for node 6, no matter the system load level. Therefore, in the science node converter design, a threshold above 5 kV can be determined. Below the threshold voltage, the converter should stop operating to avoid voltage collapse.

4.2.2 Small-signal stability

Small-signal stability problems appear in dc power systems as oscillating voltages and currents at the converters' input or output. It usually occurs when the impedance following the voltage source is large [31], or a converter is powering multiple converters at its output. In this section, appropriate models of cables and converters for small-signal stability analysis are discussed first. A detailed converter model that reveals the converter's frequency characteristics is compared with the simple constant power load model. Then the Nyquist criterion widely used to evaluate stability of cascaded converters is introduced.

A. Cable model

Small-signal stability is a characteristic determined by a system's dynamic response to small disturbances at an equilibrium point. Therefore, cable inductance and capacitance as well as resistance need to be considered. The cable can be modeled either using a distributed parameter model or a lumped-element model. If a lumped-element model is used, the parameters should closely agree with the distributed parameter model for the whole spectrum of frequencies of interest.

The frequency spectrum for small-signal stability study depends on the converter controller bandwidth. Below the controller bandwidth, the converter appears as a constant power load in the system, beyond this frequency, the converter tends to show a characteristic of constant impedance, and hence there is no stability problem.

Again, we use the cable in the NEPTUNE power system as an example.

The 10 kV to 400 V dc-dc converters in NEPTUNE have a controller bandwidth of about 10 kHz. The cable parameters are R = 1 Ω/km, L = 0.3947 mH/km, and C = 0.179 μF/km. The equivalent π circuit of a cable is shown in Figure 4.12.

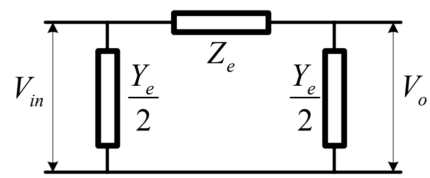

Figure 4.12 Equivalent π circuit of a cable

The parameters in Figure 4.12 can be calculated with

$$\begin{aligned} Z_e &= Z_C \sinh(\gamma l) \\ \frac{Y_e}{2} &= \frac{1}{Z_C}\tanh(\frac{\gamma l}{2}) \\ Z_C &= \sqrt{\frac{z}{y}} \\ \gamma &= \sqrt{yz} \\ z &= R + j\omega L \\ y &= G + j\omega C \end{aligned} \tag{4.25}$$

where l is cable length.

When $\gamma l \ll 1$, Z_e and Y_e can be approximated as follows

$$\begin{aligned} Z_e &\approx zl \\ \frac{Y_e}{2} &\approx \frac{yl}{2} \end{aligned} \tag{4.26}$$

At 10 kHz, for a cable of 1 km, we have

$$Z_e = 0.9090 + j23.6646$$

$$Y_e = j0.0115$$

and

$$zl = 1.0000 + j24.7997$$

$$yl = j0.0112$$

The two pairs of results are close.

When the cable is 2 km, we have

$$Z_e = 1.3163 + j40.8903$$

$$Y_e = 0.0001 + j0.0248$$

and

$$zl = 2.0000 + j49.5995$$

$$yl = j0.0225$$

The difference becomes large.

Therefore, when using small cable sections to model cables in NEPTUNE for stability analysis, the cable section length should not exceed 1 km.

B. Converter model

The constant power load model we a converter used before is an approximation of a real converter. It has a negative resistance effect in the small-signal sense, which is shown by the following.

From the definition of power, neglecting the loss of the converter, we have

$$P_o = V_{in} I_{in} \tag{4.27}$$

where P_o is the converter power output, and V_{in} and I_{in} are the converter input voltage and current, respectively.

In small-signal analysis, linearization of (4.27) gives

$$\Delta P_o = V_{in} \Delta I_{in} + \Delta V_{in} I_{in} \tag{4.28}$$

Then the small-signal impedance of the converter is

$$\frac{\Delta V_{in}}{\Delta I_{in}} = -\frac{V_{in}}{I_{in}} = -\frac{V_{in}^{\ 2}}{P_o} \tag{4.29}$$

The constant power load shows a negative resistance for all frequencies, while the impedance shown by a real converter is frequency dependent.

This section introduces a canonical model for the small-signal study for all types of dc-dc converters.

A physical converter normally can operate in continuous conduction mode (CCM) and discontinuous conduction mode (DCM). The circuit models for the two operating modes are different. However, most of the time, a converter is designed to run in CCM, hence the CCM model is the one of interest here. The canonical CCM model of a converter with its control loop is shown in Figure 4.13 [15, 18]. The model represents, with appropriate expressions for the parameters, any dc-dc converter including buck, boost, buck-boost, and various extensions from the three basic topologies. The parameter values for the three basic converters are collected in Table 4.1 [18, 24].

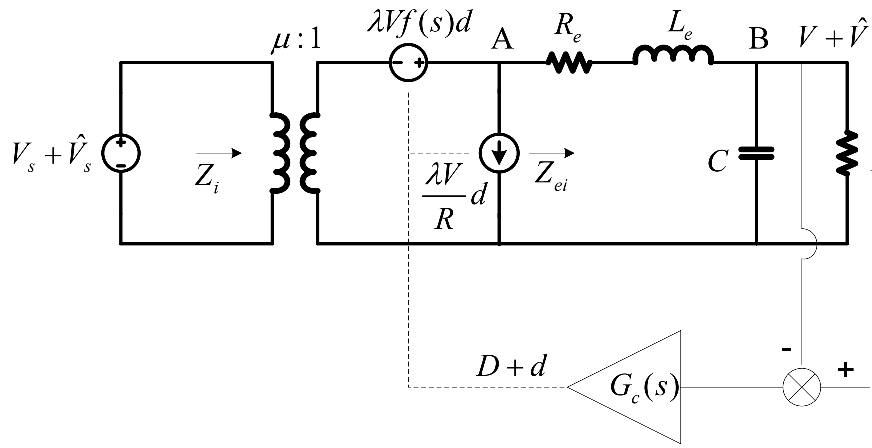

Figure 4.13 A canonical small-signal model for dc-dc converters

Table 4.1 Parameters for the three basic converters in the canonical model

	μ	λ	$f(s)$	L_e
Buck	$\frac{1}{D}$	$\frac{1}{D}$	1	L
Boost	$1-D$	$\frac{1}{1-D}$	$1-\frac{sL_e}{R}$	$\frac{L}{(1-D)^2}$
Buck-boost	$\frac{1-D}{D}$	$\frac{1}{D(1-D)}$	$1-\frac{sDL_e}{R}$	$\frac{L}{(1-D)^2}$

In Figure 4.13, $\hat{V}_s$ and $\hat{V}$ are small variations on V_s and V , respectively. The transformer is an ideal voltage conversion component, which has a ratio μ:1 for all frequencies down to dc. D is the equilibrium value of switching duty ratio, and d is the small variation on D . $G_c(s)$ represents the transfer function of the control circuit, including phase compensation circuit, amplifier and pulse width modulator. The resistance R_e is an "effective" resistance that accounts for various series ohmic resistances in the actual circuit. The element L_e is also an "effective" inductance.

Analysis of the circuit model of Figure 4.13 gives the following results [18]:

The loop gain T, which includes the effect of converter power stage and control circuit, is

$$T = G_c(s)\lambda V f(s) H_e(s) \tag{4.30}$$

where $H_e(s)$ is the voltage transfer function from point A to point B in Figure 4.13.

The converter close loop input admittance is

$$\frac{1}{Z_i} = \frac{T}{1+T}\frac{1}{f(s)}\left(-\frac{1}{\mu^2 R}\right) + \frac{1}{1+T}\frac{1}{\mu^2 Z_{ei}} \tag{4.31}$$

where Z_{ei} is the input impedance seen from point A in Figure 4.13. It includes R_e and L_e in series with C and R in parallel. $\frac{1}{\mu^2 Z_{ei}}$ is therefore the converter open loop admittance.

From (4.29) we can also get the admittance of a constant power load model

$$\frac{1}{Z_i^*} = -\left(\frac{V_{in}^{\ 2}}{P_o}\right)^{-1} = -\left(\frac{V_{in}^{\ 2}}{(V_{in}\mu^{-1})^2 / R}\right)^{-1} = -\frac{1}{\mu^2 R} \tag{4.32}$$

At frequencies lower than the controller bandwidth, the magnitude of loop gain T is large, thus, the first component in (4.31) dominates and Z_i is a little larger but very close to Z_i^*. At frequencies above the controller bandwidth, T falls below unity, therefore, the second component dominates and Z_i is close to $\mu^2 Z_{ei}$. This is the same as the converter input impedance without close loop control. Hence, the converter shows no negative resistance effect at high frequencies and will not cause a stability problem. [18] shows that at some value of loop gain *T*, usually around crossover frequency, the converter can have a more serious negative resistance effect than the constant power load model. Therefore, analyzing stability using (4.32) is not sufficient, and the more accurate form in (4.31) needs to be considered.

C. Small-signal stability criterion

In a dc power system, converters are not connected directly to an ideal voltage source. Between them there can be converter input filters, cables or output impedance of the upstream converter. In these cases, small-signal stability can be analyzed using the Nyquist criterion [18].

Assume the power source has source impedance Z_s, and voltage transfer function $F_s(s)$ when it is not loaded. The converter, as the load, has an input impedance Z_i, and voltage transfer function $F_c(s)$. The system's Thevenin equivalent is obtained as shown in Figure 4.14.

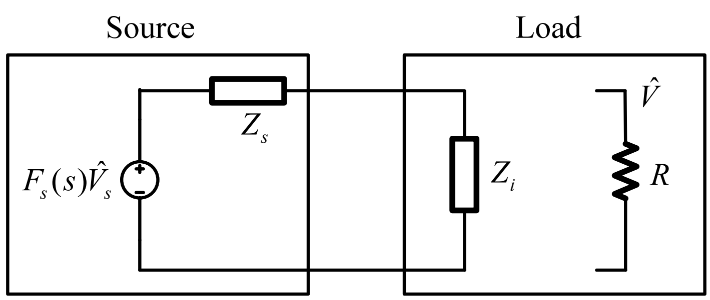

Figure 4.14 Small-signal equivalent circuit for a converter (shown as load) powered by a non-ideal source

Note that in Figure 4.14, Z_i includes the effect of resistance *R* (load of the converter). The voltage on R is

$$\hat{V} = \hat{V}_s F_s(s) F_c(s) \frac{1}{1 + Z_s / Z_i} \tag{4.33}$$

Therefore, the stability of the system can be determined by imposing Nyquist criterion on Z_s / Z_i.

Normally, in converter input filter design, $|Z_s| < |Z_i|$ is made to guarantee converter stability. However, when the converter with an input filter is connected to a voltage source through cables, equivalent source impedance is increased; therefore, potential stability problems may still exist. In a network environment, particularly, the problem is more complicated for the following reasons:

1) The power delivery cables are interconnected

2) The equivalent source impedance is affected by other converters in the system

3) The source impedance varies with load levels

These complications make the application of Nyquist criterion complicated. Methods have been proposed to ensure the stability of large dc power systems [32-36]. In [36], the design of experiments (DoE) method is used to run computer simulations with small-signal models. Frequency responses of the circuit are studied to determine the Nyquist stability margin and identify critical cases. A large number of combinations of system changes, such as load variations and component aging, are considered in DoE.

4.2.3 Large-signal stability

We have discussed the approaches to study stability problems with a dc power system in the steady-state and small-signal sense. Steady-state stability is about whether or not a system has an equilibrium point. Small-signal stability is about whether or not the system can return to the equilibrium point after a small disturbance. In a real system, large disturbances, as well as small perturbations are quite frequent, such as at system startup, short circuit faults, and loss of loads or power sources. These disturbances can cause the system's state variables to deviate largely away from the equilibrium point. If the system is linear, meaning its response is proportional to the amplitude of the disturbance, then a small or large disturbance makes no difference in terms of stability. However, a real dc power system is always nonlinear, partly because the converters are constant power loads, and partly because there are nonlinear functions in the converter circuitry. The nonlinear functions in a converter include switching actions, amplitude limitation in the compensator, over voltage and over current protections, and sometimes nonlinear control functions in the controller. Therefore, a real dc power system is nonlinear, and as shown in Section 4.1.2 C, the system may not be able to return to its equilibrium point after jumping into some region on the phase plane. The system's behavior under large disturbances must be studied to ensure it can withstand the various events happening frequently.

To study the system's large-signal property, computer modeling and hardware verification are used [37]. To simulate a dc power system using computers, one can either build a replica of the real circuit in the simulation software, or represent all or part of the circuit with mathematical functions. The advantage of the first approach is that it is easy to implement, but it usually requires longer simulation time, more powerful computer processors and larger memory. Particularly, when simulating a switching power converter, the converter's switching frequency is usually from tens of kHz to over 1 MHz. A much smaller simulation time step than the switching frequency is needed for accuracy, which can cause simulating a large system to be very time-consuming or even impractical. For this reason, average models have been developed for converters to reduce simulation time, which also makes computer simulations of large dc power systems possible. The cable model for large-signal analysis is the same with small-signal analysis, since it is a linear component. This section discusses the techniques to model a converter circuit for large-signal study. Investigating the system frequency response using the average circuit models built for large-signal analysis generates the same results as using the small-signal models discussed in Section 4.2.2 [38, 39]. Therefore, by just building a large-signal model of the system it is adequate to do dynamic stability analysis. Modeling results for the NEPTUNE power system are shown in Section 4.2.4.

A. Average model of converter switches

A general PWM switch model can be applied to all kinds of PWM converters [22, 23]. As an example, a buck converter, its switching circuit and the switches' large-signal model is shown in Figure 4.15.

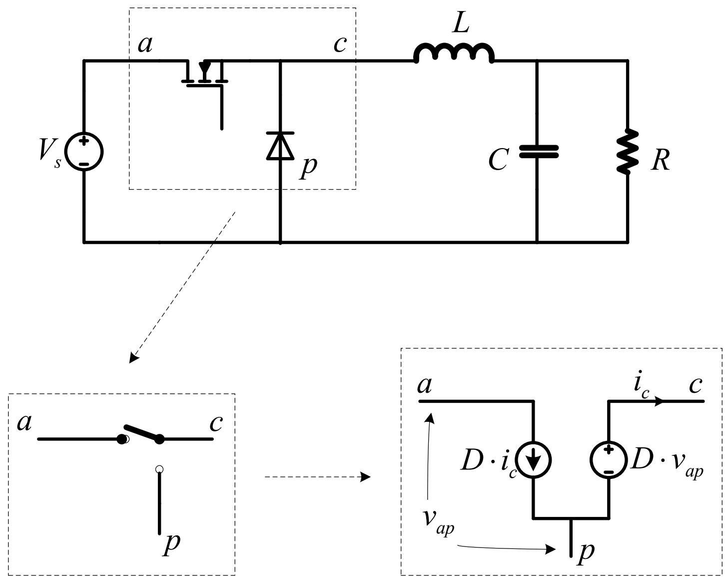

Figure 4.15 Converter switch large-signal average model with buck converter example

In Figure 4.15, the designations *a*, *c*, and *p* refer to active, common and passive, respectively. *c* terminal is the one connecting the energy storage element, which is usually an inductor. *D* is converter PWM duty ratio. It is defined as the portion of time during which *c* is connected to *a* terminal. The model is essentially an ideal transformer with conversion ratio *D*, working under all frequencies down to dc. This general switch model can be used as a basic building block to analyze any PWM converters. When doing small-signal analysis, the model can be linearized at an equilibrium point. The linearized model is omitted here, as we are only interested in using the model for large-signal analysis. In computer simulation, the switches in the converter power stage are replaced with the equivalent circuit of Figure 4.15 so that larger simulation time steps can be used.

B. Average model of voltage mode control

Voltage mode control is the simplest type among converter control approaches. It uses the difference between converter output voltage and voltage reference as the input to the compensator. The output of the compensator is compared with a saw-tooth signal and the comparison result is transformed to duty ration through a flip-flop. The diagram of voltage mode control for a buck converter is shown in Figure 4.16.

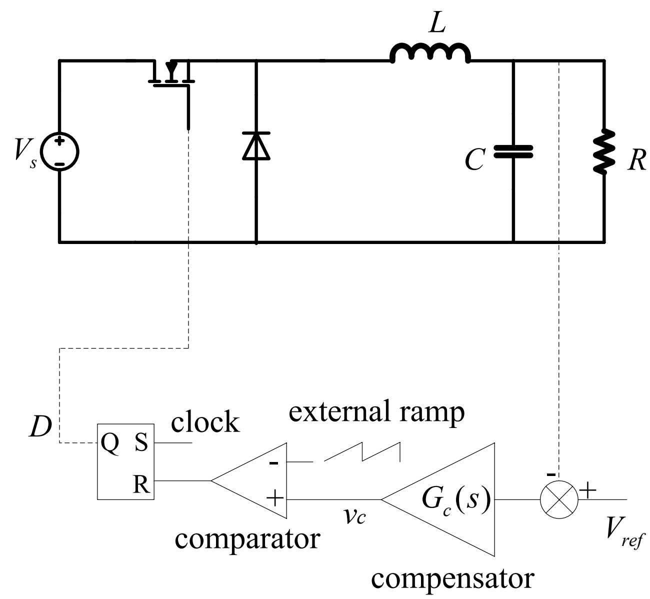

Figure 4.16 Buck converter with voltage mode control

The functionality of the pulse modulator (composed of the comparator and flip-flop) is illustrated in Figure 4.17. The input of the modulator is v_c, and the output is duty ratio D. The duty ratio is determined by

$$D = v_c / V_p \tag{4.34}$$

Therefore the modulator can be modeled as a gain $1/V_p$ with limits of minimum and maximum duty ratio levels.

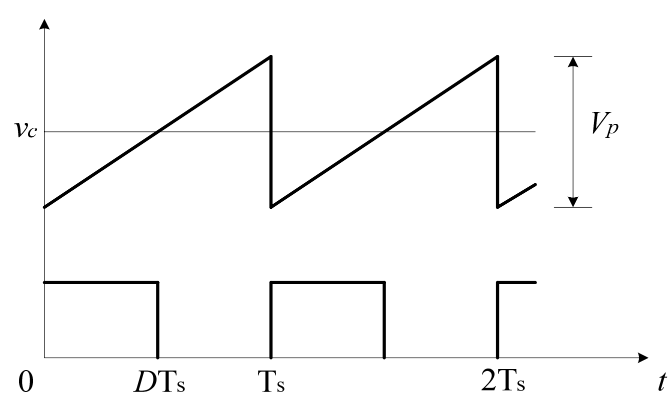

Figure 4.17 Determination of duty ratio for voltage mode control

The functional block diagram of the average model for voltage mode control is shown in Figure 4.18, where

$$F_m = 1/V_p \tag{4.35}$$

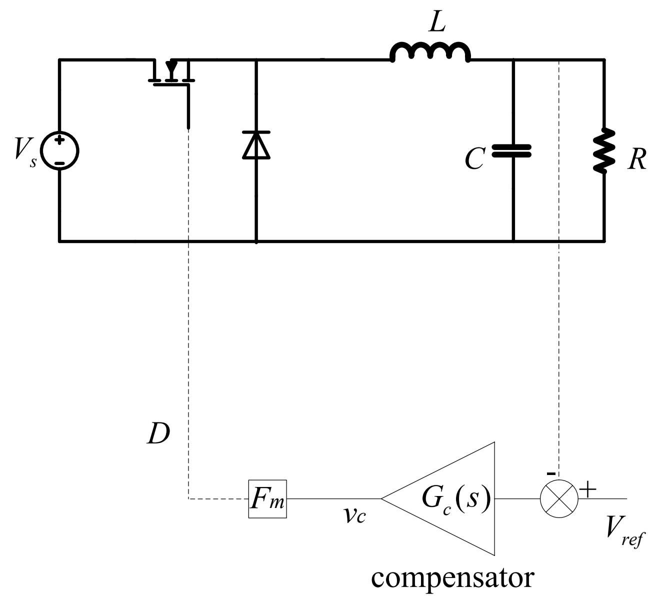

Figure 4.18 Functional block diagram of voltage mode control average model

C. Average model for peak current mode control

A lot of converters employ peak current mode control for its performance on reducing susceptibility to input voltage variations, improving stability and pulse by pulse current limiting [24]. The peak current mode control circuit is shown in Figure 4.19 with a buck converter example.

In Figure 4.19, the signal from the voltage compensator is compared with the inductor current to determine the switching duty ratio. An external saw-tooth signal is added to the current signal to improve stability [17]. The current signal can come from the inductor or the switch. The scheme of peak current mode control is directly relating current information to the pulse modulator. Therefore, an average representation of this part must be developed to obtain an average converter model.

The functionality of the pulse modulator with current mode control is illustrated in Figure 4.20. The relationship between duty ratio D and v_c and i_L is

$$R_i i_L + S_e DT_s + \frac{1}{2} S_n DT_s = v_c \tag{4.36}$$

where $S_e = V_p / T_s$, and $S_n = R_i (V_s - V)/L$ for buck converter. S_e and S_n are the rising slope of the external ramp and real-time inductor current, respectively.

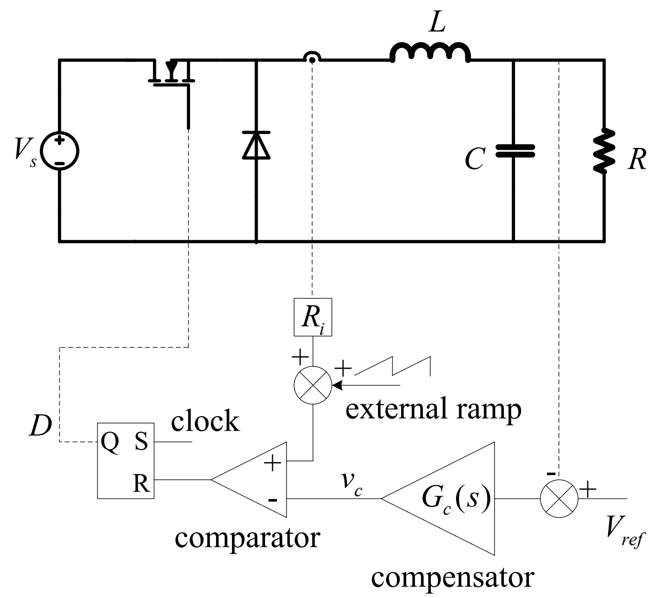

Figure 4.19 Buck converter with current mode control

From (4.36), we get

$$D = (v_c - R_i i_L) \frac{2}{(2S_e + S_n) T_s} \tag{4.37}$$

The functional block diagram of peak current mode control is shown in Figure 4.21, where

$$F_m = \frac{D}{v_c - R_i i_L} = \frac{2}{(2S_e + S_n) T_s} \tag{4.38}$$

More complicated large-signal models than that of Figure 4.21 have been proposed, usually taking into account the circuit structure change (or sampling effect) caused by switching actions [24, 25]. Normally, however, the converter controller bandwidth is far below its switching frequency, about one tenth of it, and above controller bandwidth the converter has no negative resistance effect, therefore no stability issue.

Thus, for the stability study it is not necessary to consider the sampling effect in the converter model.

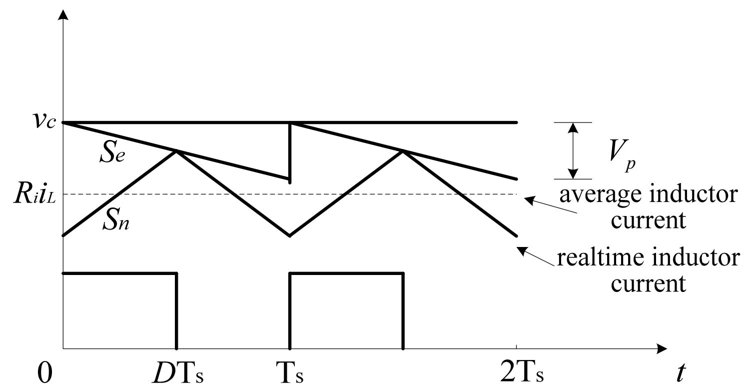

Figure 4.20 Determination of duty ratio for peak current mode control

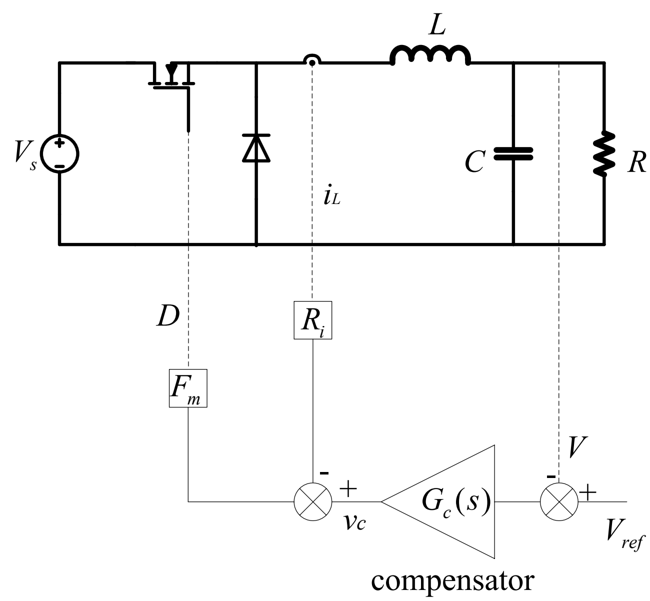

Figure 4.21 Functional block diagram of peak current mode control average model

D. Modeling of other functions in converter controllers

A real converter controller has other functions that will affect its large-signal performance, such as soft start circuit, over voltage shutdown, under voltage shutdown and over current protection. These functions can be added to the converter average model directly without any change from the circuit schematics.

4.2.4 Modeling of the NEPTUNE science node converter

This section presents the modeling results for the NEPTUNE power system science node converter. The model of the converter is built in the circuit simulation software PSIM using the approach described in Section 4.2.3. The simulation results from the model are compared with lab test results to verify its effectiveness.

A. PSIM model of the NEPTUNE power converter

Based on the modeling approaches discussed in Section 4.2.3, an average model was built in PSIM for the 10 kV to 400 V dc-dc converter designed for NEPTUNE. The converter circuit is composed of 48 small converter stages. Each converter stage has 200 V input and 50 V output. The inputs of all the 48 stages are in series. The outputs of eight stages are put in series to compose a module outputting 400 V. Then the outputs of six such modules are paralleled. All the converter stages share the same control circuit. A description of the converter circuit can be found also in Section 5.2.1. The modules for converter power stages and control circuit built in PSIM are shown in Figures 4.22 to 4.25.

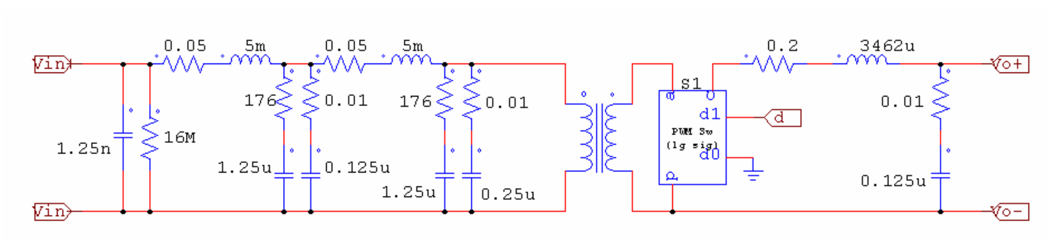

Figure 4.22 Equivalent circuit for an 8-stage converter

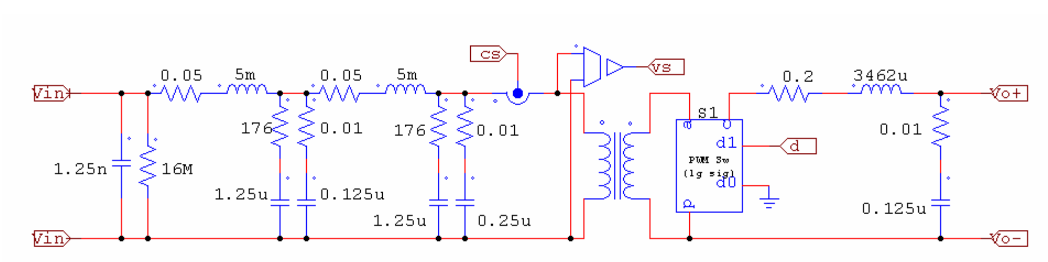

Figure 4.23 Equivalent circuit for an 8-stage converter with voltage and current sensors for control purpose

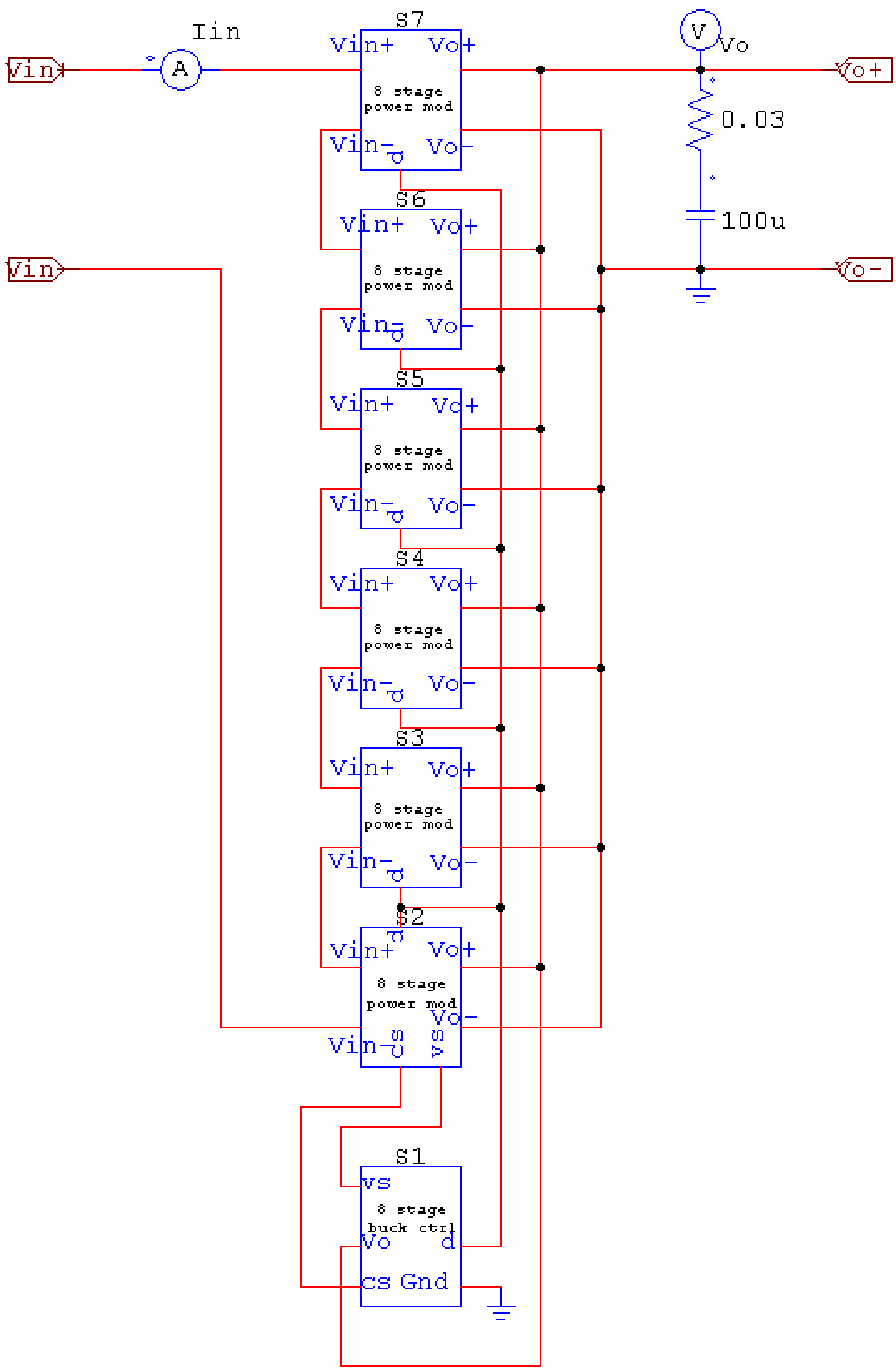

Figure 4.24 10 kV to 400 V converter (48-stage) circuit model

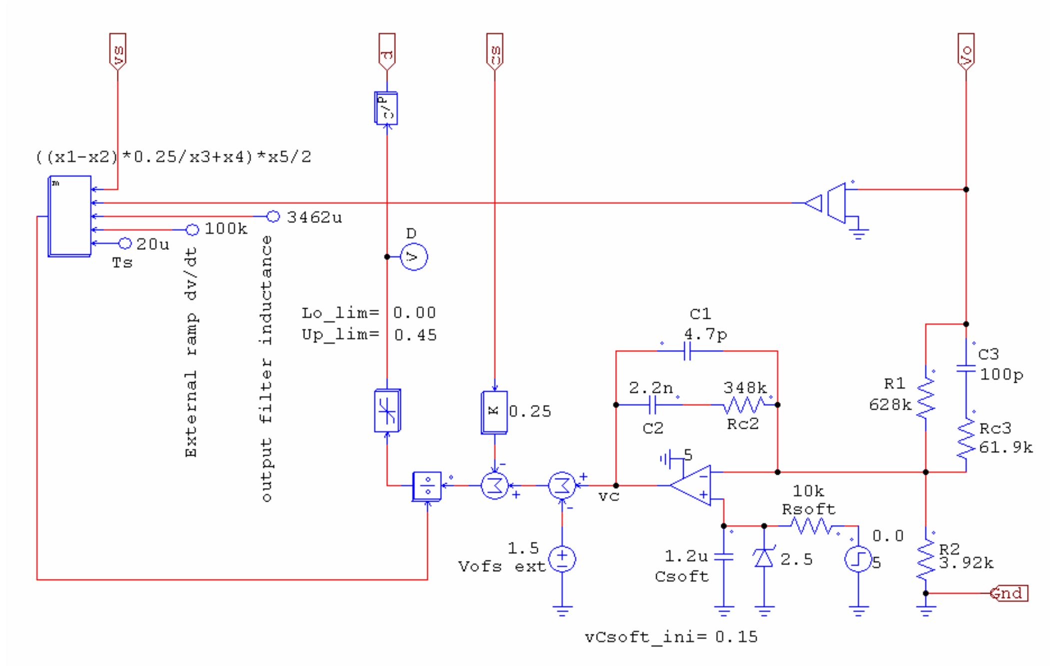

Figure 4.25 Average circuit model for NEPTUNE converter controller

B. Comparison of simulation and lab test results

To verify the model, a simple test circuit was built as shown in Figure 4.26. Comparison between the simulation results and test results are shown in Figures 4.27 to 4.30. The modeling results match very well with the test data.

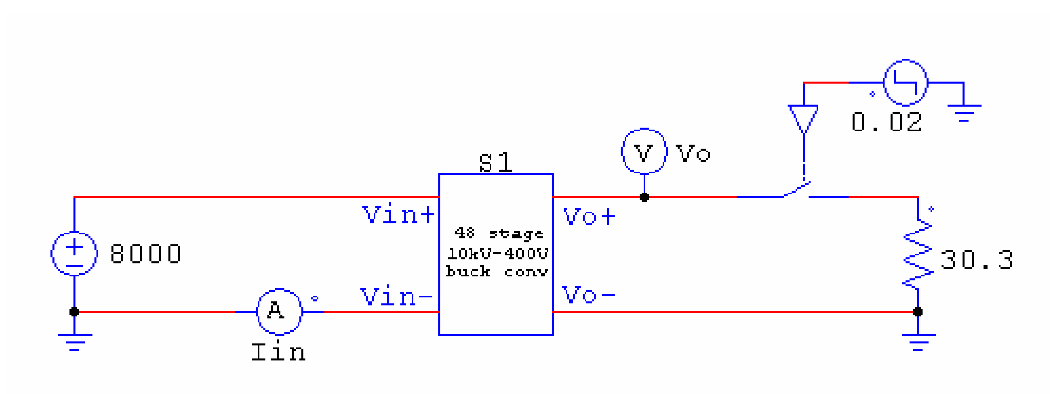

Figure 4.26 Circuit diagram for lab test and simulation

In the test shown in Figure 4.26, the startup transient and step load change transient on the input current and output voltage are monitored.

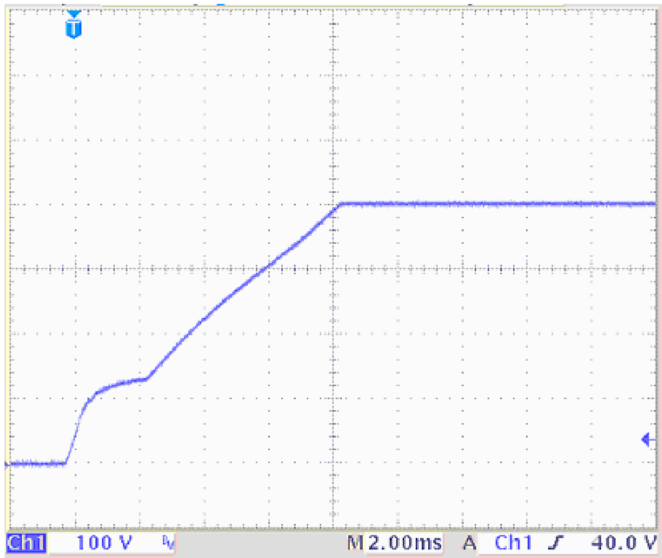

a. Lab test (Scale: 100 V/div)

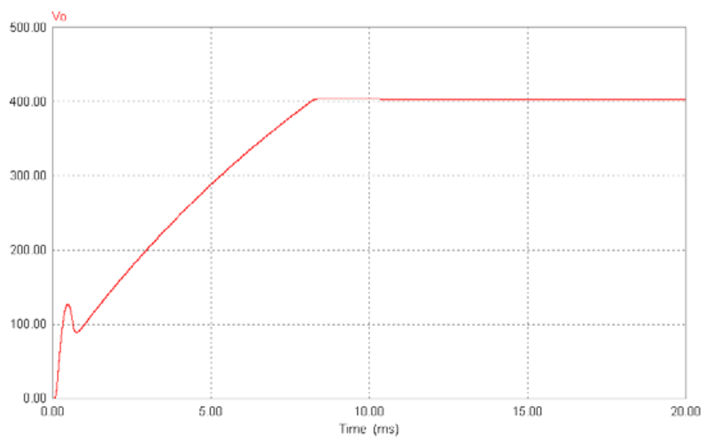

b. Simulation

Figure 4.27 Startup output voltage at no load with $V_{in} = 8$ kV

In Figure 4.27, both results show a startup ramp up time of about 8 ms, and a curl at the beginning. Output voltage of the converter is at 402.38 V, while the simulation result is 403 V.

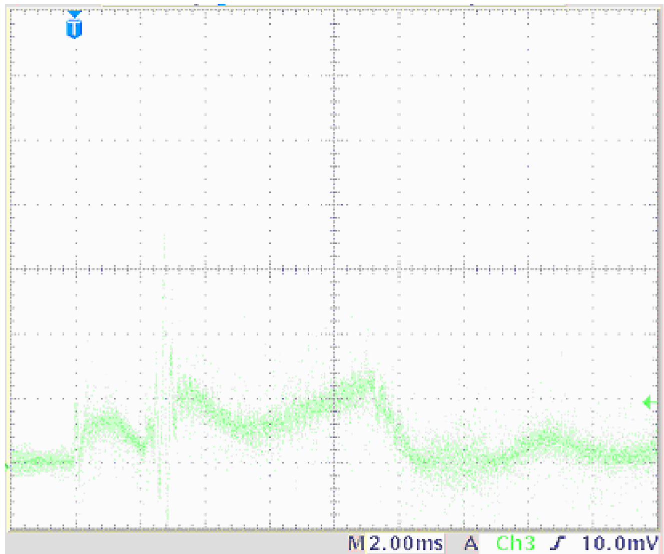

a. Lab test (scale: 250 mA/div)

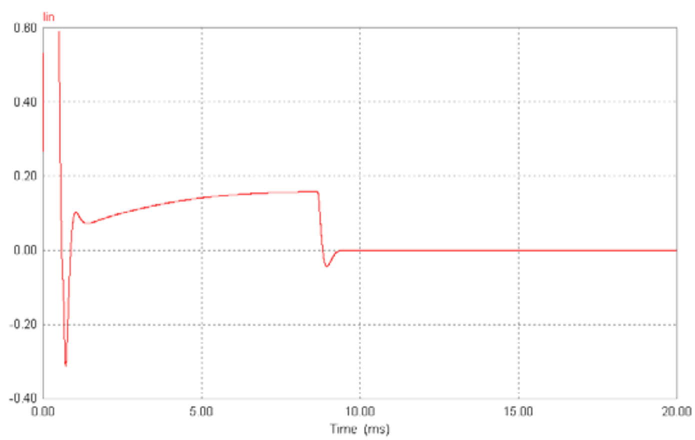

b. Simulation

Figure 4.28 Start up input current at no load with $V_{in} = 8$ kV

In Figure 4.28, both curves show that the converter input current ramps up during startup and reaches a maximum when the output voltage arrives at 400 V.

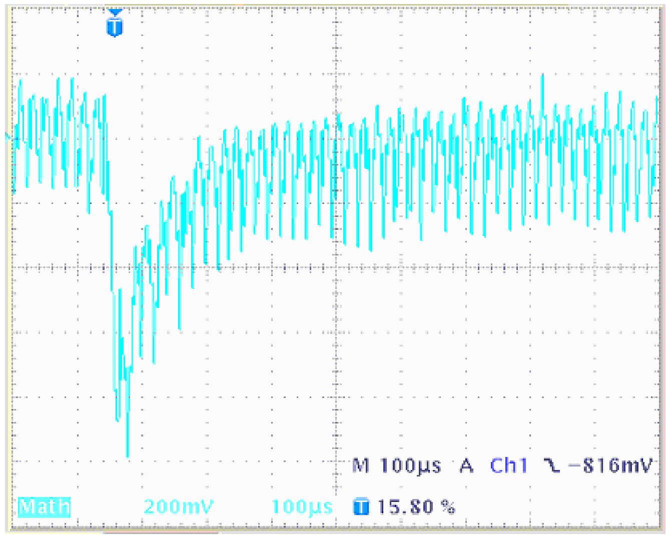

a. Lab test (scale 200 mV/div)

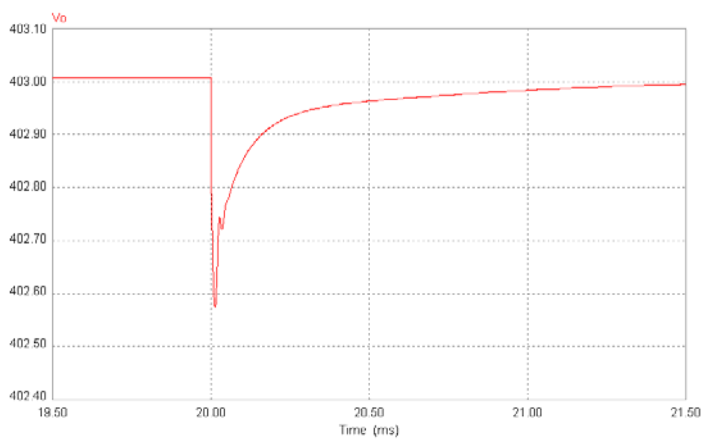

b. Simulation

Figure 4.29 Dynamic load response of the output voltage for a step load 0-5 A with $V_{in} = 8$ kV

In Figure 4.29, because of the model's "average" characteristic, the ripple at switching frequency from the test result can not be seen from the simulation. But the low frequency characteristics of the two curves are the same. Both curves show a voltage drop of about 0.4 V and a recovery time of about 1 ms.

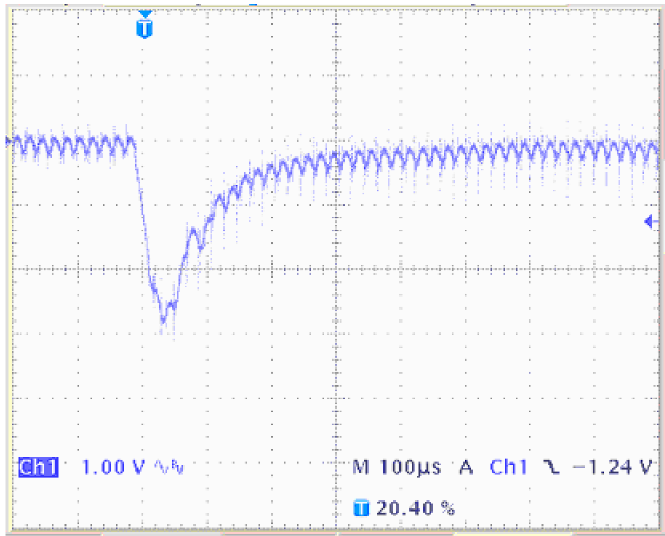

a. Lab test (scale 1 V/div)

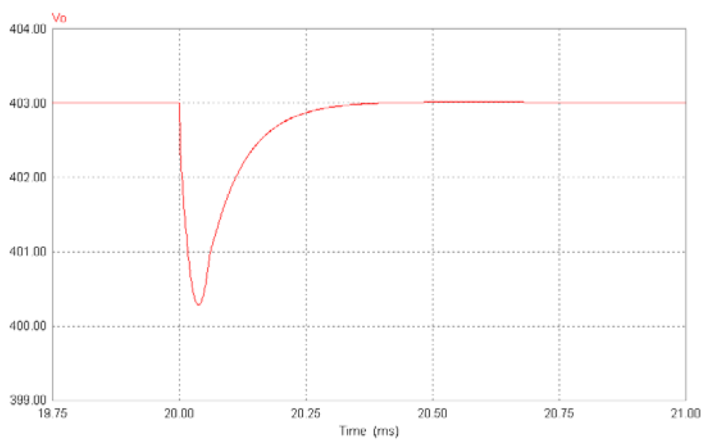

b. Simulation

Figure 4.30 Dynamic load response of the output voltage for a step load 0-13.2 A with V_{in} = 8 kV

In Figure 4.30, both curves show a voltage drop of about 2.8 V and a recovery time of about 0.25 ms.

The comparison between the simulation results and lab test results shows that the model of the NEPTUNE node converter sufficiently represents the characteristics of the real converter. With the node converter model, a model of the entire NEPTUNE power system can be built, and the various effects of system changes including source voltages, load variations and the isolation of cables, can be tested on the model.

4.3 Comparison of stability problems in ac and dc power systems

The stability problem in ac and dc power systems has similarities from the root of the concept. But because of the differences between the power source and load characteristics in the two systems, modeling approaches are different in the stability analysis.

4.3.1 Steady-state stability

Ac system steady-state stability analysis needs to consider both active and reactive power balance. Therefore, the power delivery limit is constrained by all parameters of transmission lines including R, L and C. This is also called voltage stability problem in ac power systems. The reactive power balance appears more influential in ac system voltage stability because the transmission lines have much larger L and C effect than R.

The power delivery limit in dc systems is constrained by the transmission line (or cable) resistance only, because only active power balance is involved.

4.3.2 Dynamic stability

Dynamic stability analysis in ac power systems is mainly concerned with the synchronization between generators, or angle stability. Synchronization is threatened when large variations on the generators' electric power output occurs (e.g., caused by severe faults). The changes on the electric power output can affect the kinetic energy on the rotors, which changes the rotor angle, and in turn affects maximum electric power output. Instability happens when the increased kinetic energy causes rotor angles to shift across the 90^{o} threshold, and reduces the electric power output consequently.

In dc systems there is no synchronization problem between power sources. Although large disturbances will cause oscillations on system voltage and current, the oscillations will disappear shortly if the system is well damped. When the system lacks damping, oscillations can last for a time. If the disturbance is large enough, the system can be drawn into the unstable region, and then experiences a progressive and uncontrollable decline in voltage.

The lack of damping in dc power systems is caused by the negative resistance effect of the power converters (being constant power loads). Therefore, instability is likely to happen when the system is heavily loaded, and it can be solved by adding damping, such as a shunt RC branch, to the system. For comparison, in ac power systems, there are few strict constant power loads, and they are paralleled with a majority of constant impedance loads. Therefore, lack of electric damping is not a major problem in ac power systems.

Because mechanical systems with large time constant are involved in the oscillations in ac power systems, the oscillation frequency is usually below several Hz. At the same time, the oscillation in a dc power system can be up to hundreds of kHz, depending on the scale of the system, because only small time constant electrical systems are involved. Because of this, steady-state power flow calculations can be used in ac systems to obtain the voltages and currents of the power network while analyzing generators stability; in dc systems the cable network model must be simulated together with the converter model to investigate system dynamics.

The eigenvalue approach can be used for small-signal stability analysis in both ac and dc power systems. Because many dc systems are low voltage, comparatively low power and smaller scale, measurement of power source and load impedance is possible, and small-signal stability is usually investigated using Nyquist criterion.

Transient computer simulation is used for both ac and dc power systems to perform large-signal stability analysis. Because the time constant in dc systems with switching power converters is very small (the switching frequency is very high), average models of the converters usually have to be used to simulate larger systems.

4.4 Summary

Analysis of the stability problems in a simplified dc power system, led to categorization of the problems into three aspects: steady state, small signal and large signal. (The last two aspects are also called dynamic stability.) Appropriate models and approaches for conducting stability analysis in a dc power network such as NEPTUNE were described. The steady-state stability analysis approach is proposed by the author since there is not any previous work available. The approaches for small-signal and large-signal analysis were available from the literature because the topic has been well-studied for dc power systems in space stations and computing servers. A large-signal average model with appropriate simplification for the NEPTUNE science node converter was built in PSIM and the simulation results matched well with lab test results. This model, therefore, can be used to investigate the dynamic stability of the entire NEPTUNE power system. Finally, the stability problems in ac and dc power systems were compared to help gain a greater understanding of the issue.

Chapter 5

Branching Unit and Science Node Startup System Design

The infrastructure hardware of NEPTUNE power system has three main components: the power source (shore stations), the delivery network (backbone and spur cables, BUs) and the user interface (science nodes). Among these components, the power source and undersea cables are commercially available. The BUs connecting backbone cables to spur cables are to be designed and built. The BU must implement the system operations described in Chapter 3. The science node is composed of two converters and a power monitoring and control system. This chapter is focused on the design of BU system, and the startup system for the science node converters. The information regarding other components of the science node such as the 10 kV to 400 V dc-dc converters, the 48 V and other low voltage converters, the load management circuit, and power monitoring and control system can be found in [1, 40-43].

5.1 Branching unit system

The BU system has essentially two functions:

1) To connect the backbone and spur cables by closing switches

2) To isolate faulted backbone or spur cables by opening switches

The BU system design involves the configuration of switches and their control circuit to implement the protection scheme under a given set of constraints. Among these constraints are:

1) No direct communication link exists between the BUs, or between BUs and shore stations

2) The energy needed for the switching and control functions in the BUs must be obtained from the backbone cable, which can be as low as 500 V and as high as 10 kV

3) The BU control circuit should use the minimum number of components, and they should be highly reliable

4) The BU control circuit should dissipate minimal power, in order to hold down the internal temperature and thereby allow maximum lifetime

Bounded by these constraints, the BU circuit must be simple, and yet must operate autonomously with enough intelligence to identify and complete the intended operations in various system modes. The design proposed in sections 5.1.1 and 5.1.2 will meet these challenges.

5.1.1 BU circuit for closing switches

The circuit configuration in a BU is shown in Figure 5.1. The BU control circuit can be separated into two parts based on their functions: the circuit to close switches and the circuit to isolate fault. The second part is contained in the controllers L and R underneath the zener diodes in Figure 5.1, which will be discussed in Section 5.1.2.

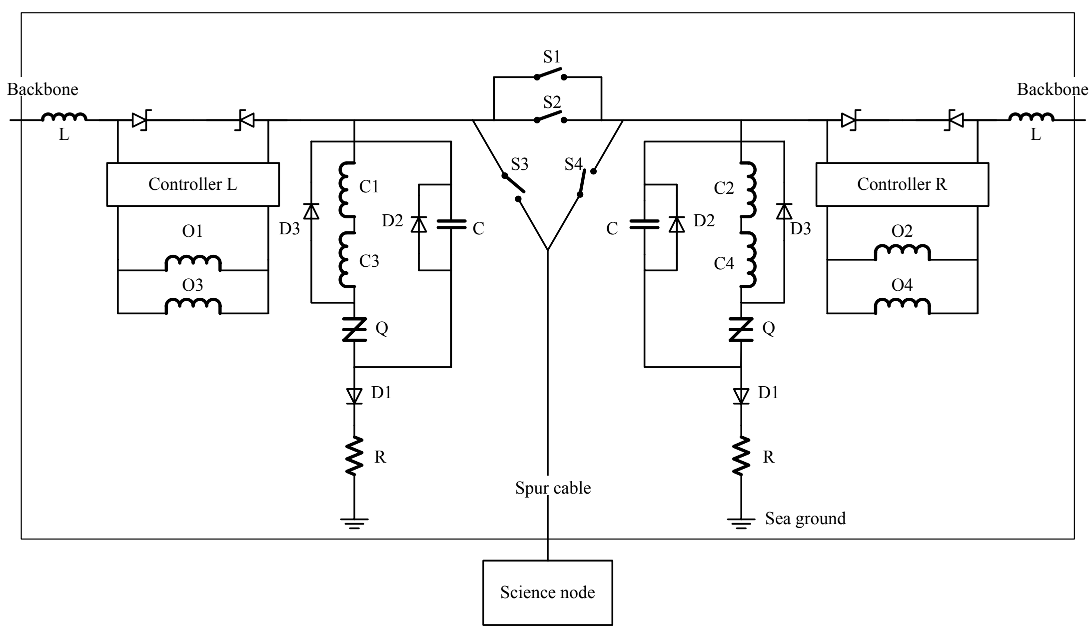

Figure 5.1 BU system configurations

The configuration of the switches and control circuits in the BU are both symmetrical (Figure 5.1). This way, the circuit will perform the same functions when the system is energized to either end.

A. Switching circuit

The BU switching circuit is composed of four high voltage switches connecting two backbone cables and one spur cable. The switches are latching type switches with two operating solenoids: one for closing (C) and one for opening (O). (The latching status is changed when either solenoid is energized.) S1 and S3 are controlled by the circuit on the left side of the switches, and S2 and S4 by the circuit on the right side. The connections between backbone cables or between backbone and the science node are redundant. Two back-to-back zener pairs are in series with the backbone cable to supply power to the BU control circuit. The series inductance L is to protect the zener diodes from possible damage caused by spikes in current in the backbone cable. The science node is connected to the backbone cable through a spur cable.

B. Control circuit

The BU control circuit for closing the switches (Figure 5.1) is the shunt circuit between the backbone and sea ground. Each shunt circuit consists of closing solenoids (C1 and C3, or C2 and C4) for the two switches (S1 and S3, or S3 and S4), a capacitor C, a Silicon Diode for Alternating Current (SIDAC) Q, a resistor R and 3 diodes D1 to D3.

To understand the closing operation of the BU switches, assume that the shore station is on the left side of the BU in Figure 5.1. The shore stations apply a positive voltage in the startup/restoration mode, thus the diode D1 in the left shunt branch allows capacitor C to charge. When the voltage across C reaches the breakover voltage of the SIDAC (V_{br}), the SIDAC conducts. After Q is closed, C discharges its energy into the closing solenoids C1 and C3. Hence, S1 and S3 are closed. After S1 is closed, the closing circuit on the right closes S2 and S4 in the same way. Then the next BU performs the same closing process until all BUs are closed.

In normal mode, the current in the shunt circuit is blocked by the high voltage diode D1. Thus, no closing actions are needed. However, the leakage current of D1 may still charge C slowly and eventually reaches the SIDAC breakover voltage. Then C will discharge through D3, which may damage Q because the discharge current is in the reverse breakdown mode of the SIDAC. This problem is prevented by adding diode D2 in parallel with C. The reverse voltage across C will be limited to D2's forward voltage when the backbone voltage is negative. D3 in the figure is a freewheeling diode for the solenoids.

C. Control circuit parameters

There are several parameters to be determined in the control circuit: SIDAC breakover voltage, charging resistor R and energy storage capacitor C.

SIDAC breakover voltage (V_{br}) should be as low as possible, because the switches can only be closed when the backbone voltage is higher than V_{br}. If there is any fault in the system during the startup mode, the backbone voltage can be very low. On the other hand, V_{br} needs to be high enough to operate the switches.

In choosing the values for R and C, we need to consider the following aspects:

1) The time required to close a single BU, i.e., the period from when the BU is energized to the moment the capacitor C is charged up to V_{br}. It is referred to as "pulse delay time" which must comply with the startup time requirement for the NEPTUNE power system. For example, the whole system needs about 5 minutes to close all switches with each BU taking 15 seconds. In operation the time will be less because the network topology allows several nodes to close at the same time.

2) The pulse generated by discharging C to close the switches must be wide enough to meet the requirement of the solenoids.

3) The energy dissipated from the charging resistor must be small so that the resistor can be housed inside the BUs where heat dissipation is poor. The shore station must maintain the positive voltage for the period needed to close all BUs, and the components must be rated to allow this time to be extended.

Define t_d as the time required to close a single BU, or pulse delay time. t_d is calculated as follows.

From the RC charging circuit

$$V_{bb}(1-e^{-\frac{t_d}{\tau_1}})=V_{br} \tag{5.1}$$

where V_{bb} is the backbone voltage, V_{br} is the SIDAC breakover voltage, and $\tau_1 = RC$.

Thus

$$t_d=\tau_1 \ln\frac{V_{bb}}{V_{bb}-V_{br}} \tag{5.2}$$

The width of the pulse t_w satisfies

$$I_0 e^{-\frac{t_w}{\tau_2}} = I_{th} \tag{5.3}$$

where $I_0 = V_{br}/R_{sol}$, I_{th} is the SDIAC holding current, and $\tau_2 = R_{sol}C$. R_{sol} is the solenoid resistance.

Thus

$$t_w = \tau_2 \ln\frac{V_{br}/R_{sol}}{I_{th}} \tag{5.4}$$

The relationship between the values of R and C and the pulse characteristic is given in Table 5.1.

Table 5.1 Pulse characteristic of BU closing circuit with different RC parameters

#	R (10^5 Ω)	C (μF)	Loss (W)	Pulse delay time t_d (s)	Pulse width t_w (ms)
1	5	170	0.5	11.21	42
2	5	340	0.5	22.4	84
3	2.5	340	1	11.19	84

Note: Loss in the circuit is calculated as $I_R \cdot V_b$ with $V_b = 500$ V.

5.1.2 BU circuit for fault isolation

The circuit must be designed to implement the second function of the BU, which is to isolate the faulted backbone or spur cables by opening its switches. In this section, all the cited time instants t_1, t_2 and t_3 are referring to the corresponding symbols in Figure 3.4.

A. Control circuit for isolating spur cable faults

According to the operation design, spur cable fault is checked in every BU at the end of t_2 in the fault isolation mode. If there is any current flowing in the spur cable in the fault isolation mode, a fault exists in the spur cable. In the circuit implementation, three conditions need to be satisfied to open the spur cable switches:

1) The present operation mode is fault isolation

2) The time t_2 has elapsed

3) There is current flowing in the spur cable.

A schematic of the circuit is shown in Figure 5.2. The first condition is checked by the voltage divider. If the backbone voltage is negative and below 500 V, the system logic is in the fault isolation mode. The timing in the second condition can be implemented using an RC delay circuit in the controller. This delay circuit gives the same delay time t_2 in every BU. The third condition requires sensing the spur cable current. It is done by the optic isolation amplifier in series with the spur cable switches S3 and S4. The current sensing need not be precise since what really matters is the existence of current. The diode anti-paralleled with the optic isolation amplifier is to bypass the optic diode when the backbone voltage is positive, therefore the optic diode does not need to bear high reverse voltages.

When the above three conditions are satisfied, the logic circuits in the controllers L and R energize the solenoids of S3 and S4. Thus the spur cable switches S3 and S4 are opened.

The circuit block diagram shows (Figure 5.3) the voltage sensing, timing and current sensing circuits for checking the these three conditions. The controllers are powered by the back-to-back zener diodes on the backbone. The logic circuit in the controller is sitting at the backbone voltage level. Both voltage sensing and current sensing output are at the same potential, hence no high voltage isolation is required, thus simplifying the implementation.

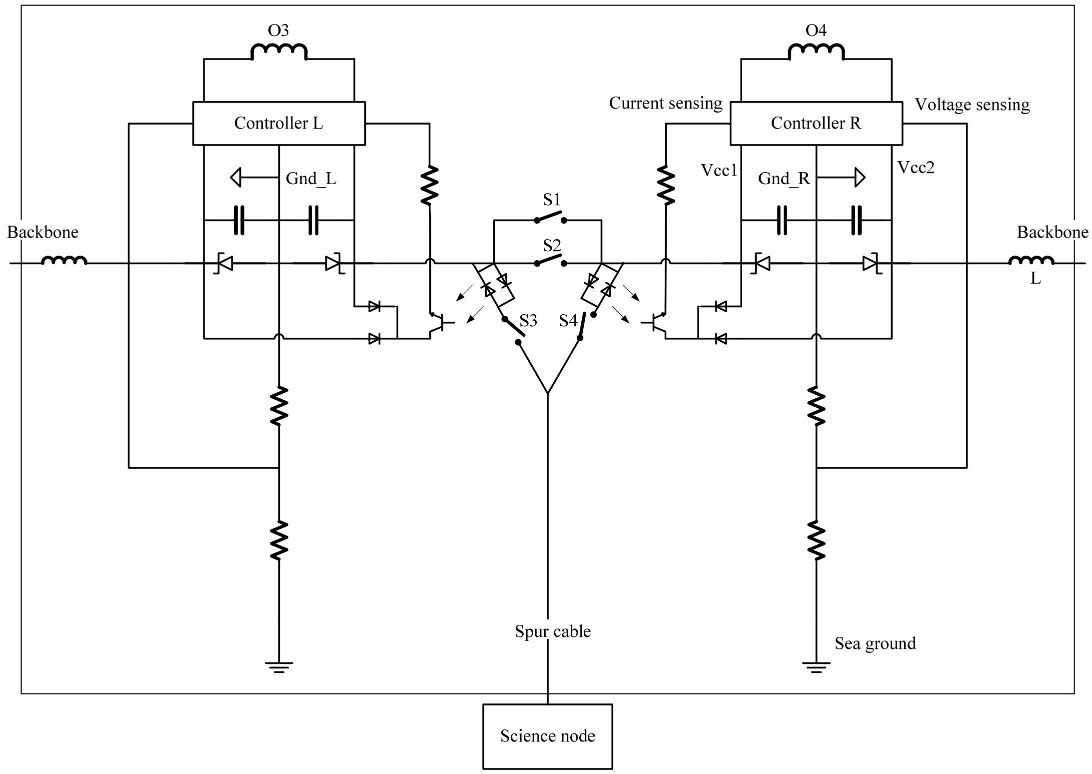

Figure 5.2 BU circuit for opening spur cable fault

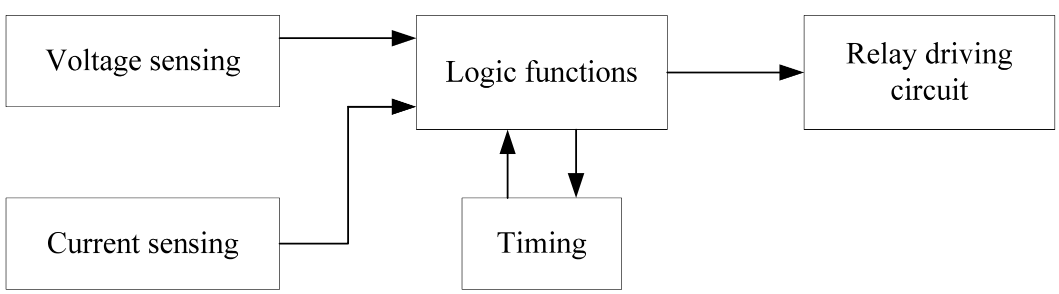

Figure 5.3 Functional block diagram of fault isolation circuit in the BU controllers

B. Control circuit for isolating backbone faults

As addressed in Section 3.3, when the backbone voltage is negative and below 500 V, the BU controllers enter fault location mode and start their timing function.

After t_2 (a preset value for all BUs) has elapsed, all spur cable faults should have been isolated. Then the controller starts another timing process ending at t_3 for fault isolation in the backbone circuit. The value of t_3 is proportional to the voltage at the BU where the controller is located, as shown in (3.1). If no voltage jump and current drop are seen at the BU before t_3, the BU controller opens the switches under its control to isolate the backbone fault. The controllers in all BUs are coordinated based on the voltage and current, instead of exchanging data through a communications system. The circuit schematic for isolating backbone faults is shown in Figure 5.4.

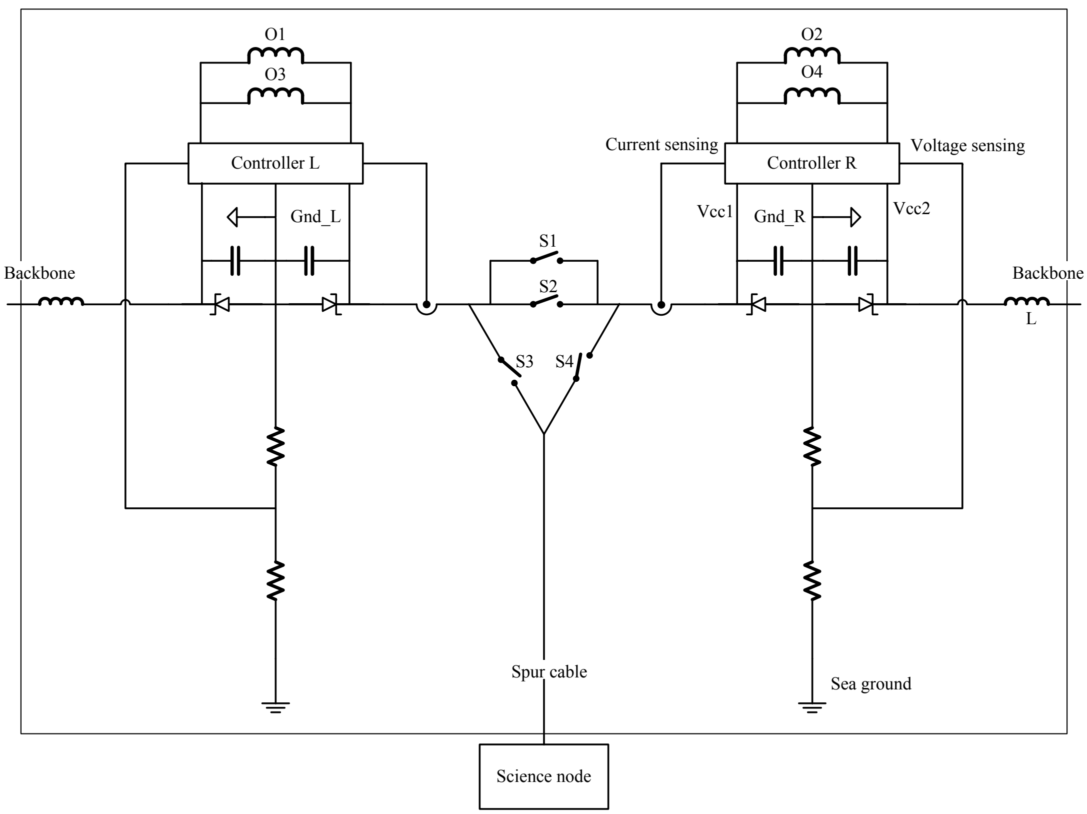

Figure 5.4 BU circuit for isolating backbone cable faults

The circuit includes voltage sensing, current sensing and logic functions inside the controller. When t_3 has elapsed and a BU needs to isolate a fault, depending on which side of the BU the fault is located, switches S1 and S2 and one of the two spur cable switches (S3 or S4) are opened. Thus, the fault is isolated while maintaining the science node connected to one side of the backbone network. The location of the fault and the status of related switches are shown in Table 5.2.

Table 5.2 location of fault and related switch status

Fault location	S1	S2	S3	S4
Left side of BU	Open	Open	Open	Closed
Right side of BU	Open	Open	Closed	Open

The conditions that need to be satisfied to open backbone switch S1 and S2 are:

1) The present operation mode is fault isolation

2) t_3 has elapsed

3) No sign of voltage jump and current drop

Similar to isolating a spur cable fault, the first condition is evaluated sensing the backbone voltage. The value of t_3 is set at the end of t_2 based on the backbone voltage at each BU. A considerable variation of voltage and current, which indicates the fault has been isolated by other BUs, can be caught by a differential circuit. The signal generated by the differential circuit is used to terminate the timing and disable any further operations in the BU.

The conditions that need to be satisfied to open spur cable switch S3 (or S4) are:

1) S1 and S2 are opened

2) The fault is on the left (or right) side of the BU

The circuit functional block diagram is similar to that in Figure 5.3. Again, it can be implemented using a small number of analog components.

5.2 Science node converter startup system

Science node converters provide an interface between the NEPTUNE power system and science users. It converts the high voltage of the backbone to usable low voltages for the scientific sensors.

A block diagram of the science node power system configuration (Figure 5.5) shows -10 kV coming from the backbone via spur cables first converted to 400 V, then to 48 V. The 10 kV to 400 V dc-dc converters in the science nodes accept input voltages ranging from -5.5 kV to -10 kV. Outside this range, the converter is disabled. The maximum power output of the converter is 10 kW [41]. In each science node, there are two 10 kV dc-dc converters, with one of them in cold standby. The converter is designed by JPL [40]. A brief introduction of the converter design is given in Section 5.2.1. For the conversion from 400 V to 48 V, there are commercially available products. The remainder of this section is dealing with the startup procedures of the converters and the associated circuit design.

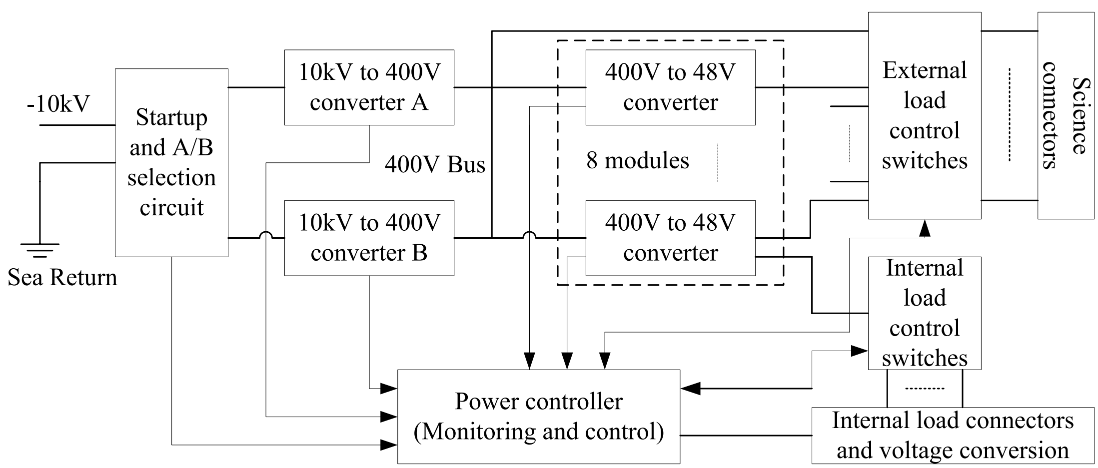

Figure 5.5 Functional block diagram of the science node power system

5.2.1 10 kV to 400 V dc-dc converters

The 10 kV to 400 V dc-dc converter consists of 48 power converter stages. The input side of each stage is connected in series so that every converter withstands 1/48 of the input voltage (approximately 200 V). The output of every converter stage is 50 V. Eight stages are connected in series at the output to give 400 V. Six of these modules are connected in parallel to give an output of 10 kW (total current is 25 A) [41]. The design is a very good embodiment of the methodology: using a large number of low-power and low-cost components to compose a high power system with some redundancy.

Each converter stage is a two-switch forward converter with peak current mode control. The current in the primary-side switches are sensed and compared to the error signal from the voltage feedback amplifier to determine the duty cycle. The secondary side uses synchronous rectification, which keeps the inductor current running in CCM even without load, which is helpful for system stability as well as simplifying the controller design. The configuration of 48 power converter stages is shown in Figure 5.6. The circuit block diagram of a converter stage is shown in Figure 5.7.

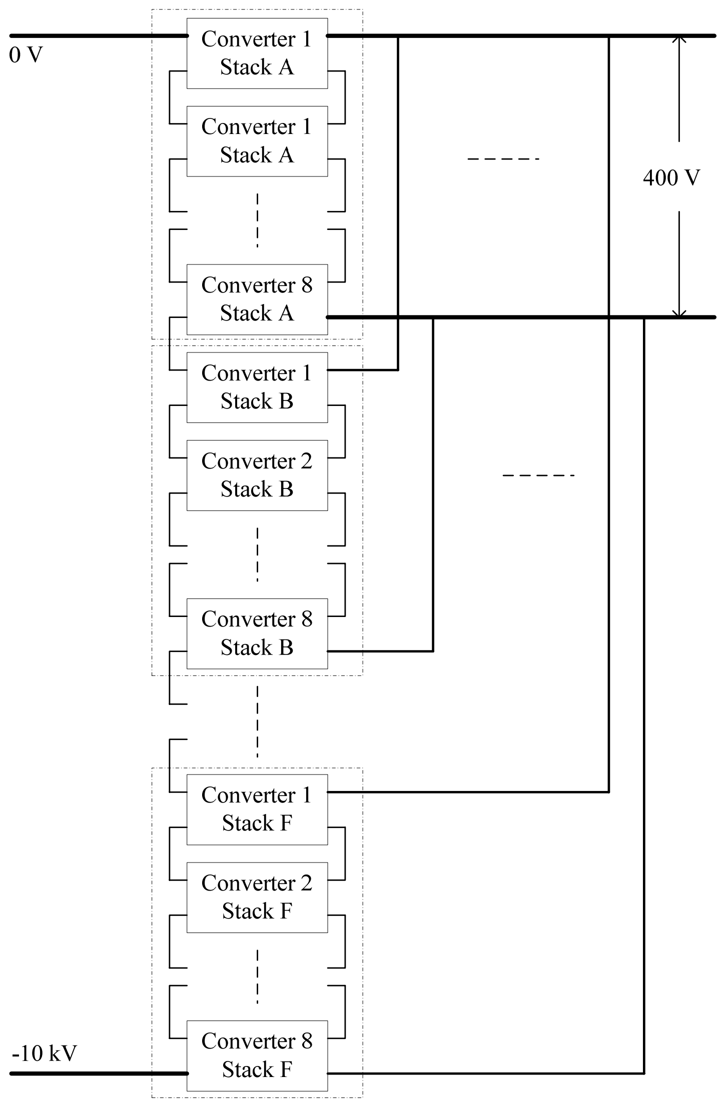

Figure 5.6 Top level block diagram of a 10 kV to 400 V dc-dc converter with interconnections between individual converter stages.

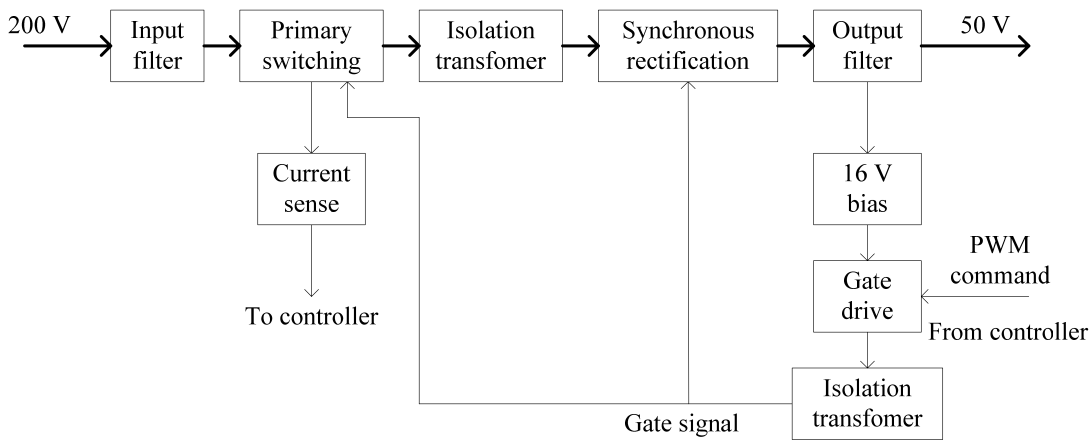

Figure 5.7 Functional block diagram of a 200 V to 50 V power converter stage

5.2.2 Science node startup operations and circuit

In the science node, a set of operations need to be performed before starting up the 10 kV to 400 V converters. These operations include the control of the 10 kV switches connecting the input power cables to the converters, checking converter faults at the converter input, and providing the converters with startup power. This section presents a solution to the startup procedure.

5.2.2.1 Startup operations

The initial startup process is controlled locally by an A/B selection circuit. After one of the two converters starts, 400 V and 48 V are available for the science loads as well as the internal loads such as the power controllers and the communications subsystem.

The converters are connected to the spur cable through the high voltage latching switches (Figure 5.8). The function of the high voltage latching switches S1_A and S1_B is to power the converters or isolate them. The converter is disconnected from V_in when it is not needed, so that less voltage stress is imposed on the components. The 3 kΩ resistor is used to limit the initial inrush current due to the capacitance of the converters' input filters. It is bypassed by S2 after the converter starts. The switches

S1_A, S1_B and S2 are vacuum type latching switches. To extend their lifetime, the control for the switches is designed to operate them at low current.

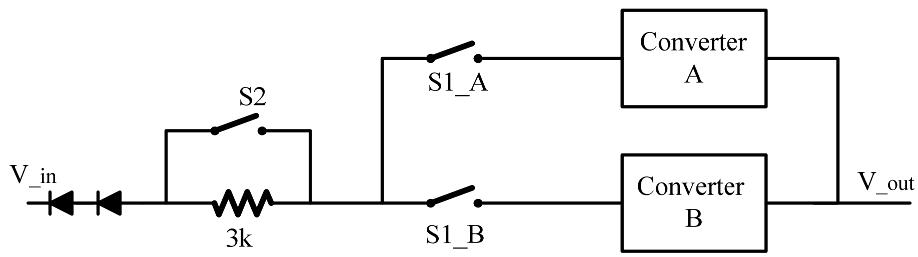

Figure 5.8 Science node converter input configuration

The science node system has to be autonomous during startup because the communications system will not be operational. The challenge is how to inform the science nodes of the intended operation. Some sort of signal must be sent from the shore stations. This is achieved using different voltage levels and polarities at the shore stations as communication signals. The startup sequence of operations is performed, in conjunction with the shore stations, in 11 steps:

1) All switches in Figure 5.8 are latched open when the shore station voltage is set to a positive voltage of about 500 V; the positive voltage is the signal for only this action

2) After a few minutes, the shore station voltage is reversed to about -500 V. This low value of negative voltage is the signal for switch S1_A (only) to be closed

3) Fault condition is checked at the input of converter A. If a fault exists, a non-zero current will flow, and switch S1_A is opened

4) Whether or not a fault is detected, switch S1_B is closed

5) Fault condition is checked at the input of converter B. If a fault exists, switch S1_B is opened

6) The shore station voltage is increased to -10 kV gradually

7) Switch S2 is closed when the voltage reaches -5.5 kV so that the resistor is bypassed before the converter starts

8) The control circuit for converter A is powered

9) If the output voltage rises to 400 V, switch S1_B is opened

10) If converter A cannot start, converter B is turned on and switch S1_A is opened

11) If converter B cannot start, switch S1_B is opened, and the system needs maintenance

Step 1 is to reset the science node power system to a fixed and known pre-start condition. Positive polarity of the operating voltage is used in this step to reduce the possibility of misinterpretation by the science nodes.

In steps 2 to 5, switches are closed to connect the converters to the input power cable unless a fault is detected. Low negative voltage and the 3 kΩ resistor insure that switches S1_A or S1_B are not damaged even if a short circuit exists.

In steps 9 or 10, switch S1_A or S1_B may be opened at high voltage. This is allowed because the converter is started at no load; therefore, the current flowing through the switches is almost zero.

After the above operations are completed, any fault at the input of the converters is isolated during the low voltage period; if one converter fails to start, it is isolated and the other converter starts. If a converter fails during normal operation, the startup operations are repeated to start the second converter.

Logic circuits have been developed to carry out the startup operations. They are presented in Section 5.2.2.2. For convenience, the startup operations in steps 1 to 5 will be referred to as switching logic and operations in steps 6 to 11 as A/B selection logic.

To carry out these operations, a low voltage power supply is required to power the logic functions and to provide startup power to the converters. It is referred to as the converter startup power supply. Specifications and solutions to implement the startup power supply are discussed in Section 5.2.2.3.

5.2.2.2 Logic circuit for startup operations

A. Switching logic circuit

The purpose of the switching logic circuit is to isolate or connect the power cable coming into the science node to the converters, and check if any fault exists at the converters' input connections (right after switches S1_A and S1_B in Figure 5.8). If a fault exists, the related converter is isolated from the input cable. The logic includes different operations at +500 V and -500 V. The functional block diagram of the switching logic circuit is shown in Figure 5.9.

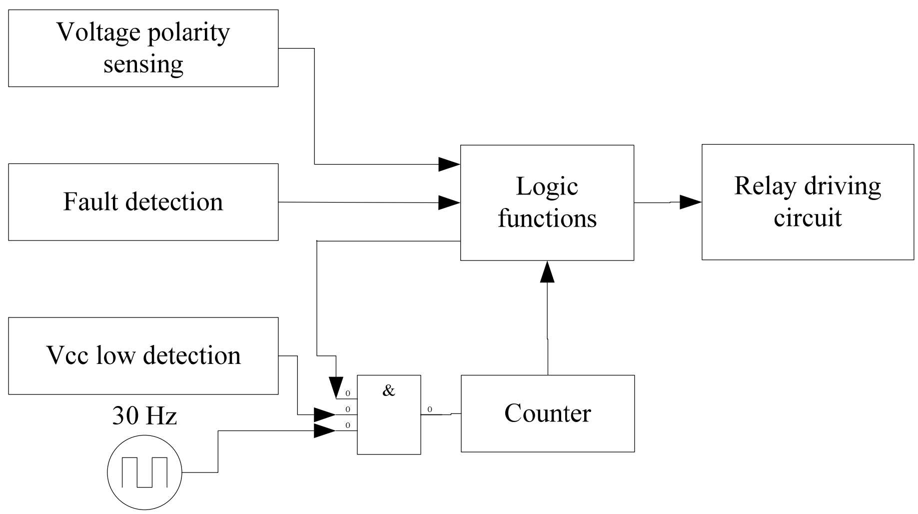

Figure 5.9 Switching logic circuit block diagram

The purpose of the voltage polarity sensing circuit is to use the system voltage polarity to determine which operations need to be performed. It compares the potential of sea ground with respect to the startup power supply voltage, using the fact that when the science node input voltage is positive, the startup power supply positive terminal is about 12 V higher than sea ground, and when the science node input voltage is negative, the positive terminal is at about the same potential of the sea ground [44].

The operation at positive voltage is relatively simple: opening all switches including S1_A, S1_B and S2. At negative voltage, a series of operations must be carried out in the sequence illustrated in Figure 5.10.

The series of operations are implemented using a clock signal, a counter and appropriate logic gates. In every clock cycle, the counter output moves forward one bit, and the logic functions connected to the next counter output are activated and performed. The method is illustrated in Figure 5.11. The operations under negative voltage are carried out from time step t_1 through t_5.

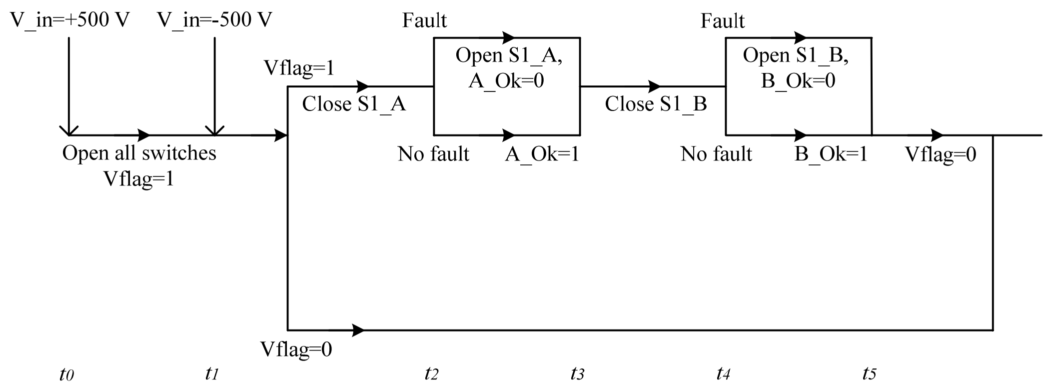

Figure 5.10 Logic sequence for switching operations

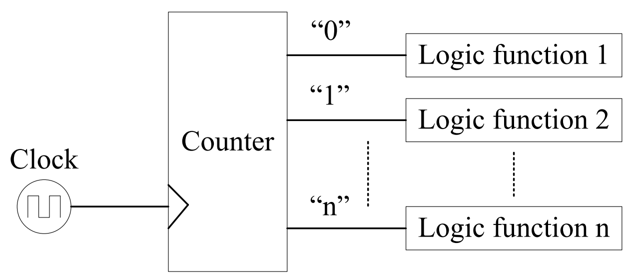

Figure 5.11 Logic sequence implementation block diagram

In Figure 5.10, Vflag is an internal status memory indicating whether or not the operations defined at -500 V have been completed. A_OK and B_OK are two memories indicating the "health condition" of converter A and converter B, respectively. The value and corresponding meaning of the memories are listed in Table 5.3. The information bits of A_OK and B_OK are sent to the power controllers in the science nodes after the whole system starts up and then transmitted to the shore stations. Thus, the converter connection status is known to the control center. These memories are implemented using small-signal latching switches.

The task to check for faults at the converters input is challenging because it is required that a current as little as 1 mA should be identified as fault current when the converter is not operating. Ideally, the current sensing should be connected to the high voltage side to better detect any fault. Presently, no accurate current sensing technique is implemented to detect such a small dc current at 10 kV because it is hard to isolate the current sensing device. A different approach is adopted in the fault current detection circuit (Figure 5.12). The scheme is in fact measuring a voltage signal instead of direct current measurement. Two voltage dividers are used to measure the voltage across the 3 kΩ current-limiting resister when S1_A or S1_B is closed. If any fault exists at the input of the converters, a current will be flowing through the 3 kΩ resistor. A voltage difference V_d will be detected between the outputs of the two voltage dividers. To reduce the heat dissipation at -10 kV, the voltage dividers have a total resistance of 150 MΩ. The output ratio for each voltage dividers is 1:100, so that it is compatible with the logic circuit input when V_in is at -500 V. However, when the fault current is small, V_d is also very small. For example, if a current of 1 mA is flowing through the 3 kΩ resistor, V_d is only 0.03 V. Further, the large output impedance makes it difficult to measure V_d. The two voltage dividers are selected carefully to match each other closely. High input impedance and common mode rejection ratio are required for the amplifier to detect V_d. An accurate instrumental amplifier followed by a carefully designed low pass filter was chosen to complete the task.

Table 5.3 Register values and meanings of switching logic circuit

state	Vflag	A_OK	B_OK
“0”	Switching operations are finished	Converter A has fault	Converter B has fault
“1”	Switching operations are to be performed	Converter A is OK	Converter B is OK

The V_{cc} low detection block in Figure 5.9 monitors the power supply voltage. The power supply has a very slow pulse-like shape [44, 45], and the logic may not be able to complete its sequence during one burst of power, which lasts about 200 ms. When the power supply voltage is below a threshold, the logic operations are disabled.

Knowledge of the status of the circuit is maintained from one cycle to the next with mechanical switches and by powering the counter with an energy storage capacitor. When the next pulse of the power supply comes, the circuit is able to continue carrying out the unfinished logic functions.

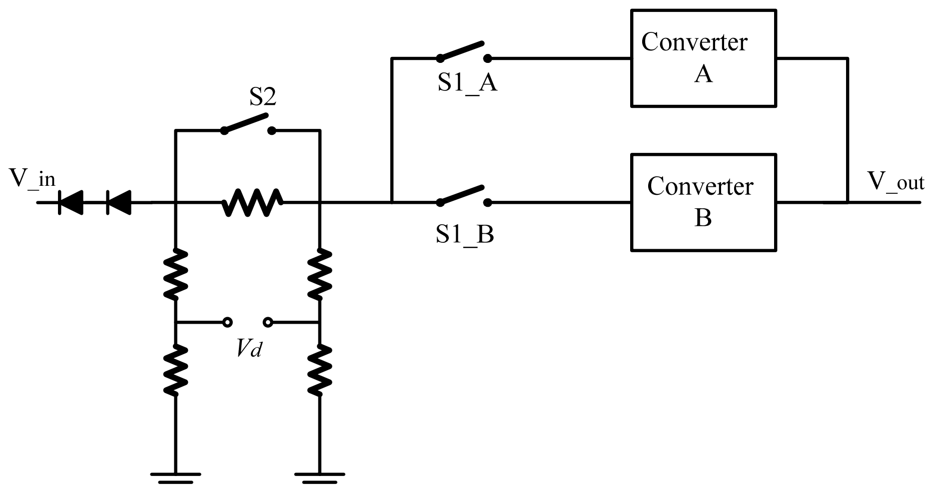

Figure 5.12 Fault detection circuit

The clock signal controls how long each operation in Figure 5.10 takes. A short clock period can reduce the energy consumed by the logic circuit, so that less energy is required from the startup power supply. However, there are constraints for the minimum clock period imposed by the operations. For example, closing or opening vacuum switches S1_A or S1_B requires no less than 10 ms. Also, the initial charging current into converters A or B takes 10 to 15 ms to subside. Therefore, the clock period needs to be longer than this time when using the circuit shown in Figure 5.12 to detect faults.

B. A/B selection logic circuit

The purpose of the A/B selection logic circuit is to start one of the two converters at an appropriate input cable voltage and switch to the other one if the first one fails. The circuit block diagram is shown in Figure 5.13.

The voltage sensing hysteresis circuit monitors the voltage on the input to the science node. When the voltage is more negative than -5.7 kV, the converter is turned on. When the voltage is less than -5.2 kV, the converter is shut off. The converter operation characteristic is shown in Figure 5.14.

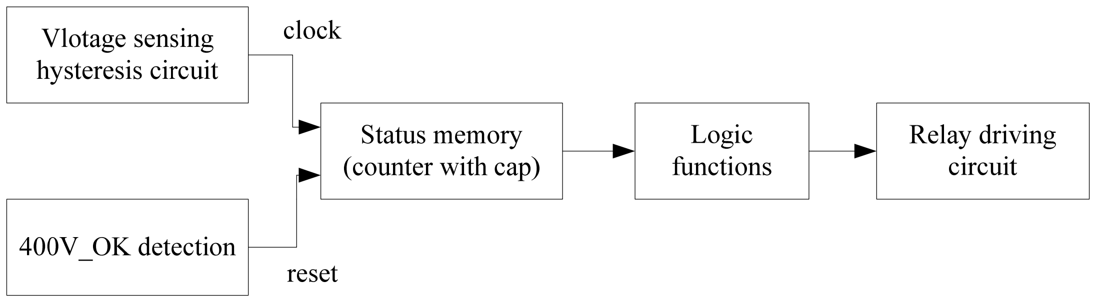

Figure 5.13 A/B selection logic circuit block diagram

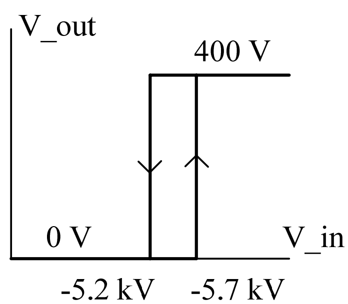

Figure 5.14 Converter input turn on characteristics

After one converter is turned on successfully, the converter house-keeping power supply (HKPS) takes over to energize the logic circuit, and the supply voltage goes up from 12 V to 16 V (Figure 5.15). The 400V_OK detection circuit sees this change as a signal indicating a converter has been started successfully.

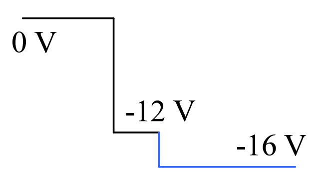

Figure 5.15 Power supply waveform when a converter is started successfully

Each time the science node power system starts up, converter A is tried first. If converter A does not start, either because a fault is detected and S1_A is opened, or because the converter fails, the logic circuit starts converter B at the next pulse of the startup power supply. The status of the converters is maintained during the interval of two power supply pulses. A counter supported by a large energy storage capacitor is used as a memory for this purpose. The output from the voltage sensing hysteresis circuit acts as the clock signal to trigger the counter.

The logic functions of the A/B selection circuit are as follows (see also Figure 5.16).

1) When the input voltage goes more negative than -5.7 kV, a positive pulse from the voltage sensing hysteresis circuit is sent to the counter. Hence the counter output moves forward to “1”, and the 10 kV switch S2 is closed to bypass the current limiting resistor. Then the PWM control circuit of converter A will be energized. After converter A outputs 400 V correctly, the counter is reset to “0” by the 400V_OK detection circuit. S1_B is opened to isolate converter B from the input voltage.

2) If for any reason, converter A does not start, the counter stays at “1” waiting for the next power pulse. The next time the startup power supply comes up, the counter receives a clock signal from the voltage sensing hysteresis circuit. Its output moves forward from “1” to “2”, and converter B starts. When converter B outputs 400 V, S1_A is opened to isolated converter A from the input cable.

3) If converter B does not start either, the counter output moves to “3”, and S1_B is opened; both converters have failed to start and the science node needs to be repaired.

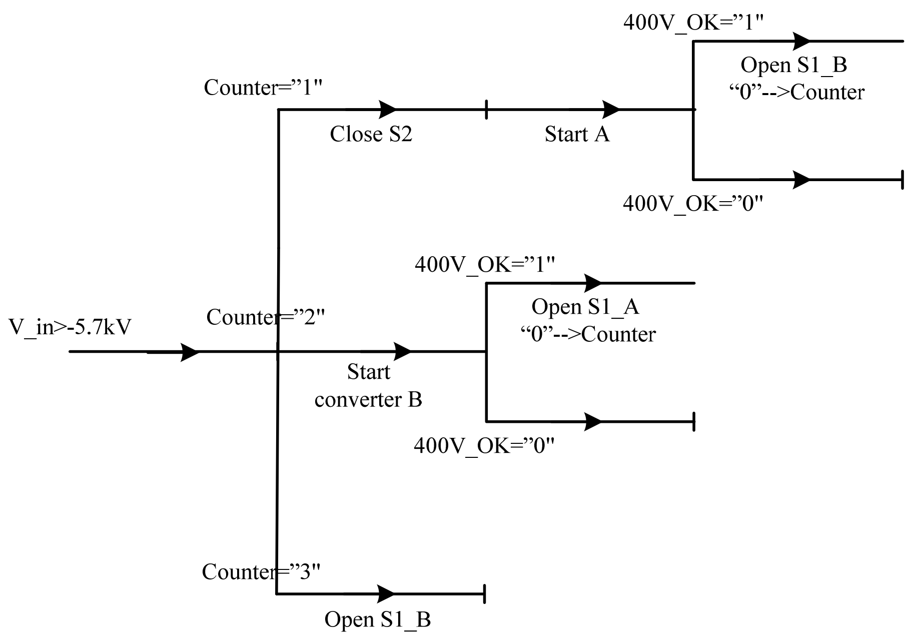

Figure 5.16 Logic sequence for converter A/B selection

The lab test results are shown in Chapter 6.

5.2.2.3 Converter startup power supply

The converter startup power supply must receive its energy directly from the backbone system when the voltage is in the range of 500 V to 10 kV. The output of this supply is 12 V with reference to the sea ground to power the various logic and MOSFET driving circuits. The continuous energy of the supply is about 0.16 Ws with an energy burst of about 40 W for 4 ms. Because of the location on the seafloor and the wide input voltage range, the startup power supply in the science node is a challenge to design. In the following, some commonly used converter startup techniques are reviewed, and their applicability to the NEPTUNE power system is discussed. Then a startup power supply design solution is presented.

A. Available converter startup techniques

Generally, a high voltage converter uses a HKPS to power its control and switching actions. However, before a converter starts, HKPS can not provide energy. Hence, there must be a temporary energy source for the control and driving circuits at the beginning of their operation. With the switching of power semiconductors in the converter, the HKPS gets its energy from an auxiliary winding of the converter's main transformer or the converter's output. Several known converter startup methods are discussed below [46-49].

Figure 5.17 shows the control circuit bias voltage supported by an energy storage capacitor. The capacitor receives its charging current from the input line via a startup resistor. After the capacitor is charged to a preset threshold voltage, the control circuit starts switching. The startup current is provided via both the startup resistor and the bypass capacitor. The voltage across the capacitor will eventually drop because of the discharging action but it must always be above the under voltage lock-out (UVLO) threshold, which is usually several volts lower than the first threshold voltage. The value of the resistor and the bypass capacitor need to be chosen appropriately so that they can supply the control circuit with the maximum required startup current and avoid triggering UVLO.

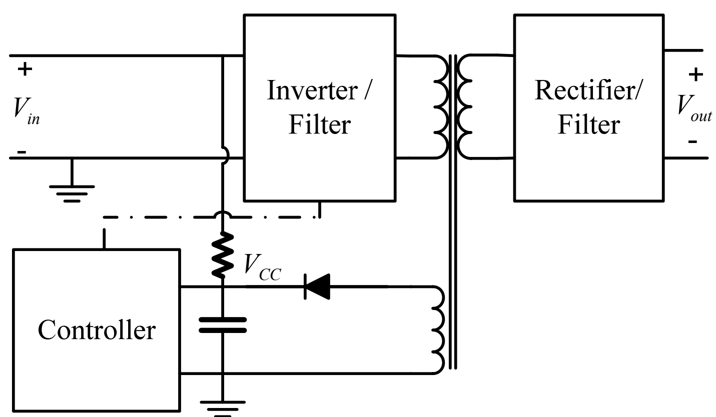

Figure 5.17 Converter startup circuit 1

It is easy to see that when large startup current is needed, small startup resistors and larger energy storage capacitors have to be used, which leads to low efficiency and large sized components.

Adding a linear regulator (Figure 5.18) improves the efficiency of the startup circuit. Thus, larger value startup resistors can be used and the size of the capacitor can be reduced. But this configuration is not suitable for high input voltage because the transistor must withstand the entire input voltage.

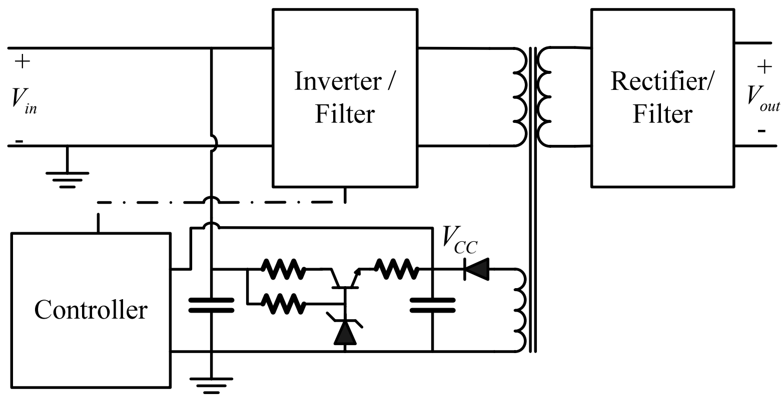

Figure 5.18 Converter startup circuit 2

Another method to generate a startup bias voltage involves a relaxation circuit composed of a startup resistor, a capacitor and a voltage regulator (Figure 5.19). The RC circuit is followed by a diode ac switch (DIAC). The DIAC blocks the current until the voltage across it reaches its breakover voltage (V_{br}), and then a pulse is generated. The energy in the capacitor is used by the voltage regulation circuit to power the initial switching operations until the auxiliary winding starts to generate output. This method does not require large capacitors or small startup resistors. In addition, the transistors only withstand low voltages. The drawback, however, is the complexity of the circuit. Also, because the DIAC ratings are usually small, it is not useful when large startup current is needed.

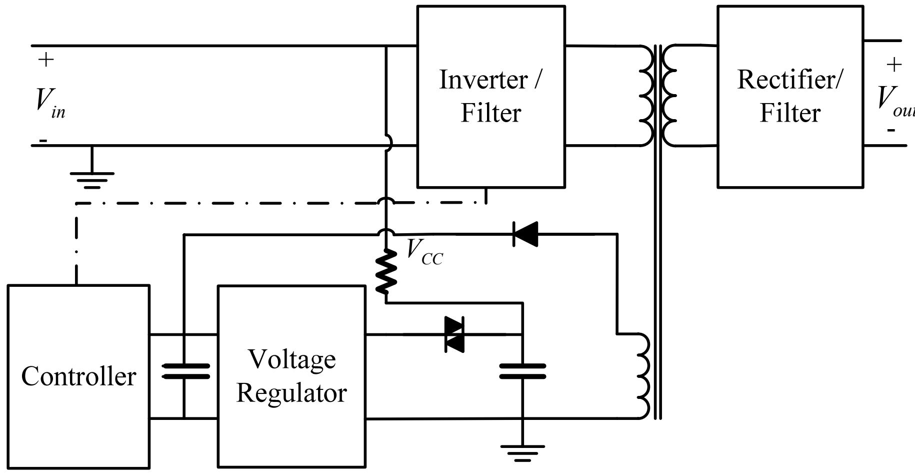

Figure 5.19 Converter startup circuit 3

A technique that is more suitable for tapping power from a high voltage input and providing large startup current uses a more complex relaxation circuit (Figure 5.20). A programmable unijunction transistor (PUT) is used to trigger the thyristor connecting the energy storage capacitor and the voltage regulation circuit. The capacitor C_1 is charged through R_1. When the PUT anode voltage reaches a point set by R_2 and R_3, the PUT gets into its conduction state, and the thyristor is triggered. The voltage regulation and isolation circuit can be a low power forward or fly back converter.

For the 10 kV converters used in NEPTUNE, more than 3 A at 12 V is needed for 4 ms to drive the MOSEFTs of the converters. This is a relatively large amount of power for commonly used converter startup techniques. The 10 kV voltage of the system poses another challenge that requires the use of multiple components or components that can withstand higher voltage. Moreover, the designed operations of the system demand that the startup circuit functions correctly for the range of 500 V to 10 kV.

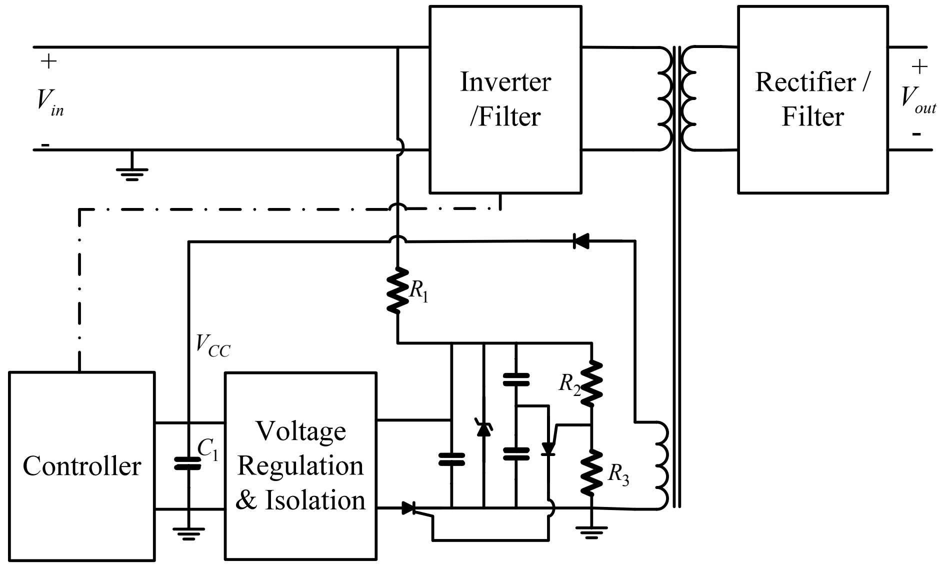

Figure 5.20 Converter startup circuit 4

Among the aforementioned startup techniques, the last one is the most applicable because of its high efficiency and capacity to provide large startup current. However, the circuit is very complex with a large number of components. The reliability is therefore impacted. A design that addresses the particular requirements for NEPTUNE application is needed.

B. Startup power supply circuit designed for NEPTUNE

The startup power supply circuit designed for NEPTUNE's 10 kV converters (Figure 5.21) is composed of a relaxation circuit and a linear regulator. At positive voltage, the capacitor C_1 is charged through R_{12} because diodes D_1 through D_{10} are conducting. At negative voltage, it is charged through both R_{11} and R_{12}. D_1 to D_{10} are small current 2.5 kV diodes put in series to withstand reverse voltage at -10 kV. A smaller size can be achieved this way than using bulky high voltage diodes. Resistors R_1 to R_{10} are used to balance the voltage across the diodes. R_{11} is a high value to limit the charging current of C_1. The RC circuit together with the SIDAC forms a relaxation circuit. The SIDAC is a voltage controlled semiconductor switch that closes at its V_{br}, which is 60 V in this circuit. Therefore, when C_1 is charged up to V_{br}, the SIDAC closes and the energy stored in C_1 is released to the linear regulator formed by R_{14}, D_{15} and Q_1.

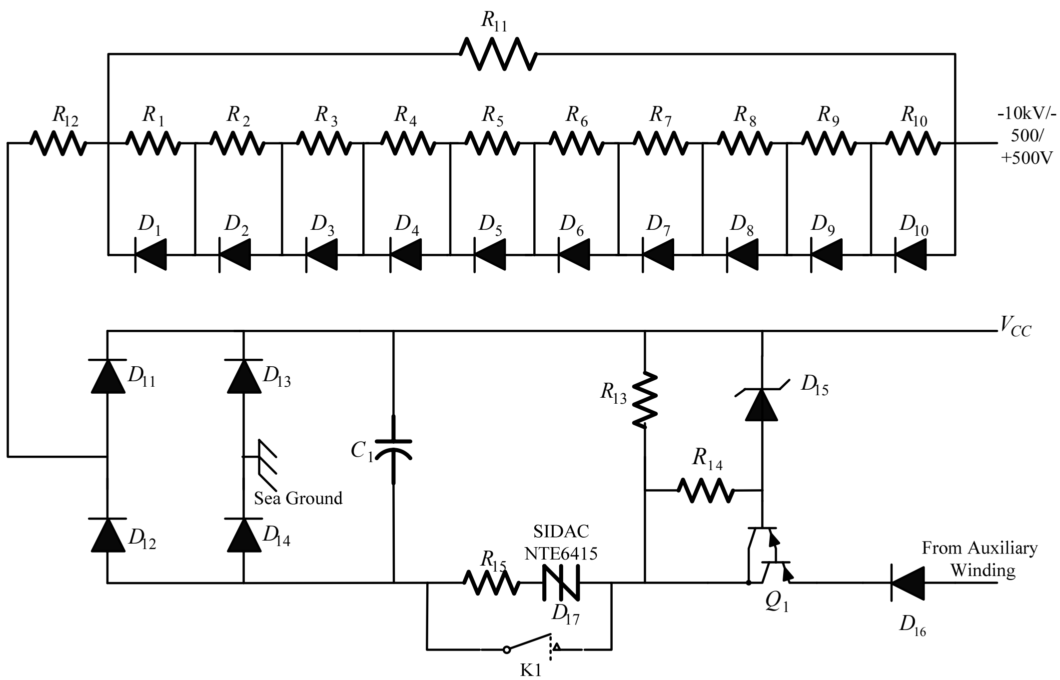

Figure 5.21 Startup power supply designed for 10 kV to 400 V dc-dc converters

A Darlington type transistor Q_1 is used in the linear regulator because the required collector current is above 3 A. A linear regulator can be inherently short circuit proof. From Figure 5.13, the maximum base current of Q_1 is determined by R_{14}. When R_{14} is large enough, the emitter current of Q_1 is limited within a safe range. The linear regulator can be replaced with a switching mode power supply to achieve higher efficiency at the cost of increased complexity. This is not adopted because keeping the circuit simple (less parts) and reliable is a greater objective.

One difficulty for implementing this power supply circuit is that the SIDAC requires holding current at about 50 mA. Normally the control logic circuit for the startup functions does not consume that much energy. One way to solve this problem is to add a bleeding resistor at the output of the linear regulator. But this certainly lowers the power supply efficiency. The approach adopted here is to parallel a normally open switch (K1) with the SIDAC. This switch is operated by the logic circuit and has no holding current requirement. After the SIDAC is closed and the logic circuits are operational, K1 is closed.

The paralleling of K1 with the SIDAC solves another problem. Under -500 V, the capacitor C_1 needs to be charged for a much longer time to reach the SIDAC V_{br} compared with +500 V, due to the difference between the charging resistors. By opening switch K1, the energy in C_1 is maintained. Thus, less charging time is required under -500 V.

Under -10 kV, the logic circuit for startup operations is powered by the HKPS. K1 is kept closed, and the voltage across C_1 is determined by the voltage distribution across R_{11}, R_{12} and R_{13}. By adjusting the value of these resistors, the voltage across C_1 can be set at a level much lower than its rating, thus prolonging its life. The present values of R_{11}, R_{12} and R_{13} are 10 MΩ, 500 kΩ, and 20 kΩ, respectively. The voltage across C_1 is about 20 V after the converter starts. Because it is lower than the V_{br} of the SIDAC, the relaxation circuit is no longer functional. This also increases the life time of capacitor C_1 and the SIDAC.

This circuit operates correctly when the input voltage is larger than V_{br}, regardless of polarities. It generates a pulsed power with an interval of about 60 seconds. The ideal waveform of the circuit output at full load is shown in Figure 5.22. When only the logic circuits are powered, the pulse lasts for several hundred milliseconds. The test results are given in Chapter 6.

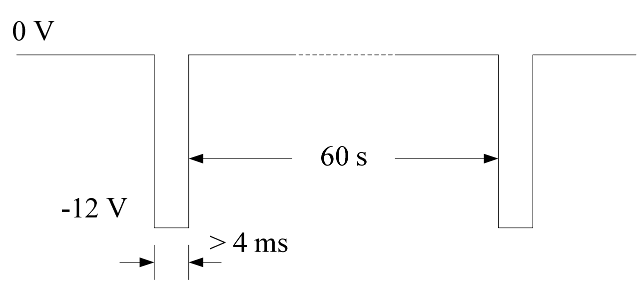

Figure 5.22 Ideal output of the startup power supply when starting a converter

5.3 Summary

In this chapter, the design and implementation circuits of the BU system and the science node startup system are described. Both designs must solve the particular challenges resulting from system's location on the seafloor, including lack of communications and no low voltage power supply. The BU system has two functions: closing switches to connect cables and opening switches to isolate a faulty cable. The BU circuit design therefore includes the switching circuit and the control circuit to close switches, to isolate spur cable and backbone cable faults. The converter startup system consists of the startup logic circuit and the startup power supply. The startup logic circuit carries out the operations designed during the startup process of the science node converters. The startup power supply obtains energy from the 10 kV input cable to provide a low voltage powering the logic circuit and converter control circuit.

Chapter 6

Test Results of Branching Unit and Science Node Startup System

This chapter presents the test results of the branching unit system and science node startup system in Chapter 5. Synchronized with the requirements of the NEPTUNE project, the test of the BU system was performed at a reduced voltage level with simulated system events to verify the required functionalities. The tests of the science node startup system were carried out under situations similar to the anticipated field environment and have proved that it will operate properly in the field.

6.1 Branching unit system

Two main parts of the BU system correspond to the two functions of a BU: closing switches and opening switches. The system was tested at a reduced voltage level in the power lab at the Electrical Engineering Department of the University of Washington.

6.1.1 Branching unit circuit for closing switches

The BU circuit for closing switches (see Section 5.1.1) was tested in the lab environment for weeks with a switching frequency of about 0.1 Hz. Functionality and reliability were the main objectives in the test. For convenience, the BU circuit configuration in Figure 5.1 is also shown here in Figure 6.1.

The voltage across capacitor C is shown in Figure 6.2 (a). The voltage across the switch solenoids C1 and C3 and the current flowing through them are shown in Figure 6.2 (b) and (c).

Circuit parameters in the lab tests are:

SIDAC break down voltage = 60 V, C = 165 μF, R = 500 kΩ, and the solenoid resistance = 50 Ω.

In Figure 6.2 (a) the capacitor voltage is charged up slowly until it reaches 60 V, at which point the SIDAC conducts. The energy in the capacitor is dumped directly into the switch solenoids [Figure 6.2 (b) and (c)]. A voltage regulator could be added between the capacitor and the solenoids for higher efficiency and a regulated voltage across the solenoids. However, this is unnecessary because the current magnitude and duration in the solenoids meets their operation specifications.

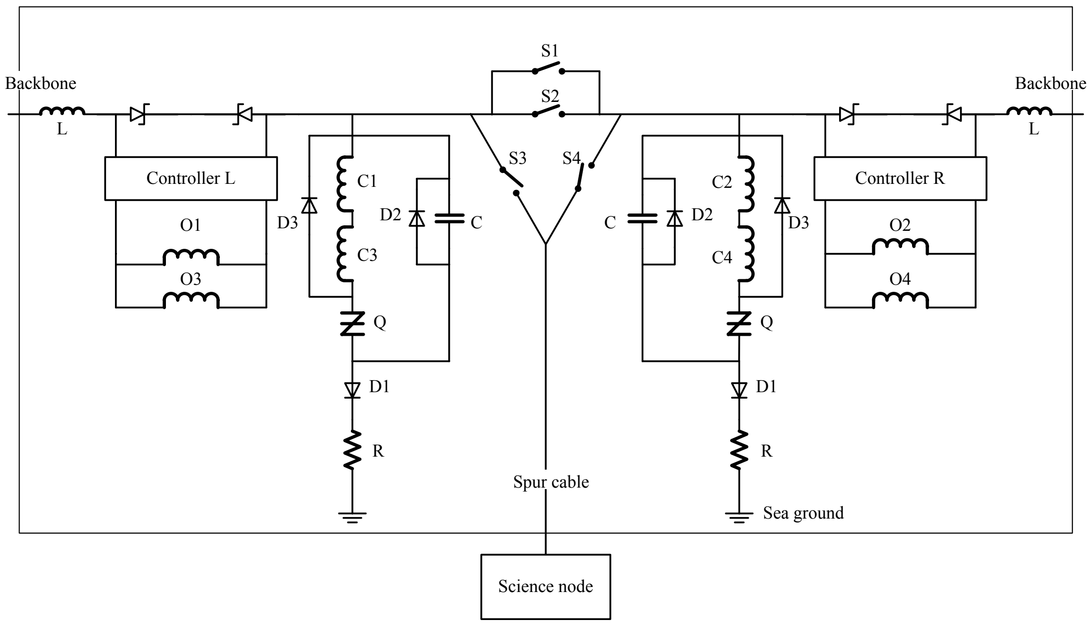

Figure 6.1 BU circuit configurations

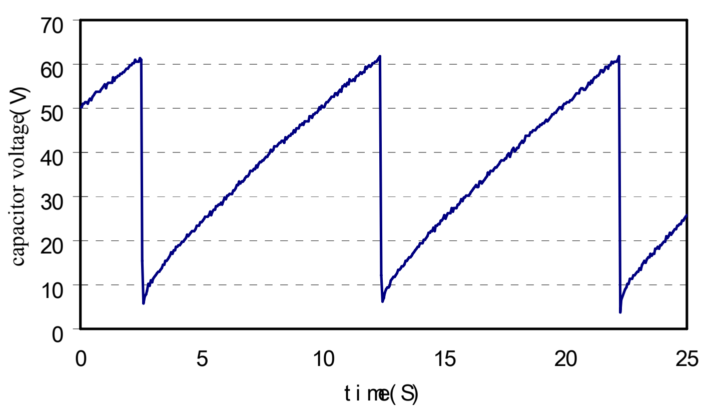

(a) Capacitor voltage in BU circuit for closing switches

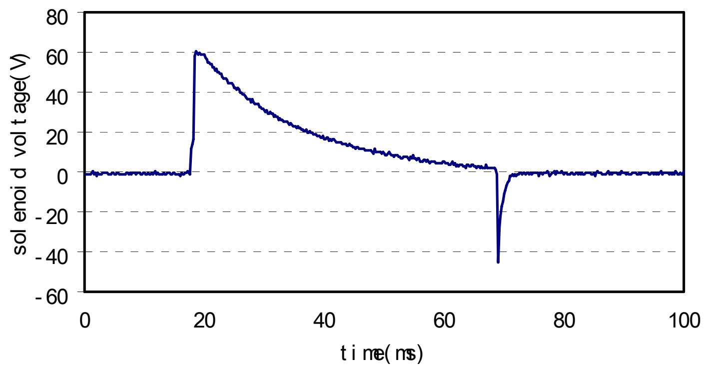

(b) Voltage across the switches solenoids

bv

(c) Current flowing through the switches solenoids

Figure 6.2 Lab test waveforms of BU circuit for closing switches

6.1.2 Branching unit circuit for opening switches

The BU circuit for opening switches to isolate a fault (Section 5.1.2) consists of two parts: circuit for isolating backbone fault and circuit for isolating spur cable fault. They have been tested preliminarily in two steps. The first part of the circuit was tested together with the circuit for closing switches in a simple network (Figure 6.3). Then, a network with two BUs and associated control circuits, including both parts of the fault isolating functions and switch closing function, was built and tested. Results from both tests verified the functionality of the design.

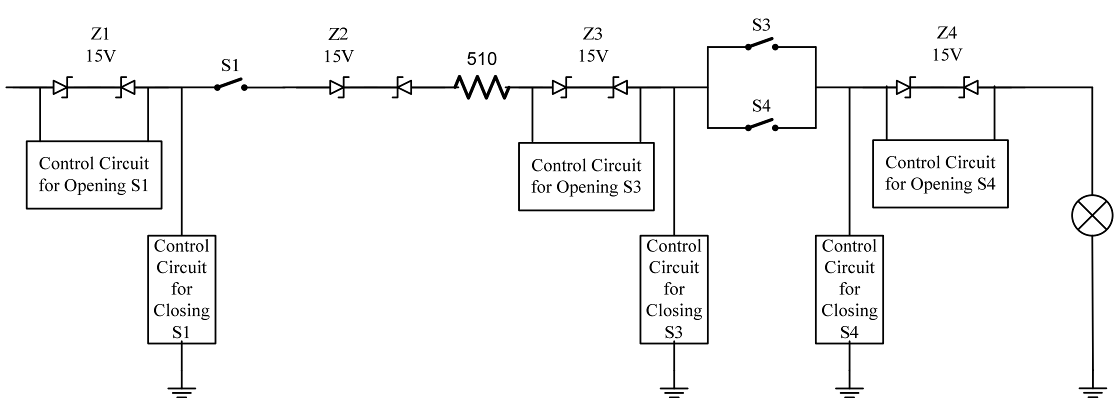

Figure 6.3 A simple network for BU circuit test

The network (Figure 6.3) is equivalent to one and one-half branching units. The light bulb at the end is simulating a fault. The circuit was energized by either +300 V or -300 V. Under the positive voltage, all switches, S1, S2 and S3, are closed. When the voltage polarity is reversed, the control circuits performed correctly to open S3 and S4, while S1 remains closed as it is supposed to.

6.2 Science node startup system

The science node startup system includes a startup logic circuit and a startup power supply. The operations of this system and the circuit design details are explained in sections 5.2.1 and 5.2.2, respectively. The startup circuit was tested both in the Applied Physics Laboratory (APL) of the University of Washington with a circuit simulating the 10 kV to 400 V converters, and in the Jet Propulsion Laboratory (JPL) of the California Institute of Technology with the real converters. Both tests gave satisfying results. The waveforms shown here are mostly from the APL test.

6.2.1 Startup logic circuit

A. Switching logic circuit

To test the switching logic circuit, the converter input circuit was simulated using an RC circuit with equivalent values as in the converter input filter. As the operation at +500 V is rather simple, the emphasis of the test is on the functions at -500 V. Two resistors are connected in front of the circuit simulating converters A and B, and after switches S1_A and S1_B (refer to Figure 5.8) to simulate faults. One is 250 kΩ and the other is 500 kΩ. Therefore, the fault current is 2 mA and 1 mA at -500 V, respectively. Using the fault detection circuit shown in Figure 5.12, the voltage drop across the 3 kΩ current limiting resistor is detected and shown in channel 2 of Figure 6.4. Channel 1 is the counter clock signal (refer to Figure 5.9).

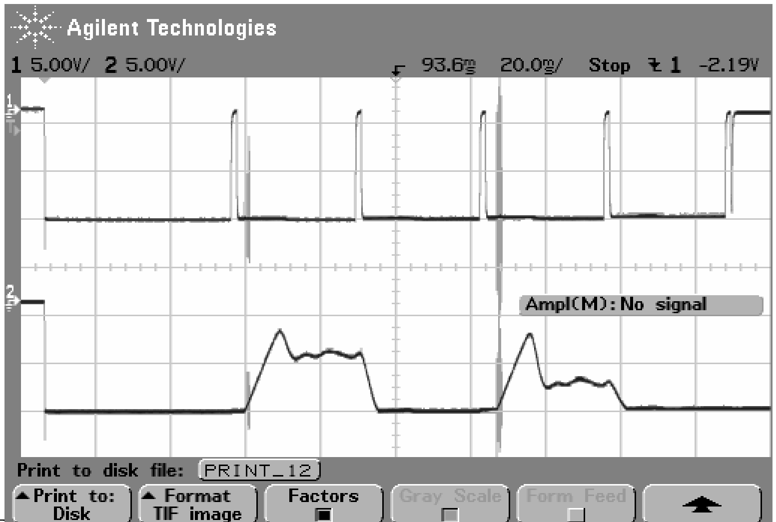

Figure 6.4 Fault detection circuit waveforms when faults exist

Further descriptions of the waveforms shown in Figure 6.4 are as follows.

1) At the first rising edge of the clock signal, switch S1_A is closed. Thus, the 250 kΩ resistor simulating a fault at converter A is connected to the -500 V input. The voltage across the current limiting resistor is detected at about 6 V.

2) At the second rising edge of the clock signal, S1_A is opened because the fault is detected. Therefore, the current flowing through the 3 kΩ resistor drops to zero. The output of the fault voltage sensing circuit becomes 0 V.

3) At the third rising edge, S1_B is closed. Thus, the 500 kΩ resistor simulating a less serious fault at converter B is connected to the -500 V input. The voltage across the 3 kΩ resistor is detected at about 3 V.

4) At the fourth rising edge, S1_B is opened because the fault is detected. Therefore the output of the fault voltage sensing circuit becomes 0 V for the same reason as in 2).

5) After these operations are completed, the clock signal is disabled to prevent any more switching operations.

When switch S1_A or S1_B is closed, the converter input capacitance is charged through the 3 kΩ current limiting resistor. This causes the initial spike on the voltage across the resistor, which is not interpreted as a fault by the fault detection circuit.

A waveform with no resistors simulating faults at the converter inputs is shown in Figure 6.5 for comparison. The initial spike on the 3 kΩ resistor voltage waveform is more distinctive in this case, because the current flowing through it goes to zero after the converter input capacitance is fully charged.

B. A/B selection logic circuit

The function of the A/B selection circuit is to start converter A when the input cable voltage is negative and its magnitude is above 5.7 kV. If converter A fails, the logic circuit tries to start converter B.

After a converter starts, the power supply V_{cc} for the logic circuit is taken over by the converter HKPS. Hence, V_{cc} increases from 12 V to 16 V. The waveform is shown in Figure 6.6. Channel 1 is the signal to start converter A. Channel 2 is V_{cc} (V_{cc} is inverted in the figure). In the test, V_{cc} is provided by a voltage source simulating the converter HKPS.

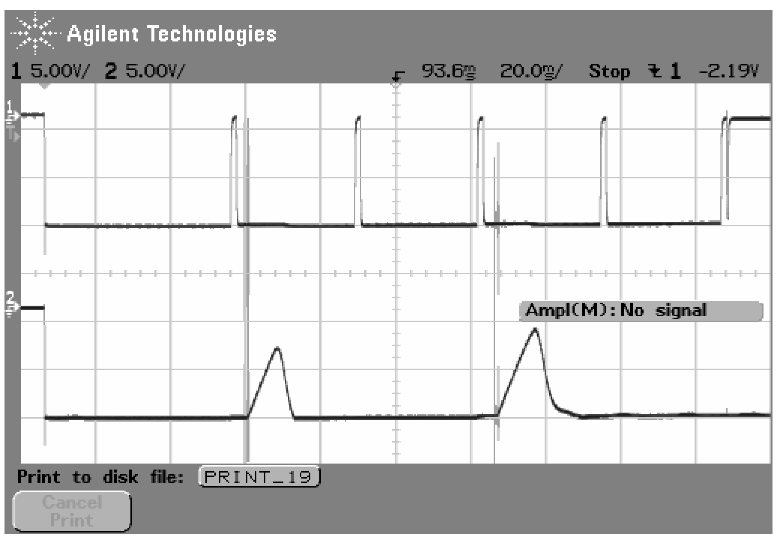

Figure 6.5 Fault detection circuit waveforms when no fault exists

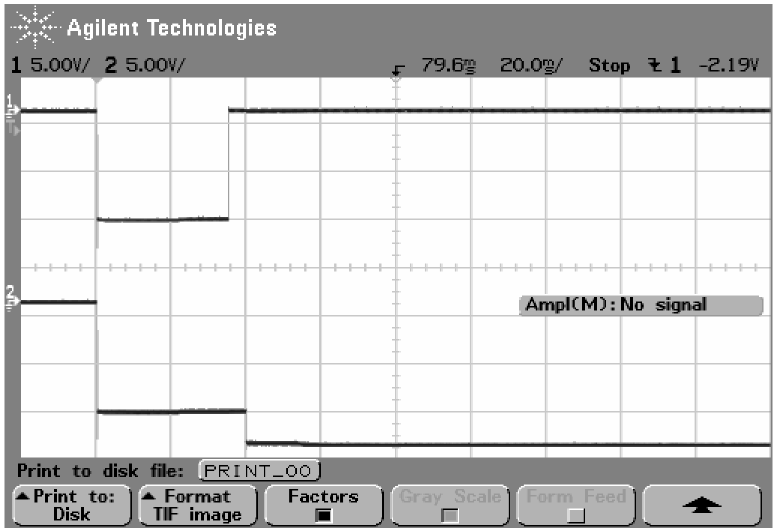

Figure 6.6 Waveforms of converter start signal and V_{cc} when the converter is started successfully

Figure 6.7 shows the waveforms of converter's start signal in Channel 1 and V_{cc} in Channel 2 when the converter fails to start. V_{cc} drops to 10 V for about 8 ms when trying to start the converter. This is because of the 4 Ω load simulating the converter's MOSFETs driver circuit. V_{cc} drops to zero after the energy in the startup power supply is depleted.

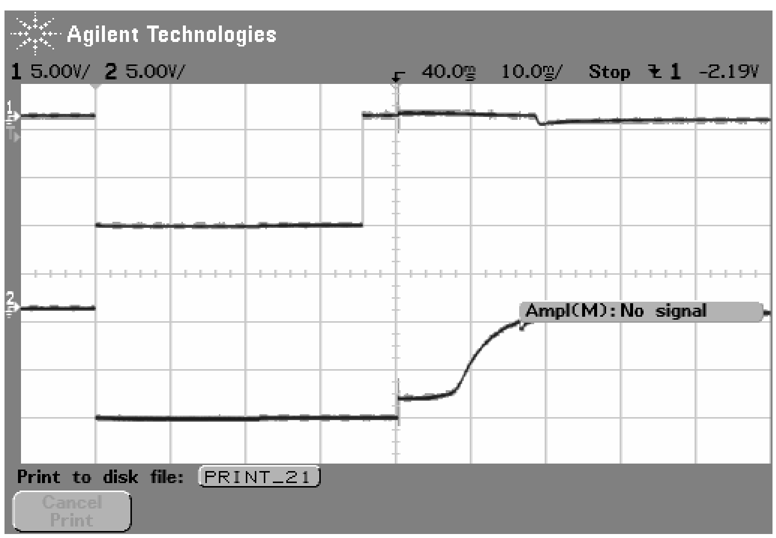

Figure 6.7 Waveforms of converter start signal and V_{cc} when the converter could not be started

6.2.2 Startup power supply

The functionality of connecting a linear regulator to a SIDAC relaxation circuit was tested by Tess McEnulty of the University of Michigan at JPL. The proposed startup power supply circuit was built and tested at APL with a 4 Ω resistive load, and later at JPL with a real converter. The input voltage in the tests varies from 100 V to -12 kV, a wider range than required by the operation design. The example waveforms generated by the startup circuit from both tests are shown in Figures 6.8 through 6.10.

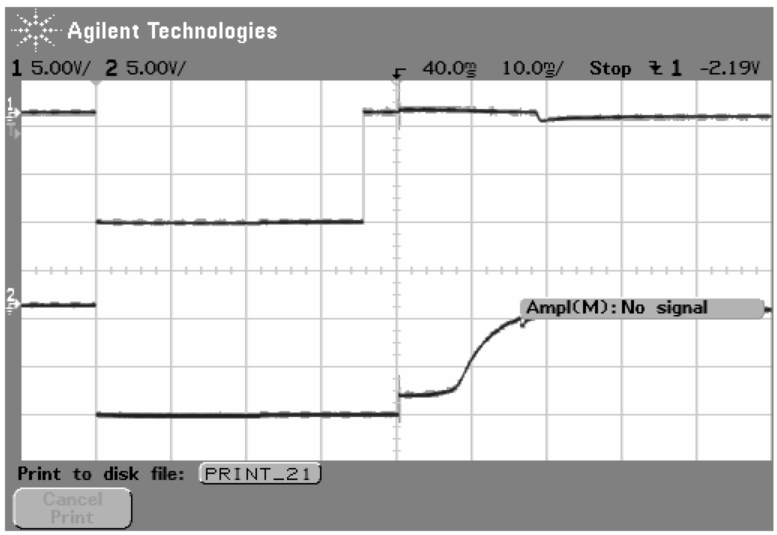

Channel (1): Command signal to power the 4 Ω load

Channel (2): Startup power supply output V_{cc}

Figure 6.8 Startup power supply output waveform with a resistive load

The waveform of V_{cc} drops to about 10 V when a command signal to power the 4 Ω load is made; and nearly 3 A current is drawn from the startup power supply (Figure 6.8). This high output current lasts for about 8 ms. The period can be lengthened by using a larger capacitor C_1 or employing a SIDAC with a higher V_{br}.

The startup power supply powers the control circuit and the MOSFETs' driving circuit of the 10 kV to 400 V converter (Figure 6.9). The converter consumes about one-third of the required startup energy. When V_{cc} reaches its target value, it lasts about 50 ms at 12 V.

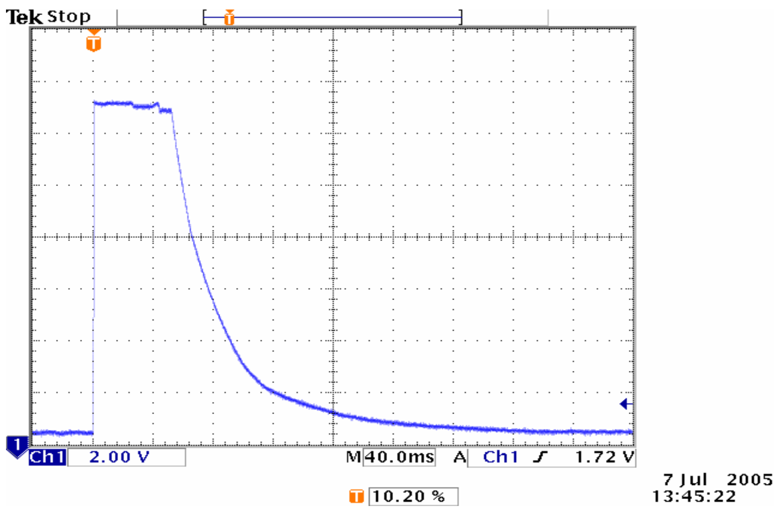

Figure 6.9 Startup power supply output when firing a converter at -8 kV (inverted)

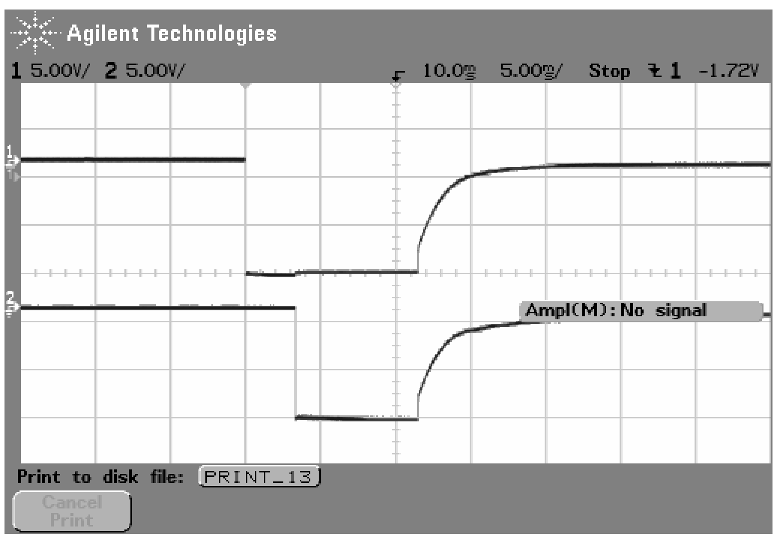

Figure 6.10 Waveform of V_{cc} and signal to open K1 at +500 V (inverted)

Figure 6.10 shows the waveform of V_{cc} when the input voltage is +500 V in channel 1 and channel 2 shows the signal to open K1. Both are inverted for the convenience of testing. K1 is a switch to bypass SIDAC in the startup power supply circuit. Opening K1 after all switches are opened at +500 V can preserve the energy in capacitor C_1, so that at -500 V the charging process is shorter. A more detailed description of the startup power supply is found in Section 5.2.2.3.

6.3 Summary

In this chapter, test results of the branching unit system and science node startup system are shown. The branching unit system consists of a circuit for opening switches and a circuit for closing switches. The tests for both circuits were performed under a lower voltage level and simulated the operations in the real situation. The results verified the required functionality of the branching unit. The science node startup system consists of a startup logic circuit and a startup power supply. The system was tested with the same operation procedures and voltages as in the field. The results show that the startup system can carry out the right functions under various situations.

Chapter 7

Concluding Remarks

Study of the Earth's ocean system requires data to be collected over a long range of time and space. NEPTUNE is a planned ocean observatory system with such capability to be deployed under the northeast Pacific Ocean. It will provide permanent power and communications to the scientific sensors on the seafloor, enabling continuous study of the ocean processes across a large region. This dissertation describes the design of the NEPTUNE power system including the infrastructure, operations, stability analysis and the implementation circuits for some important subsystems.

Located on the seafloor and being the world's first large scale interconnected dc power network, the NEPTUNE power system poses a number of challenges in its design: it requires high reliability and compact sizes, no COTS components are available for power conversion and protection, no measurements to identify topology changes or locate a fault, no communications are available to assist the system startup. Solutions to meet these challenges are proposed in this dissertation. The main contributions are summarized as follows:

1) Propose operation modes using voltage levels and polarities to separate different power system operations

2) Propose an automated and coordinated protection scheme that does not require dedicated communication capability between protection units but has coordination between them; needs only regular power switches for fault isolation instead of fault current interruption devices; has the same settings at every protection unit; and has inherent backup capability for dysfunctional protection units

3) Propose an algorithm to identify an opened backbone switch or a high impedance fault by analyzing the residual of the network node voltage equations

4) Propose an algorithm to locate a high impedance fault through a combined parameter and state estimation using the weighted least square approach

5) Propose an algorithm to locate a fault through only shore station measurements using the weighted least square approach

6) Propose approaches for steady-state stability analysis, and appropriate models for small and large-signal stability analysis

7) Propose the operation design and implementation circuits for the branching unit system and the science node startup system that require neither communications nor low voltage power supply.

Many of the challenges and constraints are unique to the undersea observatory system. With increasing research interest in the Earth's ocean system, similar observatory systems will surely be needed and constructed. The solutions proposed in this dissertation address the most typical constraints and difficulties in building the power systems for this type of observatories. They may find more applications as scientists conceive methods to explore the ocean environment.

Bibliography

[1] *North East Pacific Time-integrated Undersea Networked Experiments (NEPTUNE)*. [Online]. Available: http://www.neptune.washington.edu.

[2] *Maritime Communication Services*. [Online]. Available: http://www.mcs.harris.com.

[3] *Hawaii 2 Observatory*. [Online]. Available: http://www.soest.hawaii.edu/h2o.

[4] *Advanced Real-time Earth monitoring Network in the Area (ARENA)*. [Online]. Available: http://homepage.mac.com/ieee_oes_japan/ARENA/ARENA-E.html.

[5] *European Sea Floor Observatory Network (ESONET)*. [Online]. Available: http://www.oceanlab.abdn.ac.uk/research/esonet.shtml.

[6] J. Kojima, K. Asakawa, B. Howe, H. Kirkham, "Power Systems for Ocean Regional Cabled Observatories," in *Proc. OCEANS '04, IEEE Oceans Conference*, pp. 2176-2181, Kobe, Japan, November 2004.

[7] M. A. El-Sharkawi, et al, "North East Pacific Time-integrated Undersea Networked Experiments (NEPTUNE): Cable Switching and Protection," *IEEE Journal of Ocean Engineering*, Vol. 30, No.1, pp. 232-240, January 2005.

[8] P. Phibbs, S. Lentz, "Selection of the Technical Design of the World's First Regional Cabled Observatory- NEPTUNE Stage 1 (NEPTUNE Canada)," in *Proc. IEEE Scientific Submarine Cable 2006 Conference*, Dublin, Ireland, February 2006.

[9] A. D. Chaves, et al, "The NEPTUNE Scientific Submarine Cable System," in *Proc. OCEANS 2001 Conference*, Honolulu, Hawaii.

[10] H. Kirkham, "The Design of the NEPTUNE Power System," in *Proc. OCEANS 2001 Conference*, Honolulu, Hawaii.

[11] K. Schneider, C.C. Liu, T. McGinnis, B. Howe, H. Kirkham, "Real-Time Control and Protection of the NEPTUNE Power System," in *Proc. OCEANS 2002, MTS/IEEE Conference and Exhibition*, pp. 1799-1805, Mississippi, October 2002.

[12] A. Simoes Costa, J.A. Leao, "Identification of Topology Errors in Power System State Estimation," *IEEE Trans. Power Systems*, Vol. 8, No. 4, November 1993.

[13] K. Schneider, C.C. Liu, B. Howe, “Topology Error Identification for the NEPTUNE Power System,” *IEEE Trans. Power Systems*, Vol. 20, No. 3, pp. 1224-1232, August 2005.

[14] R.D. Middlebrook, “Modeling Current-Programmed Buck and Boost Regulators,” *IEEE Trans. Power Electronics*, Vol. 4. No. 1, pp. 36-52, January 1989.

[15] R.D. Middlebrook, “Small-Signal Modeling of Pulse-Width Modulated Switched-Mode Power Converters,” in *Proceedings of the IEEE*, Vol. 76, No. 4, pp. 343-354, April 1988.

[16] F.D. Tan, R.D. Middlebrook, “A Unified Model for Current-Programmed Converters,” *IEEE Trans. Power Electronics*, Vol. 10, No. 4, pp. 397-408, July 1995.

[17] R.B. Ridley, “An Accurate and Practical Small-Signal Model for Current-Mode Control,” [Online], Available: http://www.ridleyengineering.com.

[18] R.D. Middlebrook, “Input Filter Considerations in Design and Application of Switching Regulators,” in *Proc. IEEE Industry Applications Society Annual Meeting*, 1976, pp. 366-382. Republished in Advances in Switched-Mode Power Conversion, Vol. I, Teslaco, Pasadena, CA.

[19] C.M. Wildrick, F.C. Lee, B.H. Cho, B. Choi, “A Method of Defining the Load Impedance Specification for A Stable Distributed Power System,” *IEEE Trans. Power Electronics*, Vol. 10, No. 3, pp. 280-285, May 1995.

[20] X. Feng, J. Liu, F.C. Lee, “Impedance Specifications for Stable DC Distributed Power Systems,” *IEEE. Trans. Power Electronics*, Vol. 17, No. 2, pp. 157-162, March 2002.

[21] S.D. Sudhoff, et al, “Admittance Space Stability Analysis of Power Electronic Systems,” *IEEE Trans. Aerospace and Electronic Systems*, Vol. 36, No. 3, pp. 965-973, July 2000.

[22] V. Vorperian, “Simplified Analysis of PWM Converters Using Model of PWM Switch Part I: Continuous Conduction Mode,” *IEEE Trans. Aerospace and Electronic Systems*, Vol. 26, No. 3, pp. 490-496, May 1990.

[23] V. Vorperian, “Simplified Analysis of PWM Converters Using Model of PWM Switch Part II: Discontinuous Conduction Mode,” *IEEE Trans. Aerospace and Electronic Systems*, Vol. 26, No. 3, pp. 497-505, May 1990.

[24] R.W. Erickson, *Fundamentals of Power Electronics*. Boulder, CO: Chapman & Hall, 1997, pp. 408-451.

[25] F. Guinjoan, J. Calvente, A. Poveda, L. Martinez, "Large-Signal Modeling and Simulation of Switching DC-DC Converters," *IEEE Trans. Power Electronics*, Vol. 12, No. 3, pp. 485-494, May 1997.

[26] *NEPTUNE Feasibility Study*, [Online], Available: http://www.neptune.washington.edu

[27] B. Howe, H. Kirkham,V. Vorperian, "Power System Considerations for Undersea Observatories," *IEEE Journal of Oceanic Engineering*, Vol. 27, No. 2, 267-274, April 2002

[28] K. Schneider, C.C. Liu, T. McGinnis, B. Howe, H. Kirkham, "Real-Time Control and Protection of the NEPTUNE Power System," in *Proc. OCEANS, 2002, MTS/IEEE Conference and Exhibition*, pp. 1799-1805, Mississippi, October 2002

[29] Shuai Lu, Mohamed A. El-Sharkawi, "NEPTUNE Power System: Detection and Location of Switch Malfunctions and High Impedance Faults," in *Proc. International Symposium on Industrial Electronics 2006*, Montreal, Canada, July 2006.

[30] P. Kundur, *Power System Stability and Control*, McGFraw-Hill Inc., 1993

[31] K. Siri, "Study of System Instability in Solar-Array-Based Power Systems," *IEEE Trans. Aerospace and Electronic Systems*, Vol. 36, No. 3, pp. 957-964, July 2000.

[32] J.R. Lee, B.H. Cho, S.J. Kim, F.C. Lee, "Modeling and Simulation of Spacecraft Power Systems," *IEEE Trans. Aerospace and Electronic Systems*, Vol. 24, No. 3, pp. 295-304, May 1988.

[33] A. Emadi, J.P. Johnson, M. Ebsani, "Stability Analysis of Large DC Solid-State Power Systems for Space," *IEEE AES Systems Magazine*, pp. 25-30, February 2000.

[34] J.G. Ciezki, R.W. Ashton, "Selection and Stability Issues Associated with a Navy Shipboard DC Zonal Electric Distribution System," *IEEE Trans. Power Delivery*, Vol. 15, No. 2, pp. 665-669, April 2000.

[35] J. Liu, X. Feng, F.C. Lee, D. Borojevich, "Stability Margin Monitoring for DC Distributed Power Systems via Perturbation Approaches," *IEEE Trans. Power Electronics*, Vol. 18, No. 6, pp. 1254-1261, November 2003.

[36] K.J. Karimi, A. Booker, A. Mong, "Modeling, Simulation, and Verification of Large Power Electronics Systems," in *Proc. IEEE 27th Annual Power Electronics Specialists Conference*, PESC '96 Record, 1996.

[37] E.W. Gholdston, et al, "Stability of large DC power systems using switching converters, with application to the International Space Station," in *Proc. 31st Intersociety Energy Conversion Engineering Conference*, IECEC 96, 1996.

[38] B.R. Needham, P.H. Eckerling, K. Siri, "Simulation of Large Distributed DC Power Systems Using Averaged Modelling Techniques and The Saber Simulator," in *Proc. Applied Power Electronics Conference*, *APEC '94*, pp. 801 -807, Vol. 2, 13-17 February 1994.

[39] J.H. Ly, K. Siri, "Frequency Response Analysis for DC-DC Converters Without Small-Signal Linearization," in *Proc. Applied Power Electronics Conference and Exposition*, 2003, pp. 1008-1013.

[40] V. Vorperian, "*Test results of the 10kV-to-400V dc-to-dc converter for the MARS project*," JPL Document No. D-33812, December 26, 2005.

[41] V. Vorperian, "Synthesis of Medium Voltage Dc-to-Dc Converters from Low-Voltage, High-Frequency PWM Switching Converters," to be published in *IEEE Trans. Power Electronics*.

[42] B. Howe, et al, "Power System for the MARS Ocean Cabled Observatory," in *Proc. Scientific Submarine Cable 2006 Conference*, pp. 121-126, Marine Institute, Dublin, Ireland, February 2006.

[43] P. Lancaster, R. Jacques, G. Nicol, G. Waterworth, H. Kirkham, "NEPTUNE: dc power beyond MARS," in *Proc. Scientific Submarine Cable 2006 Conference*, pp. 118-120, Marine Institute, Dublin, Ireland, February 2006.

[44] Shuai Lu, Mohamed A. El-Sharkawi, Harold Kirkham, Bruce M. Howe, "NEPTUNE Power System: Startup Power Supply for 10 kV to 400 V Dc-Dc Converters", in *Proc. Applied Power Electronics Conference 2006*, Dallas, Texas, pp. 1385-1389, March 2006.

[45] Shuai Lu, Mohamed A. El-Sharkawi, "NEPTUNE Power System: Science Node Converter Startup Operations Design and Implementation Circuit", in *Proc. 4th International Energy Conversion Engineering Conference*, San Diego, California, June 2006.

[46] J. Adams, "Designing a Power Supply Using IRIS40xx Series" *Application Note AN1025*, International Rectifier, February 2001.

[47] G. J. Miller, "A 50W, 48V-to-5V DC-DC Converter Using the HIP2100," *Application note 9605*, Intersil Corporation, April 1996.

[48] V. Vorperian, "Node Converter Design," *NEPTUNE project Concept Design Review*, [Online]. Available: http://www.neptune.washington.edu

[49] M. Madigan, M. Dennis, "50W Forward Converter with Synchronous Rectification and Secondary Side Control," *Technical document*, Texas Instruments, 2001.

[50] W. Xu, Y. Mansour, "Voltage Stability Analysis Using Generic Dynamic Load Models", *IEEE Trans. Power Systems*, Vol. 9, No. 1, pp. 470-493, Feb. 1994.

[51] J.A. Momoh, L.G. Dias, D.N. Laird, "An Implementation of a Hybrid Intelligent Tool for distribution System Fault diagnosis", *IEEE Trans. Power Delivery*, Vol. 12, No. 2, pp. 1035-1040, April 1997.

[52] R.C. Dorf, R.H. Bishop, *Modern Control Systems*, Prentice Hall, Inc, 2003.

[53] V. Vorperian, *Fast Analytical Techniques for Electrical and Electronic Circuits*, Cambridge University Press, 2002.

Vita

Shuai Lu was born in Luoyang, People's Republic of China in 1976. He entered Tsinghua University in Beijing in 1994 and received his Bachelor of Science degree and Master of Science degree, both in Electrical Engineering, in Beijing in 1999 and 2002, respectively. Following that, he enrolled in the Ph.D. program in the Department of Electrical Engineering at the University of Washington. With the completion and successful defense of this dissertation, he will have earned a Doctor of Philosophy in Electrical Engineering from the University of Washington.